Investigating the role of neutral sphingomyelinases in membrane vesicle trafficking

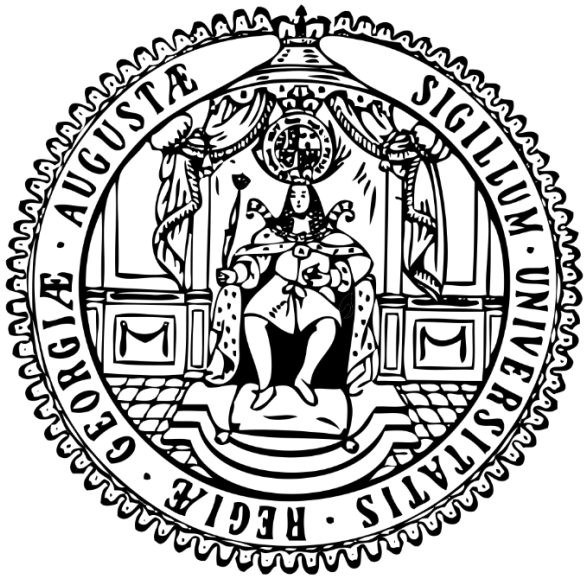

Dissertation
For the award of the degree “Doctor rerum naturalium”
of the Georg-August-Universität Göttingen

within the doctoral program Molecular Medicine
of the Georg-August University School of Science (GAUSS)

submitted by
Dolma Choezom
from Lithang, Tibet

Göttingen, 2022

Thesis Committee:

Prof. Dr. Julia Christina Groß

Health and Medical University Potsdam & Institute for Developmental Biochemistry/ Haematology and Oncology, University Medical Center Göttingen

Prof. Dr. Michael Meinecke

Heidelberg University Biochemistry Center (BZH), Heidelberg University

Prof. Dr. Jörg Enderlein

Third Institute of Physics (Biophysics), Georg August University Göttingen

Members of the Examination Board:

Prof. Dr. Julia Christina Groß

Health and Medical University Potsdam & Institute for Developmental Biochemistry/ Haematology and Oncology, University Medical Center Göttingen

Prof. Dr. Michael Meinecke

Heidelberg University Biochemistry Center (BZH), Heidelberg University

Further members of the Examination Board:

Prof. Dr. Jörg Enderlein

Third Institute of Physics (Biophysics), Georg August University Göttingen

Prof. Dr. Ralph Kehlenback

Department of Molecular Biology, University Medical Center Göttingen

PD. Dr. Laura Zelarayán-Behrend

Institute of Pharmacology and Toxicology, University Medical Center Göttingen

Prof. Dr. Matthias Dobbelstein

Department of Molecular Oncology, University Medical Center Göttingen

Date of Oral examination: 26.04.2022

Affidavit

I hereby declare that I prepared the PhD thesis “Investigating the role of neutral sphingomyelinases in membrane vesicle trafficking” on my own with no other sources and aids than quoted.

This chapter-based thesis includes two manuscripts. The first manuscript is accepted for publication in the Journal of Cell Science and the second manuscript is available on the preprint server bio-archive (bioRxiv) and is submitted to Review Commons for peer-review publication.

Author contribution for both manuscripts is as follow:

Dolma Choezom: Conceptualization; Investigation; Formal analysis; Writing-original draft, review, and editing.

Prof. Dr. Julia Christina Groß: Conceptualization; Writing-review and editing; Funding acquisition.

For my parents; for their sacrifices and selfless love

And for my uncle Ngawang Lobsang; for his unrelenting support, guidance, and love

Acknowledgments

I would like to express my heartfelt gratitude to many people whose contributions and support made this dissertation possible.

Firstly, I would like to thank my supervisor Prof. Dr. Julia Christina Groß not only for the opportunity to work with her but also for her supervision and guidance. Above all, thank you for creating a conducive and stimulating environment for learning and research with your openness, optimism, empathy, and support. Your mentorship has been truly instrumental in my both personal and scientific growth.

I am very grateful to all the members of Exo-Lab; thank you for providing a strong, supportive, and lively work environment. Thank you Dr. Karen Linnemannstöns for being very generous in helping me out with both personal and professional matters. I truly appreciate not only your scientific input but also your pragmatic support. My sincere thanks also go to Mona Honemann-Capito, for always being just a call-away (Mona!) whenever I needed to ask for help. Thank you for efficiently keeping the lab organized and running. I am especially thankful for your company towards the end of my PhD. I am also thankful to Dr. Leonie Witte, for your supervision during my lab rotation, for always being so patient in clearing out conceptual doubts, and for giving me motivation and positive pep talks whenever I needed those. I am equally thankful to Dr. Pradhipa Karuna M, for your advice and motivation, for our philosophical evening conversations, and for always being ready to help me out to draw up plans for important deadlines. I also want to thank Dr. Jan-Moritz Plum for being a supportive SMPD-companion, and for always answering medical-related questions.

Collectively, I am very thankful to Exo-Lab for their friendship and team spirit, I am happy that I got to share one of the most life-enriching experiences with you all.

I am forever indebted to my parents and my uncle Jamyang Samten for not only their courage to envision a better future for me but also for their sacrifices and efforts to ensure it. I am equally thankful to my relatives both in India and abroad for their unwavering support and love throughout my journey. I am especially grateful to my uncle Ngawang

Lobsang whose constant love, support, and guidance made many things possible in my life.

I am very grateful to Roswitha and Hartmut Boeck for making me feel at home in Germany, thank you for making my initial transition into German culture so much easier, and for your continued love and care. I am so lucky to have you both in my life. I also want to thank Dr. Abhinadan Shrestha for his guidance and advice since my bachelor's; I learned a lot from you.

Finally, I want to thank Kunchok Tharlam whose love, understanding, and support made this journey so much easier and fun. I also want to thank my sister Dolma Lhakyi, my best friend Dechen Yangkyi, and all my other friends for always checking on me with love and care.

Abstract

Evidence collected over the years has established small extracellular vesicle (sEV) or exosome secretion as a novel paradigm for intercellular communication under both physiological and pathological conditions. SEVs are generated as intraluminal vesicles (ILVs) during multivesicular body (MVB) maturation in the endocytic pathway. Upon fusion of MVBs with the plasma membrane, ILVs are released into the extracellular space as sEVs. The molecular mechanisms that underlies ILV generation and the subsequent sorting of these secretory MVBs from the conventional degradative MVBs remain largely unraveled.

Neutral sphingomyelinase 2 (nSMase2, encoded by *SMPD3*) activity drives intraluminal vesicle (ILV) generation for sEV secretion. In addition to its role in producing ceramide required for membrane invagination to form ILVs, here, we report that nSMase2 regulates sEV secretion through modulation of vacuolar H^+-ATPase (V-ATPase) activity. Specifically, we show that nSMase2 inhibition induces V-ATPase complex assembly that drives MVB lumen acidification and consequently reduces sEV secretion. Conversely, we demonstrate that stimulating nSMase2 activity with the inflammatory cytokine TNFα decreases acidification and increases sEV secretion. Thus, we unravel that nSMase2 activity affects MVB membrane lipid composition to counteract V-ATPase-mediated endosome acidification, and thereby shift MVB fate towards sEV secretion.

The second part of this thesis focuses on neutral sphingomyelinase 1 (nSMase1, encoded by *SMPD2*), which also belongs to the sphingomyelinase enzyme family. The molecular characterization and biological function of nSMase1 remain poorly studied. Here, we show that *SMPD2* knockdown (KD) reduces LAMP1 at the mRNA levels and is required for initiating a full-potential unfolded protein response under ER stress. Additionally, *SMPD2* KD dramatically reduces the global protein translation rate. We further show that *SMPD2* KD cells are arrested in the G1 phase of the cell cycle and that two important cell cycle regulating processes - PI3K/Akt pathway and Wnt signaling pathway are altered. Taken together, we propose a role for nSMase1 in buffering ER stress and modulating cellular fitness via cell cycle regulation.

Table of contents

List of figures

Introduction and discussion

Results

(Manuscript I)

(Manuscript II)

Abbreviations

AB	Amyloid-β
ALIX	ESCRT-accessory protein ALG-2-interacting protein X
ALK	Anaplastic lymphoma kinase
ALL	Acute lymphoid leukemia
AML	Acute myeloid leukemia
APP	Amyloid-β precursor protein
ARF6	ADP-ribosylation factor 6
ARNO	ADP-ribosylation factor nucleotide site opener
ATG	Autophagy-related gene
ATM	Ataxia-telangiectasia mutated
Chk	Checkpoint kinase
EED	Embryonic ectoderm
EGFR	Epidermal growth factor receptor
ESCRT	Endosomal sorting complexes required for transport machinery
EV	Extracellular vesicles
GAP	GTPase-activating protein
GEF	Guanine-nucleotide exchange factor
GPAA1	Glycosylphosphatidylinositol anchor attachment 1
GPI	Glycosylphosphatidylinositol
GSKβ	Glycogen synthase kinase β
GUVs	Giant unilamellar vesicles
HRS	Hepatocyte growth factor-regulated tyrosine kinase substrate
ILV	Intraluminal vesicle
LAMP1	Lysosomal-associated membrane protein 1
LDL	Low-density lipoprotein
LRP1	Lipoprotein receptor-related protein 1
MAPK	Mitogen-activated protein kinase
MBP	Myelin basic protein
mTOR	Mammalian target of rapamycin
MVB	Multivesicular bodies
NES	Nuclear export signal
NLS	Nuclear localization signal
NSMAF	Neutral sphingomyelinase activation associated factor
PAF	Platelet-activating factor
PDI	Protein disulfide-isomerase
PIG-S	Phosphatidylinositol glycan anchor biosynthesis, class S
PLP	Proteolipid protein
PP2A	Protein phosphatase 2 A

PTEN	Phosphatase and tensin Homolog
RIDD	Regulated IRE-1-dependent decay of mRNA
ROCK	Rho-associated protein kinase
S1P	Sphingosine-1 phosphate
S1PR	Sphingosine-1 phosphate receptor
SCAP	SREBP cleavage-activating protein
SERCA	Sarco/endoplasmic reticulum Ca^{2+} ATPase
sEV	Small extracellular vesicle
SMPD	Sphingomyelindiesterase
SNX	Sorting nexin
SPC	Sphingosylphosphocholine
SREBP	Sterol regulatory element-binding protein
SRPRB	Signal recognition particle receptor B
SSR2	Signal sequence receptor 2
TNF	Tumor necrosis factor
TNF-R1	Tumor necrosis factor receptor 1
UPR	Unfolded protein response
V-ATPase	Vacuolar-type adenosine triphosphatase
VPS	Vacuolar protein-sorting-associated protein
XBP	X-box binding protein

1 Introduction

1.1 Intracellular membrane trafficking: Relaying intracellular messages

Targeting of cargo molecules to their correct locations is indispensable for proper cellular function. Eukaryotic cells have evolved an elaborate internal membrane system to transport cellular cargos, which include proteins and different macromolecules, from one organelle to another within the same cell or across the plasma membrane to and from the extracellular space. Transport vesicles with cargos enclosed within or associated with the membrane, bud off from one donor membrane and can fuse with another membrane or split up into several smaller vesicles in a highly regulated and dynamic manner (Johannes M. Herrmann and Anne Spang, 2015).

Based on the direction of the cargo movement, membrane trafficking can be broadly grouped into two basic pathways: endocytosis and exocytosis (Fig.1). Exocytosis refers to the movement of intracellular cargo to the plasma membrane or into the extracellular space. For example, as a part of the biosynthetic secretory pathway, newly synthesized proteins, carbohydrates, and lipids in the endoplasmic reticulum are targeted to the plasma membrane or into the extracellular space via the Golgi Apparatus (Barlowe & Miller, 2013). Conversely, endocytosis refers to the movement of cargos into the cell from the plasma membrane or extracellular space. Endocytosis not only achieves the uptake of essential nutrients such as iron, vitamins, and cholesterol but also directs cargos such as cell surface receptors for recycling or lysosomal degradation (McMahon & Boucrot, 2011). Additionally, lysosomes also receive cargos for degradation via autophagy (Yang & Klionsky, 2010). Cell-specific endocytic mechanisms such as phagocytosis and micropinocytosis achieve the internalization of pathogens or extracellular particles (Liu & Roche, 2015). To achieve both long- and short-range intercellular communications, cells release diverse cargo-bound small vesicles from their surface that are collectively termed extracellular vesicles (Tricarico *et al*, 2017; van Niel *et al*, 2018). Therefore, intracellular membrane traffic allows the continuous exchange of components not only between

different cellular compartments but between different cells, thereby relaying important biological messages in a spatiotemporal manner (Fig. 1).

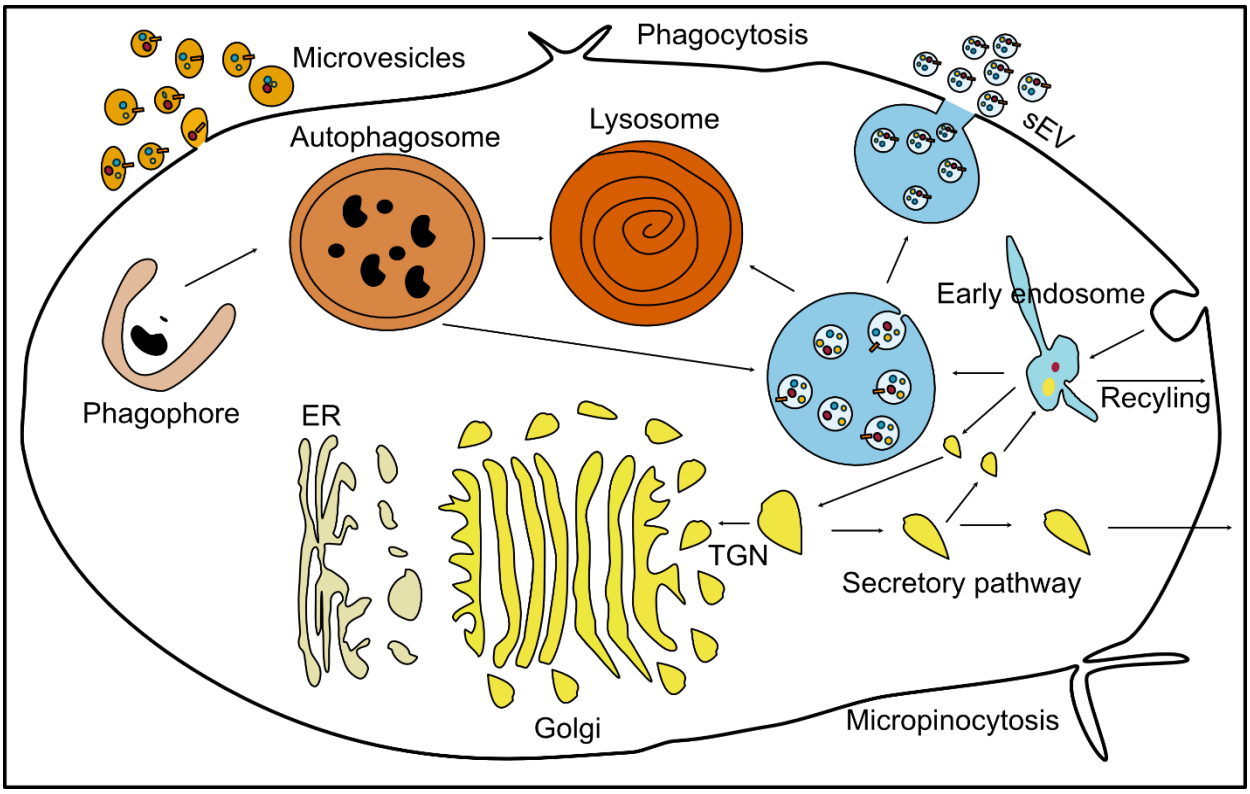

Figure 1: Intracellular membrane vesicle trafficking: Membrane vesicle trafficking comprises many cellular processes that make extensive connections with each other. It includes the conventional secretory pathway, the endosomal pathway including sEV secretion, and the autophagy pathway which culminates in the cellular degradative pathway at the lysosome. It also includes processes occurring at the cell surface such as phagocytosis, micropinocytosis and microvesicle secretion.

1.2 Extracellular vesicles: biological messages in small vesicles

All cell types, from bacteria to plants, secrete various types of membrane-bound vesicles collectively termed extracellular vesicles (EVs) (reviewed in van Niel *et al*, 2018). Although initially regarded as a mere route for spewing out intracellular waste, the loading and secretion of extracellular vesicles are now gaining intense research interest with a focus on its capacity to mediate intercellular communications. The molecular cargos of EVs varying from nucleic acids to lipids and proteins are enclosed within the lumen or associated with the lipid bilayer. In this way, EVs act as signaling vehicles by allowing the

exchange of these components between the secreting and the recipient cells (Van Niel *et al*, 2018).

Intact EVs can be isolated from most bodily fluids including blood (Nomura, 2017), saliva and tears (Aqrawi *et al*, 2017), urine (Dong *et al*, 2020), and milk (Sanwlani *et al*, 2020), thus reflecting their diverse origin. With the ability to incorporate a vast range of cargo molecules and with the added stability provided by the lipid bilayer encapsulation, EVs mediate both short- and long-range intercellular communications necessary for various physiological and pathological processes (Kalluri & LeBleu, 2020; Becker *et al*, 2016). For example, EVs play major roles in various immunological functions (Hu *et al*, 2020; Gutiérrez-Vázquez *et al*, 2013). Specifically, EVs derived from both human and mouse B-lymphocytes activate the major histocompatibility (MHC-II)-restricted T-cell response by presenting the antigen bound to the MHC-II complex on their surfaces (Muntasell *et al*, 2007; Admyre *et al*, 2007). Similarly, Oligodendrocytes in the central nervous system (CNS) secrete EVs containing myelin proteolipid (PLP), myelin basic protein (MBP), and myelin oligodendrocyte glycoprotein (MOG) that are thought to provide axon trophic support (Krämer-Albers *et al*, 2007).

More importantly, EVs also play a role in different pathological processes including cancer and neurological disorders. EVs are thought to contribute to the pathological mechanisms of various neurological disorders by disseminating aggregating proteins such as β-amyloid and Tau in Alzheimer's disease (Bellingham *et al*, 2012; Soares Martins *et al*, 2021), α-Synuclein in Parkinson's disease (Guo *et al*, 2020), and Huntingtin and Polyglutamine in Huntington's disease (Ananbeh *et al*, 2021). Tumor cells release EVs with pro-tumorigenic cargo to induce cell proliferation (Jabbari *et al*, 2020), migration (Ghoroghi *et al*, 2021), metastasis niche establishment (Costa-Silva *et al*, 2015), and immune modulation (Hood *et al*, 2011; Hu *et al*, 2020).

EVs, based on their subcellular origins, are categorized into three subpopulations: microvesicles, apoptotic vesicles, and small extracellular vesicles (sEVs) or exosomes (Théry *et al*, 2018).

1.2.1 Microvesicles

Microvesicles, also known as ectosomes or microparticles, are generated by outward budding and fission of the plasma membrane and subsequent release of the vesicles into the extracellular space (Heijnen *et al*, 1999). Microvesicles are typically 50-1000 nm in diameter (Van Niel *et al*, 2018). Microvesicle biogenesis starts with the trafficking of cargo molecules to a distinct site in the plasma membrane, a redistribution of lipids in this domain, and the action of contractile machinery to drive vesicle pinching (Tricarico *et al*, 2017). The detailed step-wise molecular mechanisms that underlie microvesicle biogenesis including cargo recruitment, membrane budding, and membrane fission for final vesicle release are still being unraveled.

Lipids and other intracellular cargo molecules, targeted for extracellular secretion via microvesicles, associate to a specific site in the plasma membrane which eventually buds outward. Lipids are sorted to this budding site through their affinity to lipid rafts. Cytoplasmic soluble proteins fated for secretion associate to the budding site by binding to inner leaflet lipids of the plasma membrane through different anchors such as palmitoylation, prenylation, and myristoylation (van Niel *et al*, 2018). Cellular components are selectively recruited for microvesicle secretion. While ADP-ribosylation factor 6 (ARF6) on recycling endosomes selectively incorporates cargo such as VAMP-3, β-1 integrin, and MHC-I into microvesicles for secretion, transferrin receptor, which is also trafficked via ARF6-positive endosomes, is actively excluded from incorporation (Muralidharan-Chari *et al*, 2009). Additionally, Rab22a mediates microvesicle generation under hypoxic conditions, most likely by recruiting proteins targeted for secretion or required for microvesicle biogenesis under this condition (Wang *et al*, 2014). Furthermore, surface protease MT1-MMP cargo, in association with VAMP-7, is selectively recruited into microvesicles in a CD9-dependent manner where it facilitates matrix invasion by tumor cells (Clancy *et al*, 2015). Interestingly, nucleic acids are also targeted for microvesicle secretion most likely through co-trafficking with protein cargos (Miranda *et al*, 2010). These results suggest that cells employ multiple mechanisms for selective cargo recruitment depending on the cellular context or the cell type for microvesicle secretion.

Microvesicle budding, fission, and the subsequent release from the cell surface entail drastic physical bending and constriction of the lipid-bilayer domains. Based on the known findings, it is clear that microvesicle biogenesis requires concerted action from both proteins and lipids (Pap *et al*, 2009). Rearrangements in the plasma membrane asymmetry driven by different enzymes including scramblases and aminophospholipid translocases generate physical bending of the membrane and restructuring of the underlying actin cytoskeleton that favor membrane budding and microvesicle formation (Al-Nedawi *et al*, 2009; Lima *et al*, 2009). Therefore, defects in the phosphatidylserine exposure in scramblase activity mutant cells failed to release pro-coagulant-containing microvesicles in blood platelets (Fujii *et al*, 2015). Another important player in microvesicle biogenesis is cholesterol. Cell surface depletion of cholesterol impairs microvesicle biogenesis in activated neutrophils (Del Conde *et al*, 2005). Conceivably, the cellular contractile machinery such as cytoskeleton elements and their regulators play important roles in microvesicle biogenesis. For example, the GTPase protein ARF6, the Rho family of small GTPases, and Rho-associated protein kinase (ROCK) activate contractile actin-myosin networks to drive membrane budding and fission for microvesicle release (Tricarico *et al*, 2017; Muralidharan-Chari *et al*, 2009; Li *et al*, 2012).

Released microvesicles then elicit different cellular responses by transferring their bioactive cargo molecules to the recipient cells. Importantly, microvesicles released by tumor cells carry potential biomarkers for cancer prognosis and diagnosis (Pap *et al*, 2009). Therefore, understanding the precise molecular pathways and mechanisms that drive microvesicle biogenesis could lead to the exploitation of these vesicles as both therapeutic targets as well as drug-delivery vehicles.

1.2.2 Apoptotic vesicles

Apoptotic vesicles, as the name suggests, are another group of subcellular vesicles released from cells undergoing programmed cell death or apoptosis (Wolf, 1967). In contrast to apoptotic bodies, whose size can reach up to 5 µm in diameter, apoptotic vesicles are relatively smaller in size (50-1000 nm) (Kakarla *et al*, 2020). These vesicles contain nuclear fragments and cellular organelles such as mitochondria and parts of the

endoplasmic reticulum as a result of apoptosis. Like other sub-groups of extracellular vesicles, apoptotic vesicles contain bioactive molecules that can elicit different cellular functions in the recipient cells (Li *et al*, 2020). Phosphatidylserine exposed on these vesicles serves as “eat me” signals to the patrolling phagocytes that consequently engulf these apoptotic remnants and thereby facilitate a controlled clearance by the immune system (Truman *et al*, 2008).

1.2.3 Small extracellular vesicles or exosomes

Exosomes or small extracellular vesicles (herein referred to as sEVs) are generated as intraluminal vesicles (ILVs) during multivesicular body (MVB) maturation in the endocytic pathway. MVBs loaded with ILVs are then trafficked towards the cell periphery where they fuse with the plasma membrane to release ILVs as sEVs into the extracellular space (van Niel *et al*, 2018; Pant *et al*, 2012). These vesicles are 50-150 nm in diameter and enriched for proteins that mediate their biogenesis such as protein subunits of the Endosomal Sorting Complexes Required for Transport machinery (ESCRT): HRS, Tsg101, or ESCRT-associated proteins such as Alix and syntenin (Colombo *et al*, 2013; Baietti *et al*, 2012).

Owing to the extensive network of contact sites the endosomal system makes with various organelles, ILVs receive a vast variety of molecular cargos from different cellular origins including the nucleus (Hurley, 2008; van Niel *et al*, 2018). This cargo diversity eventually translates into a complex list of cellular responses that the sEVs elicit in target cells under both physiological and pathological conditions.

1.3 The endosomal system – the biological sorting station

The eukaryotic endosomal system provides a central controlling hub where the decision for recycling versus degradation of its membrane components is made. And thereby it regulates fundamental cellular processes in nutrient uptake, signal transduction, adhesion, and membrane composition regulation in response to changing extracellular conditions (Gruenberg, 2001; Cullen & Steinberg, 2018). Endocytosis starts when a cargo

to be ingested is progressively enclosed by a small portion of the plasma membrane, which first buds inward and then pinches off to form a vesicle containing the ingested cargo. Through endocytosis, cells ingest a wide array of materials: receptor-ligand complexes, various nutrient and their carriers, extracellular matrix components, pathogens, and in some specialized cases even whole other cells (Gruenberg, 2001; Cullen & Steinberg, 2018). Once formed, these endocytic vesicles fuse with a common receiving compartment, the early endosome, where these ingested materials are efficiently sorted. Thus, the early endosome with its tubular membrane portions undergoing constant fusion and fission serves as the first sorting station in the endocytic pathway: some cargo molecules are transported back to the plasma membrane directly or via recycling endosomes, some go to the trans-Golgi network, and others are transported for lysosomal degradation through late endosomes (Gruenberg, 2001; Cullen & Steinberg, 2018). For example, after receptor-ligand uncoupling in mildly acidic pH, house-keeping recycling receptors such as LDL (low-density lipoprotein) receptors are rapidly transported back to the cell surface directly or through recycling endosomes (Arias-Moreno *et al*, 2008). For signal downregulation, some receptors, in particular activated EGFR (epidermal growth factor receptor), are efficiently sorted towards late endosomes for lysosomal degradation (Taub *et al*, 2007).

How are recycled and downregulated cargos efficiently discriminated from each other in early endosomes? Based on the earlier observation on the intact recycling of the transferrin receptor even in the absence of its cytoplasmic tail domain, a sequence-independent geometric-based sorting was described (Jing *et al*, 1990). This model, described after elucidating cargo-ubiquitylation as the sorting signal for degradation in the endosomal system (Katzmann *et al*, 2001), proposed that an integral membrane protein with high lateral mobility in principle follows the bulk membrane flow into the tubular extensions of the early endosomes and can be retrieved and recycled (Maxfield & McGraw, 2004). A critical re-evaluation of the transferrin receptor and other recycling cargos later indeed showed the involvement of sorting motifs in these cargos essential for their recycling (Hsu *et al*, 2012; Dai *et al*, 2004; Chen *et al*, 2013). These recycling sorting motifs found in the cytoplasmic tail of the cargos are recognized by cargo adaptor proteins, for example, sorting nexin (SNX) family proteins, which then engage retromer

[vacuolar protein-sorting-associated protein 35 (VPS35), VPS29, and VPS26] or retriever complexes (VPS35L and VPS26C) for efficient recycling of the cargos to the plasma membrane (Cullen & Steinberg, 2018). For example, specific recycling sorting motifs found in P-selectin (Fjorback *et al*, 2012), lipoprotein receptor-related protein 1 (LRP1) (Van Kerkhof *et al*, 2005), and β-Integrin-1 (Böttcher *et al*, 2012) are recognized by the cargo adaptor protein SNX17, which then recycles these cargos to the plasma membrane by associating with the retrieval complex.

As early endosomes slowly mature into the bulbous late endosomes, also known as the MVBs (Multivesicular bodies), they progressively lose their extensive tubular membrane extensions and migrate along the microtubule tracks towards the perinuclear area (Piper & Katzmann, 2010). The cargos destined for lysosomal degradation are sorted in the MVB membrane subdomains which then bud inward to form ILVs. This gradual maturation process is also accompanied by changes in membrane lipid and protein composition as phosphoinositide conversion as well as recruitment of MVB-specific Rab proteins and their effector proteins (Piper & Katzmann, 2010; Cullen & Steinberg, 2018; Gruenberg, 2001). A V-type ATPase localized in the membrane pumps protons from the cytosol inside the lumen and thus acidifies the MVB (Marshansky & Futai, 2008). In this way, the MVB achieves a distinct molecular and functional identity as an organelle.

The cargo-sorting and inclusion into ILVs for degradation, which initiates at the central bulbous part of the early endosomes, is orchestrated by a series of ESCRT-complex proteins in a highly systematic manner. The ESCRT-0 subunits, hepatocyte growth factor-regulated tyrosine kinase substrate (HRS) and signal-transducing adaptor molecule 1 (STAM); ESCRT-I subunits, tumor susceptibility gene 101 (Tsg101) and ubiquitin-associated protein (UBA-1); ESCRT-II component VPS36, recognize incoming ubiquitin-containing cargos and clusters them in a degradative subdomain on the endosome. Then through ESCRT-II, ESCRT-III components, including SNF7, are recruited to perform budding and fission of these cargo-clustered subdomains to generate ILVs (Cullen & Steinberg, 2018).

Although ubiquitylation and ESCRT-dependent fission are described as the major mechanims, some cargos are included in ILVs even upon depletion of ESCRT-components. This led to the identification of ESCRT-independent mechanisms for ILV

biogenesis (Stuffers *et al*, 2009; Babst, 2011). For example, protease-activated receptor 1 (PAR1) and P2Y1 purinogenic receptor are included into ILVs in an ESCRT-accessory protein ALG-2-interacting protein X (Alix)-dependent manner (Dores *et al*, 2012, 2016; Edgar *et al*, 2014). For the majority of MVBs, their fate is to fuse with the lysosome, giving rise to an endolysosome compartment that facilitates a controlled acidic environment for the efficient degradation of cargo-loaded ILVs (Huotari & Helenius, 2011).

1.3.1 ILV biogenesis and MVB trafficking for small extracellular vesicle secretion

Interestingly, a subpopulation of MVBs avoid the degradative fate and, through an insufficiently understood mechanism, are instead trafficked towards cell-periphery where they fuse with the plasma membrane to release ILVs as sEVs into the extracellular space. The exact molecular mechanisms that underlie selective cargo sorting into a subset of ILVs destined for secretion are not entirely understood (van Niel *et al*, 2018). Conceivably, depletion of various ESCRT-components results in either decreased sEV secretion or affects sEV cargo composition, thus implicating the role of some ESCRT-components in ILV biogenesis for sEV secretion as well (Colombo *et al*, 2013) (Fig. 2). Additionally, the syndecan-syntenin-Alix axis engages with the ESCRT machinery to generate ILVs for sEV secretion (Baietti *et al*, 2012)

However, the formation of ILVs loaded with Cluster of differentiation 63 (CD63) even upon depletion of ESCRT-complex components indicates the possibility of an ESCRT-independent ILV biogenesis route for sEV secretion (Stuffers *et al*, 2009). Interestingly, CD63 and other members of the tetraspanins as CD81, CD82, and CD9 are involved in sorting various cargos into sEV possibly by clustering them together to capture sEV cargos in distinct MVB membrane subdomains (Theos *et al*, 2006; van Niel *et al*, 2011, 2015; Buschow *et al*, 2009; Chairoungdua *et al*, 2010) (Fig. 2). Another ESCRT-independent ILV generation requires ceramide generated by neutral sphingomyelinase-2 (nSMase2 encoded by *SMPD3*) at the endosomal membrane (Fig. 2). In a mouse oligodendroglial cell line, it has been shown that ceramide produced by nSMase2 is required for sorting proteolipid protein (PLP) into ILVs destined for secretion (Trajkovic et al. 2008). Complementary *in-vitro* results have shown the formation of intravesicular

membranes upon ceramide generation in giant unilamellar vesicles (GUVs). Accordingly, it was argued that ceramide generated at the limiting membrane of MVBs drives spontaneous negative membrane curvature and budding, leading to the formation of ILVs (Trajkovic, 2008). Additionally, a recent study has shown that the ceramide metabolite sphingosine-1-phosphate activates its receptor on MVBs to segregate the sEV cargo CD63 into ILVs for secretion (Kajimoto *et al*, 2013). Whether ILV formation through nSMase2 activity is independent of ESCRT proteins or whether they cooperate at the same MVBs for ILV formation and cargo loading is so far not well understood.

Although the presence of a specific sorting motif in the cargo for sEV secretion has not been elucidated yet, the first hint came from studying the loading of the galectin-3 into ILVs for its subsequent secretion on sEVs (Bänfer *et al*, 2018). A highly conserved tetrapeptide motif in the amino-terminus of the galactin-3 was shown to be essential for its interaction with ESCRT-I component Tsg101, which mediates its ILV loading for subsequent secretion on sEVs (Bänfer *et al*, 2018).

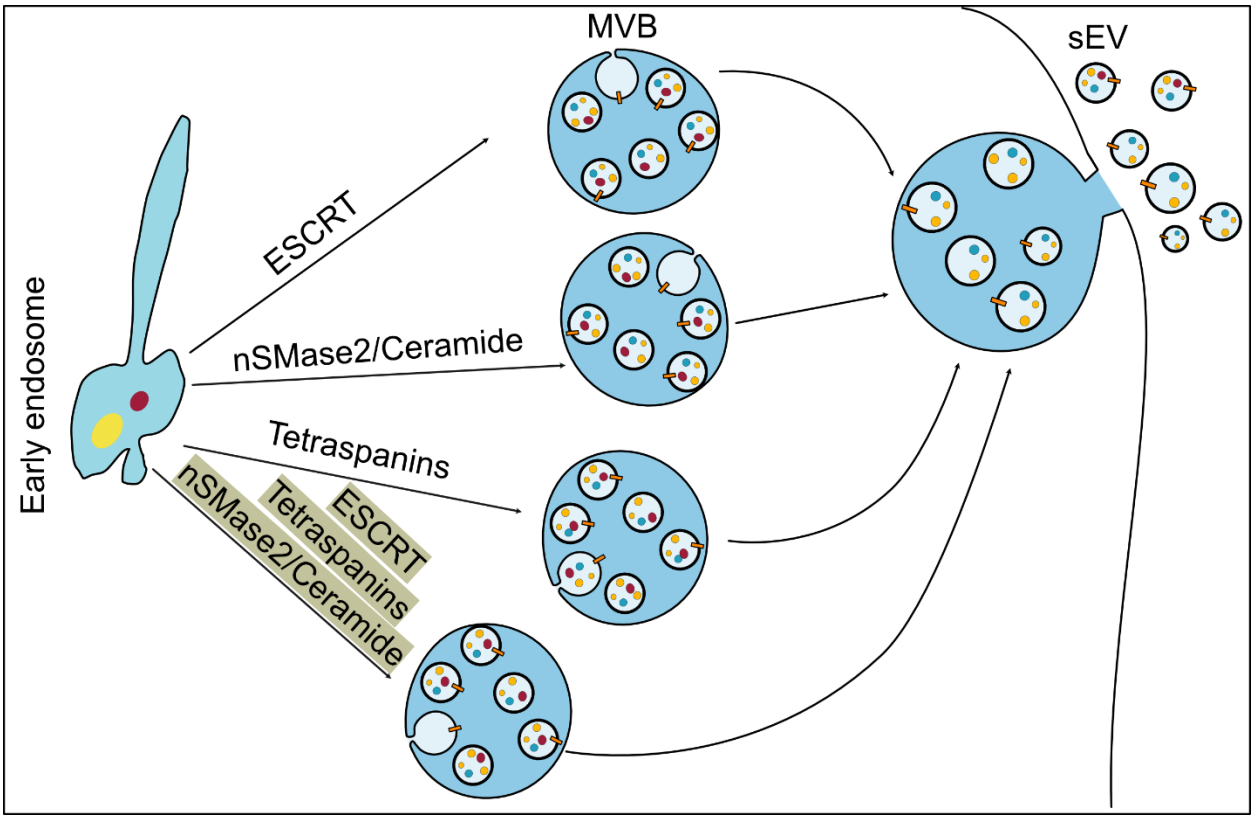

Figure 2: **Molecular mechanisms that underlie intraluminal vesicle biogenesis at the MVB for sEV secretion**. So far, three mechanisms for sEV cargo sorting and subsequent ILV

generation have been shown. ESCRT-dependent, nSMase2 dependent (ESCRT-independent), and Tetraspanin-dependent pathways. It is also proposed that the three pathways can contribute to the same MVB for ILV biogenesis.

Similarly, the regulatory factors that control the fate of MVB trafficking after ILV generation and their subsequent fusion with the plasma membrane remain largely unknown. It was shown that MVBs harboring a high concentration of cholesterol in the ILV membrane are preferentially trafficked for sEV secretion (Möbius *et al*, 2003). Interestingly, numerous studies established a connection between endosomal acidification and sEV secretion – decreasing endosomal acidification increases sEV secretion (Villarroya-Beltri et al, 2016; Edgar et al, 2016; Guo et al, 2017; Latifkar et al, 2019). V-ATPase is a multi-subunit proton pump responsible for endosomal acidification (Forgac, 2007). Cancer cells downregulate Sirtuin-1 (SIRT-1) that destabilizes the mRNA of ATP6V1A, a subunit of the complex (Latifkar et al, 2019). This impairs V-ATPase activity to acidify the MVB lumen and instead favors the sorting of these MVBs for sEV release. Similarly, another study has shown that autophagy-related gene 5 (ATG5), a protein involved in the autophagy pathway, dissociates the ATP6V1E1 subunit from the V-ATPase complex to reduce its activity and thus promote sEV secretion (Guo et al, 2017). Overall, these studies indicate that acidification plays a significant role in determining MVB sorting fate - with less acidic MVBs more likely to be targeted for secretion. Despite these recent findings, the molecular mechanisms involved in fine-tuning MVB lumen acidification to regulate their sorting decision are not well understood.

1.4 V-ATPase

Vacuolar-type adenosine triphosphatases (V-ATPases) are large membrane-embedded multisubunit protein complexes that function as ATP hydrolysis-driven proton pumps. They primarily mediate organelle acidification in all eukaryotic cells (Vasanthakumar & Rubinstein, 2020; Forgac, 2007). The establishment of the characteristic luminal pH of an intracellular compartment allows organelle-specific biochemical reactions; targeting and post-translational modifications of proteins in the Golgi apparatus (Kellokumpu, 2019), degradation of biological materials in lysosomes (Mindell, 2012), and uptake and release

of neurotransmitters in synaptic vesicles (Hnasko & Edwards, 2012). Plasma membrane V-ATPases in some specialized cells acidify the extracellular space critical for bone resorption, sperm maturation, and acid excretion by the kidney (Forgac, 2007). Plasma membrane V-ATPases in cancer cells acidify extracellular space to degrade extracellular matrix components to facilitate cell proliferation and metastasis (Stransky *et al*, 2016; Cotter *et al*, 2015). The V-ATPase activity also associates with and regulates signaling complexes in Notch, Wnt, and mTOR pathways (Sun-Wada & Wada, 2015; Pamarthy *et al*, 2018). The complete disruption of V-ATPase activity is embryonic lethal, thus, highlighting the importance of this protein complex (Sun-Wada *et al*, 2000). Aberrant expression or activity of the enzyme is associated with cancer (Stransky *et al*, 2016) and several neurological disorders (Colacurcio & Nixon, 2016). Mutations in specific subunit isoforms are associated with autosomal recessive osteoporosis (Ochotny *et al*, 2006), cutis laxa (Esmail *et al*, 2018), and distal renal tubular acidosis (Karet *et al*, 1999).

V-ATPases are rotary ATPase enzymes that are structurally and evolutionarily related to the F-type ATP synthases found in bacteria, mitochondria, and chloroplasts (Toei *et al*, 2010; Forgac, 2007). The multisubunit V-ATPase complex is organized into two domains – the soluble cytoplasm-facing V1 domain which is responsible for ATP hydrolysis and the membrane-embedded V0 domain which is responsible for proton translocation from the cytoplasm into the lumen or extracellular space in the case of plasma membrane V-ATPase. (Vasanthakumar & Rubinstein, 2020). The mammalian V1 domain comprises eight subunits ATP6V1A, ATP6V1B, ATP6V1C, ATP6V1D, ATP6V1E, ATP6V1F, ATP6V1G, and ATP6H, whereas the V0 domain consists of five different subunits ATP6V0A, ATP6V0C, ATP6V0C”, ATP6V0D, ATP6V0E, and two accessory subunits ATP6AP1(also known as Ac45) and ATP6AP2 also known as (pro)renin receptor (Abbas *et al*, 2020).

Many subunits of the V-ATPase have multiple isoforms in different tissues and organelles. The latest structural analysis of human V-ATPase has shown that the V1 complex is composed of three copies of subunits ATP6V1A, ATP6V1B2, ATP6V1E1, and ATP6V1G1 and one copy of subunits ATP6V1C1, ATP6V1D, ATP6V1F, and ATP6V1H. The V0 complex comprises subunits ATP6V0A1, ATP6V0D1, ATP6V0E1, ATP6V0C”, RNase K, ATP6AP1, ATP6AP2, and 9 copies of ATP6V0C (Wang *et al*, 2020).

V1 complex is organized in the following structures - three pairs of each subunit ATP6V1A and ATP6V1B form the hexamer top head which tilt and twist upon ATP hydrolysis. Subunits ATP6V1D and ATP6V1F form the central stalk and three pairs of the subunits ATP6V1G and ATP6V1E form the three peripheral stalks. Subunits ATP6V1H and ATP6V1C along with the N-terminal domain of the subunit ATP6V0A of the V0 region make a bottom collar at the membrane interface. The V0 complex comprises the c-ring made up of one copy of ATP6V0C" and 9 copies of ATP6V0C; the adjacent C-terminal domain of subunit ATP6V0A, subunit ATP6V0E, and RNaseK; the ATP6AP1 and ATP6AP2 subunits inside the c-ring; and subunit ATP6V0D at the cytosolic side of the c-ring (Wang *et al*, 2020).

Mechanistically, V-ATPase works as a proton pump by coupling the energy derived from ATP-hydrolysis by the V1 domain to the proton translocation by the V0 domain. Sequential ATP hydrolysis by the three pairs of catalytic ATP6V1A/B subunits produces conformational changes in the hexamer top head that induce rotation of the central stalk and the c-ring. The c-ring has conserved lipid-exposed glutamic acid residues which undergo protonation and deprotonation for coupled proton transfer into the lumen (Wang *et al*, 2020).

Bafilomycin A1 is widely used in studies to inhibit V-ATPase activity (Bowman & Bowman, 2005). The structural analysis of Bafilomycin A1 bound bovine V-ATPase has revealed that six Bafilomycin A1 molecules bind to the c-ring. One Bafilomycin A1 molecule engages with two ATP6V0C subunits and disrupts the interactions between the c-ring and subunit ATP6V0A and thereby prevents proton translocation. Further structural and sequence analyses have shown that the bafilomycin A1-binding residues are conserved in yeast and mammalian species and that the 7'-hydroxyl group of bafilomycin A1 acts as a unique feature recognized by subunit ATP6V0C (Wang *et al*, 2021).

1.4.1 Cellular and physiology functions of the V-ATPase

V-ATPases pump protons into the Golgi apparatus, which becomes progressively acidic from *cis* Golgi to *trans*-Golgi. Newly synthesized proteins undergo post-translational modifications – glycosylation, sulfation, and phosphorylation in a pH-dependent manner

- as they traverse the Golgi apparatus (Kellokumpu, 2019). These post-translational modifications are vital for their correct subcellular targeting. For example, increasing the pH of the Golgi apparatus mislocalizes and thereby impairs the function of the resident glycosyltransferases (Rivinoja *et al*, 2009). Likewise, mutations in Golgi-resident human V-ATPase subunits result in autosomal recessive Cutis laxa type-II, a disorder characterized by impaired protein glycosylation and membrane trafficking (Kornak *et al*, 2008; Esmail *et al*, 2018). The establishment of proper pH along the secretory pathway is also important for the processing of peptide prohormones and the subsequent secretion of mature hormones. For example, the acidic environment of secretory vesicles in pancreatic β-cells allows the cleavage of proinsulin into its mature form which is then secreted in a V-ATPase activity-dependent manner (Sun-wada *et al*, 2006). In neurons, the loading of neurotransmitters into synaptic vesicles is energized by the pH gradient and the membrane potential generated by V-ATPase (Hnasko & Edwards, 2012). Furthermore, V-ATPases modulate exocytosis of the synaptic vesicles at the pre-synaptic membrane (Bodzęta *et al*, 2017).

At the physiological level, V-ATPases play important roles in kidney acid excretion, sperm maturation, and bone resorption (Forgac, 2007). In the kidney, type A intercalated cells express plasma membrane V-ATPases that pump protons into the urine to maintain systemic pH homeostasis (Breton & Brown, 2013; Forgac, 2007). Mutations in the ATP6V0A4 and ATP6V1B1 subunit isoforms result in distal renal tubular acidosis (Kornak *et al*, 2008; Esmail *et al*, 2018). Osteoclasts target V-ATPases to the ruffled plasma membrane where they acidify the extracellular space for bone demineralization during bone resorption. Mutations in the ATP6V0A3 subunit isoform are associated with autosomal recessive osteoporosis, which is characterized by dense bones due to impaired bone resorption by osteoclasts (Frattini *et al*, 2000). In the epididymis, V-ATPase expressing clear cells acidify the lumen, a process that is crucial for the proper maturation and motility of spermatozoa, making them a potential contraceptive target (Pietrement *et al*, 2006). ATP6V0E1 subunit isoform that is exclusively expressed in the sperm could be another more specific potential contraceptive target (Sun-Wada *et al*, 2002). Most importantly, some cancer cells express V-ATPase on their plasma membranes to acidify

the extracellular space that allows the degradation of the extracellular matrix thereby mediating tumor cell metastasis and invasion (Stransky *et al*, 2016).

1.4.2 V-ATPase activity regulation

V-ATPase activity regulation is therefore important in maintaining pH homeostasis – both at the organelle and cellular level – in response to changing cellular environmental conditions. For instance, during acute systemic acidosis, type A intercalated cells increase V-ATPase trafficking to the apical cell surface to pump out more protons into the urine (Breton & Brown, 2013). In addition to their regulated intracellular trafficking, V-ATPase activity can also be modulated by regulating the reversible assembly/disassembly of the complex, differential localization of the multiple subunit isoforms, and the coupling efficiency of ATP hydrolysis to the proton translocation (Toei *et al*, 2010; Oot *et al*, 2017). The trigger and the signaling pathways involved in V-ATPase assembly are not entirely understood now. For instance, glucose starvation in HEK293T cells increases V-ATPase assembly in an adenosine monophosphate (AMP) kinase and PI3K pathway-dependent manner (McGuire & Forgac, 2018). Likewise, amino acid starvation in HEK293T cells also induces V-ATPase activity to increase the lysosomal output of free amino acids (Stransky & Forgac, 2015). In contrast to these studies, glucose starvation in the human immortalized kidney tubule distal cells rather induces V1 and V0 disassembly in a PI3K pathway-dependent manner (Sautin *et al*, 2005). Therefore, V-ATPase activity regulation is complex and can depend on the cellular compartment or the cell or tissue type.

V-ATPase activity can also be regulated by modulating the coupling efficiency of proton transport with ATP hydrolysis (Kawasaki-Nishi *et al*, 2001). V-ATPase subunit ATP6V0A isoforms have different coupling efficiencies: isoform ATP6V0A2 which localizes to the Golgi apparatus has a much lower coupling efficiency than the V-ATPase in the vacuole. This difference could explain why the pH of the Golgi is more alkaline than that of the vacuole (Kawasaki-Nishi *et al*, 2001). Therefore, V-ATPase activity can also be regulated by targeting different subunit isoforms to specific organelles or cell types.

1.4.3 Endosomal V-ATPase and its regulation

Endocytosis, sorting, trafficking of endosomal cargos to their target subcellular location, and degradation occur in a pH-dependent manner (Bayer *et al*, 1998). Low pH-induced ligand release and receptor recycling are important steps for endocytosis. For instance, the β-propeller containing endocytosis receptor Sortillin which internalizes a wide range of ligands, dimerizes in the acidic environment of endosomes and thereby releases the ligands (Leloup *et al*, 2017). The pH of the endosomal compartments gets progressively more acidic from the early endosomes to the lysosomes. Receptors are decoupled from their ligands in the mildly acidic lumen of early endosomes and then recycled back to the plasma membrane (Cullen & Steinberg, 2018). In contrast, for signal downregulation, receptor-ligand complexes are degraded by acidic hydrolases which are active in the more acidic lysosomes (Cullen & Steinberg, 2018). Likewise, important proteins involved in endosomal trafficking including cytosolic small GTPases are recruited to the endosomal membrane in an acidification-dependent manner. The Ras-superfamily of small GTPases which exist in the active GTP-bound or inactive GDP-bound state function as 'molecular switches' regulating a wide array of cellular processes (Bourne *et al*, 1991). The ADP-ribosylation factor (Arf) family belongs to the Ras-superfamily and functions as a molecular switch to regulate endosomal trafficking (Klausner & Donaldson, 1994; Donaldson & Jackson, 2011). Guanine-nucleotide exchange factors (GEFs) mediate ARF activation (GTP-bound) while GTPase-activating proteins (GAPS) mediate ARF inactivation (GDP bound). Small GTPases Arf6 and Arf1, which regulate endosomal trafficking by recruiting coat components, modifying phospholipids, and remodeling the cytoskeleton near vesicular membranes are recruited to the endosomal membrane in an acidification-dependent manner. (Gu & Gruenberg, 2000; Maranda *et al*, 2001). Specifically, the transmembrane ATP6V0A2 subunit and ATP6V0AC subunit of the endosomal V-ATPase directly interact with ARF6 and its cognate GEF ARNO (ADP-ribosylation factor nucleotide site opener) in the early endosomes. This endosomal acidification-dependent ARNO/ARF6/V-ATPase interaction regulates protein degradation in the endocytic pathway (Hurtado-Lorenzo *et al*, 2006). Therefore, V-ATPase activity is

regulated along the endocytic pathway to establish the required pH environment specific for the function of each compartment.

MVBs or late endosomes, which are slightly more acidic than early endosomes either fuse with lysosomes for content degradation or are trafficked to the cell surface for sEV release (van Niel *et al*, 2018). Several lines of evidence suggest that V-ATPase-mediated endosomal acidification regulates the fate of the MVB trafficking - with less acidic MVBs more likely to be targeted for secretion (Guo *et al*, 2017; Latifkar *et al*, 2019). Therefore, V-ATPase activity is fine-tuned along the endocytic pathway to establish the required pH environment specific for the function of each compartment.

V-ATPase activity can be regulated by differential subcellular targeting of the subunit isoforms. The ATP6V0A1, a predominantly neuronal isoform localizing to the synaptic vesicles, is targeted to endolysosomal compartments in non-neuronal tissues. The ATP6V0A2 is targeted to the Golgi apparatus and the isoform ATP6V0A3 localizes to endolysosomal compartments (Toei *et al*, 2010).

Lipids play an important role in V-ATPase activity regulation in both yeast and mammalian cells – especially in the endocytic compartments. For example, PI(3,5)P2, the predominant phosphatidylinositol lipid species in the yeast vacuole binds to the N-terminal domain of Vph1p for recruitment and increases V-ATPase assembly and activity (Li *et al*, 2014; Banerjee *et al*, 2019). Likewise, ergosterol, the major sterol species in fungi, is required for vacuolar acidification and V-ATPase activity in yeast (Zhang *et al*, 2010). In mammalian cells, the increased acidity of late endosomes is not due to a higher density of proton pumps on the membrane but rather an increased assembly of V-ATPase V1 and V0 regions of the V-ATPase when compared with the early endocytic compartments (Banerjee & Kane, 2020). Most importantly, this increased V-ATPase assembly on that the late endosomes is regulated by the local lipid environment (Lafourcade *et al*, 2008). In agreement with previous studies on the crucial role of lipids in V-ATPase activity regulation, a recent mass spectrometry analysis of the isolated human V0 complex has revealed that ordered lipid molecules including cholesterol are an integral part of the V0 complex (Wang *et al*, 2020).

1.5 Sphingomyelinases

Catabolism of sphingomyelin, a lipid found abundantly but not exclusively in the plasma membrane, yields several lipid metabolites with signaling capacity as second messengers: Ceramide, sphingosine, and sphingosine-1 phosphate (Airola & Hannun, 2013). Sphingomyelinase or sphingomyelindiesterase (SMPD), a member of the DNase-I superfamily of enzymes, hydrolyzes the phosphodiester bond of the sphingomyelin to generate two products: ceramide and phosphorylcholine (Airola & Hannun, 2013). Ceramide acts as a lipid signaling molecule in multiple cellular signaling pathways including cell growth, differentiation, and apoptosis (Arana *et al*, 2010).

So far, six sphingomyelinases have been identified in mammalian cells and are categorized based on their pH optima of activity into acid, neutral, and alkaline sphingomyelinases. In mammals, four neutral sphingomyelinase members have been identified, nSMase1 (encoded by *SMPD2*) (Tomiuk *et al*, 1998; Sawai *et al*, 1999), nSMase2 (encoded by *SMPD3*) (Hofmann *et al*, 2000), nSMase3 (*SMPD4*) (Krut *et al*, 2006), and mitochondrial associated nSMase (MA-nSMase; *SMPD5*) (Wu *et al*, 2010). There is one acid sphingomyelinase (*SMPD1*) (Schuchman *et al*, 1992) and one alkaline sphingomyelinase (*ENPP7*) (Duan *et al*, 2003). Of note, two SMPD-like proteins SMPDL3A and SMPDL3B with phosphodiesterase activity have also been described (Traini *et al*, 2014; Fornoni *et al*, 2011).

1.5.1 *SMPD3*/nSMase2

NSMase2 is a 655 amino acids long protein with a molecular weight of 71 kDa. It is a membrane-associating enzyme with an N-terminal domain and a C-terminal catalytic domain (Marchesini *et al*, 2003). The N-terminal domain has a short juxtamembrane region and two hydrophobic segments through which nSMase2 associates with the membrane. The C-terminal catalytic domain contains a large insertion region where different regulatory elements like five phosphoserine sites and a calcineurin-binding site are found (Airola *et al*, 2017) (Fig. 3). The catalytic domain adopts a DNase-1-type fold with a β-sandwich core and connecting loops and secondary structure elements forming

the active site pocket. The β-sandwich core of nSMase2 contains all the essential residues involved in Mg^{2+} ion binding and catalysis. NSMase2 requires stimulation by phosphatidylserine for full activation and the N-terminal domain has two phosphatidylserine-binding sites (Airola *et al*, 2017). NSmase2 activation is regulated by an interdomain allosteric mechanism; upon binding to phosphatidylserine the N-terminal domain interacts with the soluble catalytic domain and activates it. Therefore, the N-terminal domain serves as both a membrane anchor and an allosteric activator (Airola *et al*, 2017). GW4869 is a non-competitive (for the substrate sphingomyelin) nSMase2 inhibitor that competes with phosphatidylserine binding to the N-terminal domain of the nSMase2 and thereby inhibits its activation (Luberto *et al*, 2002; Airola *et al*, 2017).

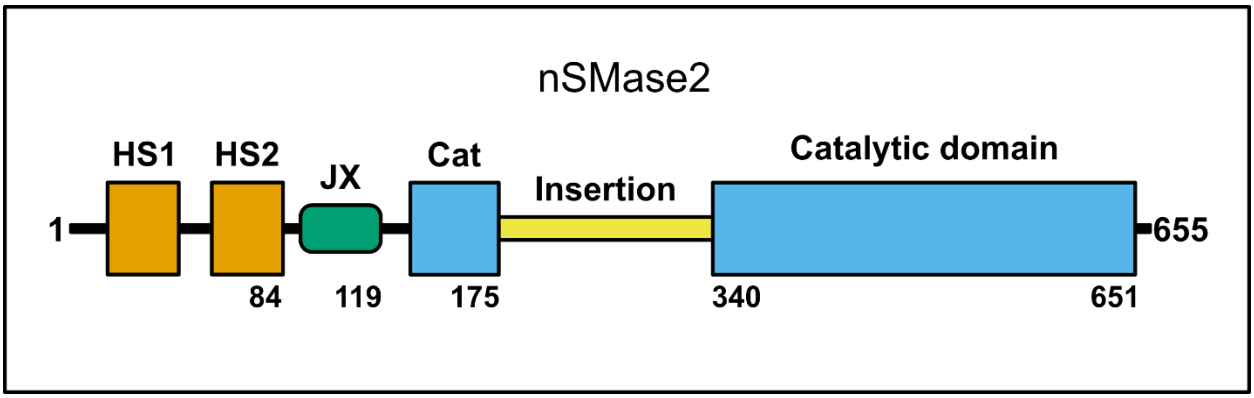

Figure 3: **The domain architecture of nSMase2**: The domain architecture of nSMase2 consists of two N-terminal hydrophobic segments (HS1 and HS2), a JX region, and a catalytic domain (CAT) that contains a large insertion region. The insertion region contains many regulatory elements including a calcineurin-binding site and five phosphoserine sites.

NSMase2 is described as the major sphingomyelin hydrolyzing enzyme with its overexpression resulting in a significant decrease in sphingomyelin levels with a concomitant increase in ceramide levels in MCF-7 cells (Marchesini *et al*, 2003) and primary hepatocytes (Karakashian *et al*, 2004). NSMase2 is predominantly expressed in the brain (Hofmann *et al*, 2000). At the cellular level, although nSMase2 was described to be localized mainly at the plasma membrane (Airola & Hannun, 2013), later studies have shown that it localizes to different subcellular compartments including the Golgi (Stoffel *et al*, 2016; Back *et al*, 2018), the endoplasmic reticulum, nucleus, and endosomes (Shamseddine *et al*, 2015b; Airola & Hannun, 2013; Shamseddine *et al*,

2015a). Different stimuli, including TNFα (Clarke *et al*, 2007), H_2O_2 (Garoby-Salom *et al*, 2015), and high cell confluence (Tani & Hannun, 2007) further increase its plasma membrane localization. The different subcellular localizations of nSMase2 reflects its ability to function in various cellular processes.

NSMase2 is involved in different cellular stress response pathways. It is described as the major stress-induced ceramide-producing enzyme. For example, nSMase2 was implicated in the anti-cancer drug daunorubicin-induced cell death by generating ceramide (Ito *et al*, 2009). Additionally, nSMase2 was shown to play a role in stress-induced bronchial and lung injury in pulmonary diseases by inducing apoptosis (Levy *et al*, 2006). In line with this study, nSMase2 is also involved in inducing apoptosis by generating ceramide in bronchial epithelial cells exposed to cigarette smoke (Levy *et al*, 2009). Additionally, nSMase2 was shown to mediate hypoxia-induced pulmonary vasoconstriction *in-vivo* (Cogolludo *et al*, 2009). In rat neuroblastoma PC12-cells, nutrient starvation upregulates nSMase2 to generate ceramide at the Golgi that is required for autophagy induction by activating p38 mitogen-activated protein kinase (MAPK) and mTOR inhibition (Back *et al*, 2018).

In addition to its role in stress responses, nSMase2 also regulates the cell cycle by mediating growth arrest under different conditions in MCF-7 cells. NSMase2 mediates confluence-induced growth arrest by modulating the phosphorylation status of retinoblastoma (Rb) protein and induction of P21 (Marchesini *et al*, 2004). Through modulating ribosomal S6 kinase (RS6K), nSMase2 also mediates retinoic acid-induced growth arrest (Christopher J Clarke., 2010).

So far the best-described pathway for nSMase2 activation is through tumor necrosis factor α (TNFα) stimulation. Among its pleiotropic actions, TNFα activates nSmase2 by translocating the polycomb group protein embryonic ectoderm (EED) from the nucleus. This translocation of EED allows the recruitment of nSMase2 to the TFNR1-FAN-RACK1-complex for its activation at the plasma membrane (Philipp et al, 2010).

Of note, nSMase2 plays a key role in ILV biogenesis for sEV secretion by hydrolyzing sphingomyelin in the MVB membrane to generate ceramide. Ceramide generates negative membrane curvature required for ILV budding into the MVB lumen (Trajkovic, 2008). A recent study has shown that ceramide produced by nSMase2 activity is further

metabolized into sphingosine-1 phosphate (S1P) which activates its cognate S1P receptor (S1PR) on the MVB membrane that drives CD63-cargo loading into ILVs for sEV secretion (Kajimoto *et al*, 2013). In agreement with these studies, nSMase2 activity is required for packing prion proteins into ILVs for their eventual release on sEV and thereby implicates a potential role for nSMase2 in neurodegenerative disorder progression (Guo *et al*, 2015).

Interestingly, the *SMPD3* gene was found to be mutated in 5% of 92 acute myeloid leukemias (AMLs) and 6% of 131 acute lymphoid leukemias (ALLs). Functional analysis of a subset of these mutations indicated defects in nSMase2 protein stability and localization (Kim *et al*, 2009). Likewise, a recent study has implicated the role of nSMase2 in T cell recruitment and directional migration (Mueller *et al*, 2014). Moreover, a genome-wide study has shown that *SMPD3* is a potential repressor of hepatocellular carcinoma (Revill *et al*, 2013). A subsequent study indeed confirmed that *SMPD3* deficient mice show increased liver tumor formation (Zhong *et al*, 2018). Non-small-cell lung cancer harbors different anaplastic lymphoma kinase (ALK)-fusion variants. The ALK gene can fuse with different genes and an *ALK-SMPD3* fusion gene is described in a case of lung adenocarcinoma (Liang *et al*, 2021). Although based on the current studies, it is not clear whether it is a pro-tumor and anti-tumor gene, these data indicate a potential role for *SMPD3* in cancer progression.

Given the role of nSMase2 in a wide array of cellular processes, *SMPD3*$^{-/-}$ mutant mice develop a pleiotropic phenotype with severe retardation of late embryonic and postnatal growth; a novel form of dwarfism and delayed puberty as a part of a hypothalamus-induced combined pituitary hormone deficiency (Stoffel *et al*, 2005). Unlike SMPD1$^{-/-}$ mutant mice, which mimic Niemann-Pick disease type A with a massive sphingomyelin accumulation in the lysosome, *SMPD3*$^{-/-}$ mutant mice develop no lipid storage abnormalities (Stoffel *et al*, 2005). Although the detailed molecular pathway and mechanisms that underpin the pleiotropic phenotypes of *SMPD3*$^{-/-}$ mutant mice are not known, the study proposes a role of *SMPD3*, which is segregated into a detergent-resistant subdomain of the Golgi membrane, in modifying the lipid bilayer that is essential for the Golgi-secretory pathway in hypothalamic neurosecretory neurons (Stoffel *et al*, 2005)(Wilhem Stoffel., 2005). A follow-up study later confirmed the molecular link

between *SMPD3* and the Golgi complex in neurons. *SMPD3* deficiency in neurons disrupts a Golgi membrane-remodeling step required for budding, vesiculation, and protein transport of amyloid-β precursor protein (APP), amyloid-β (AB), and pTau and thereby cause neurodegeneration and Alzheimer's disease-like cognitive decline in *SMPD3*$^{-/-}$ mutant mice (Stoffel *et al*, 2016, 2019).

1.5.2 *SMPD2*/nSMase1

NSMase1 (encoded by *SMPD2*) is a ubiquitously expressed integral membrane protein identified and cloned based on the sequence homology to the bacterial sphingomyelinases (Tomiuk *et al*, 1998). Similar to nSMase2, nSMase1 also exhibits a Mg^{2+}-dependent activity (Fensome *et al*, 2000). NSMase1 shares identical domain architecture to ISC1, the yeast homolog to neutral sphingomyelinases (Tomiuk *et al*, 1998)(Tomiuk 1998). The secondary structure prediction of mammalian nSMase1 suggests a catalytic domain adopting the DNase-1-like structure and two possible transmembrane domains (Rodrigues-Lima *et al*, 2000). Unlike nSMase2, nSMase1 activity does not respond to TNFα stimulation (Tomiuk *et al*, 1998). Despite being the first neutral sphingomyelinase in mammals to get cloned and identified, the structural, biochemical, and biological studies on nSMase1 remain very low in comparison with nSMase2.

Overexpressed nSMase1 conjugated to a tag localizes in the ER (Fensome *et al*, 2000; Rodrigues-Lima *et al*, 2000; Tomiuk *et al*, 2000). Furthermore, one of the predicted C-terminal transmembrane domains is required for its ER-localization (Rodrigues-Lima *et al*, 2000). In contrast to the overexpressed nSMase1, endogenous nSMase1 exclusively localizes to the nuclear matrix (Mizutani *et al*, 2001). A conventional nuclear localization signal (NLS) is missing, but nSMase1 contains a sequence LLVLHLSGLVL at the amino acid position between 120-130, which is homologous to the nuclear export signal (NES) (Mizutani *et al*, 2001).

Although nSMase1 hydrolyzes sphingomyelin *in-vitro*, sphingomyelin metabolism remains unaffected upon its overexpression in cells (Tomiuk *et al*, 1998; Sawai *et al*, 1999). Likewise, nSMase1 mouse knockout shows no obvious phenotype with no

detectable changes in sphingomyelin metabolism (Zumbansen & Stoffel, 2002). Instead of sphingomyelin, nSMase1 hydrolyzes lyso platelet-activating factor (lyso-PAF) *in-vitro* and in cells. This indicates the putative nSMase1 could be a lyso-PAF phospholipase C with lyso-PAF as its biological substrate (Sawai *et al*, 1999). A later study further has shown that, in addition to lyso-PAF, nSMase1 also hydrolyzes the other two lysocholinephosphopholipids: sphingosylphosphocholine (SPC) and lysophosphatidylcholine (lyso-PtdCho) (Miura *et al*, 2004). SPC is a naturally occurring lipid mediator which elicits different responses when exogenously added to the cell including mitogenesis, focal contact assembly, Ca^{2+} mobilization, and apoptosis depending on the concentration and type of the cell (Miura *et al*, 2004).

In contrast to the above biochemical studies, several studies later have shown that ceramide generated by nSMase1 activity induces cellular death via different pathways under different stress conditions (Jaffrézou *et al*, 1996; Jana & Pahan, 2004; Lee *et al*, 2004). For example, JNK-signaling activates nSMase1 by phosphorylation to generate ceramide for apoptosis induction upon different environmental stresses such as heat shock and UV irradiation (Yabu *et al*, 2015). Additionally, a study has shown that trivalent chromium induces autophagy in renal HK2 cells by activating nSMase1 to increase cellular ceramide levels (Yang *et al*, 2017). The molecular and structural characterization, as well as the biological functions of nSMase1, remain insufficiently known.

1.6 The aim of the study

Aim 1: Dissecting the molecular mechanism that underlies the regulatory role of nSMase2 in sEV secretion

sEV secretion represents an important paradigm for intercellular communications under both homeostatic and pathological conditions. The detailed step-wise molecular mechanisms that underlie sEV biogenesis starting from cargo sorting into the ILVs at the MVB membrane to plasma membrane targeting of these mature MVBs for sEV secretion are gradually being dissected. An important step in sEV secretion lies at the crossroad of lysosomal degradation and anterograde MVB trafficking of the MVB – where the ultimate

fate for the MVB is decided. The regulatory factors that discriminate secretory MVBs from degradative MVBs, as well as the molecular motors that facilitate the anterograde trafficking of secretory MVBs, are not yet elucidated.

NSMase2 is one the best-described regulators of sEV biogenesis at the MVB (Menck *et al*, 2017; Trajkovic *et al*, 2008; Kajimoto *et al*, 2013). Therefore, nSMase2 inhibition is widely used in both biogenesis and functional studies of sEVs. Ceramide generated by nSMase2 upon sphingomyelin hydrolysis at the MVB membrane was shown to induce negative membrane curvature required for ILV biogenesis (Trajkovic, 2008). Alternatively, a later study has unraveled that ceramide generated by nSMase2 is further metabolized into sphingosine-1 phosphate (S1P) which activates its cognate receptor S1PR on the MVB. The ongoing activated S1PR subsequently drives ILV budding into the MVB for sEV secretion (Kajimoto *et al*, 2013).

With increasingly complex molecular regulations described for ILV generation at the MVB for sEV secretion including through both ESCRT-dependent and ESCRT-independent pathways (van Niel *et al*, 2018). And with sEV cargo sorting into ILVs remaining unaffected by nSMase2 inhibition (Groß *et al*, 2012), the exact molecular mechanism and the step at which nSMase2 activity regulates sEV biogenesis is not sufficiently understood. Therefore, this study aimed to further dissect the role of nSMase2 in sEV secretion. To this end, firstly, the role of nSMase2 in sEV secretion was confirmed in the HeLa cells. Thereafter, the molecular mechanism of nSMase2 activity at the MVB that underlie sEV secretion was determined by analyzing its potential connection with V-ATPase-mediated endosomal acidification. In connection with the role of lipids in endosomal acidification, the role of cholesterol in the sEV secretion was also studied. Finally, the functional relevance of nSMase2 regulated sEV secretion was explored by studying the effects of the known nSMase2 agonist TNFα.

Aim 2: Investigating the biological functions of nSMase1/*SMPD2*

NSMase1 or *SMPD2*, another member of the neutral sphingomyelinase family, exhibits $Mg2^{+}$-dependent but phosphatidylserine-independent activity. Initially identified as sphingomyelinase based on the sequence similarity between the bacterial

sphingomyelinase and a yeast protein, the subsequent biochemical studies indicated that its biological function is less likely to be sphingomyelinase but rather a lysophospholipase (Tomiuk *et al*, 1998). Therefore, both the structural and functional insights on nSMase1 remain poor.

Given the insufficient and contrasting results on the function of nSMase1, we aimed to ascertain the biological role of nSMase1 by using siRNA-mediated gene knockdown (KD) in two human cell lines: HCT116, a human colorectal cancer cell line, and HeLa, a cervical cancer line. Since previous studies implicated nSMase1 in various stress response pathways, the potential role of nSMase1 in two cellular stress responses – autophagy and ER stress pathway - was analyzed. Finally, the role of nSMase1 in the cell cycle progression was explored by uncovering possible molecular pathways through which it could regulate cell cycle progression.

2 Results

2.1 Manuscript I: Neutral Sphingomyelinase 2 controls exosomes secretion by counteracting V-ATPase-mediated endosome acidification

This manuscript is accepted for publication in the Journal of Cell Science:
https://journals.biologists.com/jcs/article/doi/10.1242/jcs.259324/274058/Neutral-Sphingomyelinase-2-controls-exosomes

Neutral Sphingomyelinase 2 controls exosomes secretion by counteracting V-ATPase-mediated endosome acidification

Dolma Choezom[1], and Julia Christina Groß[1,2,3]

Affiliations:

[1]Developmental Biochemistry, University Medical Center Goettingen, Goettingen, Germany
[2]Hematology and Oncology, University Medical Center Goettingen, Goettingen, Germany
[3]Health and Medical University, Potsdam, Germany

*** Correspondence:**

Julia Christina Groß, Health and Medical University, Potsdam, Germany, julia.gross@health-and-medical-university.de

Abstract

During endosome maturation, neutral sphingomyelinase 2 (nSMase2, encoded by *SMPD3*) is involved in budding of intraluminal vesicles (ILVs) into late endosomes or multivesicular bodies (MVBs). Fusion of these with the plasma membrane results in the secretion of exosomes or small extracellular vesicles (sEVs). Here, we report that nSMase2 activity controls sEV secretion through modulation of vacuolar H^+-ATPase (V-ATPase) activity. Specifically, we show that nSMase2 inhibition induces V-ATPase complex assembly that drives MVB lumen acidification and consequently reduces sEV secretion. Conversely, we further demonstrate that stimulating nSMase2 activity with the inflammatory cytokine TNFα decreases acidification and increases sEV secretion. Thus, we find that nSMase2 activity affects MVB membrane lipid composition to counteract V-ATPase-mediated endosome acidification, thereby shifting MVB fate towards sEV secretion.

Keywords

Small extracellular vesicles, Endosomal maturation, Secretory Multivesicular Bodies, Intraluminal vesicles, endosomal cargo sorting

Introduction

Exosomes are small extracellular vesicles (sEVs) of endosomal origin that are released into the extracellular space and contain bioactive signaling molecules (Ciardiello *et al*, 2016). Initially considered cellular waste, recent studies have proven that sEVs play key roles in cell-cell communication, for example during erythrocyte maturation, antigen presentation, and progression of various diseases including Alzheimer's disease and cancer (Danzer *et al*, 2012; Bebelman *et al*, 2018). Cancer cells highly upregulate exosome secretion, and this significantly contributes to tumor progression by mediating different processes including proliferation, metastasis, and organ tropism (Kanada *et al*, 2016). Therefore, it is crucial to understand the molecular mechanisms that underlie exosome biogenesis and its regulation.

Exosomes are generated as intraluminal vesicles (ILVs) during endosome maturation into late endosomes or multivesicular bodies (MVBs). ILVs are secreted out as exosomes into the extracellular space when MVBs fuse with the plasma membrane. As early endosomes mature into MVBs, cargos are sorted on the endosomal membrane, which then buds inward to form ILVs (van Niel *et al*, 2018). Different molecular machineries and pathways are involved in ILV biogenesis. As one route of biogenesis, the syndecan-syntenin-Alix (also known as PDCD6IP) axis engages with the endosomal sorting complex required for transport (ESCRT) machinery to generate ILVs for exosome secretion (Baietti *et al*, 2012). Interestingly, the ESCRT-machinery also generates ILVs in MVBs that are targeted for lysosomal degradation. For example, the ubiquitylated epidermal growth factor receptors (EGFRs) that are internalized into ILVs in an ESCRT-dependent manner are targeted for lysosomal degradation (Roxrud et al. 2008; Raiborg and Stenmark 2009).

In addition, ILVs can be generated by ESCRT-independent pathways that involve neutral sphingomyelinase 2 (nSMase2, encoded by *SMPD3*). NSMase2 hydrolyzes sphingomyelin into ceramide and phosphorylcholine (Hofmann *et al*, 2000). In a mouse oligodendroglial cell line, it has been shown that ceramide produced by nSMase2 is

required for sorting proteolipid protein (PLP) into ILVs destined for secretion (Trajkovic et al. 2008). Complementary *in-vitro* results have shown the formation of intravesicular membranes upon ceramide generation in giant unilamellar vesicles (GUVs). Accordingly, it has been argued that ceramide generated at the limiting membrane of MVBs drives spontaneous negative membrane curvature and budding leading to the formation of ILVs. Additionally, a recent study has shown that the ceramide metabolite sphingosine-1-phosphate activates its receptor on MVBs to segregate cargos into ILVs for exosome secretion (Kajimoto *et al*, 2013). Whether ILV formation by nSMase2 is independent of ESCRT proteins or whether they cooperate at the same MVBs for ILV formation and cargo loading is so far not well understood.

Similarly, it is unclear, what discriminates and controls the fate of MVBs. MVBs can either be sorted for lysosomal degradation (degradative MVBs) or be transported towards the cell periphery for plasma membrane fusion (secretory MVBs) to release exosomes (van Niel *et al*, 2018). Regulatory factors that control the fate of MVB trafficking after ILV generation and their subsequent fusion with the plasma membrane remain largely unknown. Interestingly, numerous studies have established a connection between endosomal acidification and sEV secretion – decreasing endosomal acidification increases exosome secretion (Villarroya-Beltri *et al*, 2016; Edgar *et al*, 2016; Guo *et al*, 2017; Latifkar *et al*, 2019). The vacuolar H^+-ATPase (V-ATPase) is a multi-subunit proton pump responsible for endosomal acidification (Forgac, 2007). Cancer cells downregulate sirtuin-1 (SIRT-1), which destabilizes the mRNA of ATP6V1A, a subunit of the complex (Latifkar *et al*, 2019). This impairs V-ATPase activity that acidifies the MVB lumen and instead favors the sorting of these MVBs for exosome release. Similarly, another study has shown that autophagy-related gene 5 (ATG5), a protein involved in the autophagy pathway, dissociates the ATP6V1E1 subunit from the V-ATPase complex to reduce its activity and thus promote exosome secretion (Guo *et al*, 2017). Overall, these studies indicate that acidification plays a significant role in determining MVB sorting fate - with less acidic MVBs more likely to be targeted for secretion. Despite these recent findings, the molecular mechanism involved in fine-tuning MVB lumen acidification to regulate their sorting decision is not well understood.

We discovered that nSMase2 activity regulates endolysosomal acidification by modulating V-ATPase activity and thereby controls sEV secretion. Specifically, we show that nSMase2 inhibition and *SMPD3* knockdown renders the V-ATPase complex assembled and active for further MVB lumen acidification, which consequently reduces sEV secretion. Conversely, we further demonstrate that stimulating nSMase2 activity with the inflammatory cytokine TNFα decreases acidification and in turn increases sEV secretion. We show that nSMase2 activity counteracts V-ATPase-mediated endosome acidification and thereby shifts MVB fate towards sEV secretion.

Results

NSMase2 regulates sEV secretion in HeLa cells

NSMase2 hydrolyzes sphingomyelin into ceramide and phosphorylcholine (Hofmann *et al*, 2000), a reaction that can be blocked by the inhibitor GW4869, which has been used in many studies to inhibit exosome secretion (Trajkovic et al. 2008; Menck et al. 2017; Li et al. 2016; Hu et al. 2019). However, several lines of evidence indicate that even after nSMase2 inhibition, exosome cargo loading and thereby ILV generation is not completely blocked (Gross *et al*, 2012). nSMase2 inhibition with GW4869 furthermore seems to affect large EV subpopulations and alter exosome composition and even fails to reduce EV secretion in other cells (Menck *et al*, 2017; Leidal *et al*, 2020; Panigrahi *et al*, 2018). This prompted us to further dissect the role of nSMase2 in the endosomal pathway. As a first step, we analyzed sEV secretion upon nSMase2 inhibition with GW4869. Conditioned medium from equal numbers of HeLa cells treated with GW4869 or DMSO were subjected to serial ultracentrifugation to recover sEVs at 100,000 x g (Fig. S1A). Following the guidelines recommended by the International Society for Extracellular vesicles (ISEV; Théry *et al*, 2018), we hereafter refer to the isolated vesicles as sEVs rather than exosomes. Medium samples corresponding to equal amounts of cells were used to evaluate sEV secretion. Although HeLa cell viability remained unaffected (Fig. S1B), GW4869 treatment significantly reduced the secretion of Alix, syntenin, and CD63 in the sEV fraction (Fig. 1A, B). In line with their reduced secretion, GW4869 slightly increased

the intracellular levels of these markers (Fig. 1C, D). This indicates that due to their reduced secretion, the markers accumulated, possibly inside the endosomal pathway.

To exclude possible off-target effects of GW4869, we used siRNA against nSMase2 (targeting expression of *SMPD3*) to phenocopy the effects of the inhibitor. Knockdown (KD) of *SMDP3* was confirmed using qPCR (Fig. S1C) and did not affect the cell viability (Fig. S1D). *SMPD3* KD in HeLa cells significantly decreased the secretion of Alix, CD63, syntenin, and CD81 in the sEV fraction (Fig. 1E, F) and significantly increased the corresponding intracellular levels of these exosomal markers (Fig. 1G, H). Moreover, nanotracking particle analysis (NTA) showed that most of the sEVs were between 100 nm and 200 nm in diameter (Fig. 1I, K) and confirmed their reduced secretion upon GW4869 treatment and *SMPD3* KD (Fig. 1J, L). Furthemore, KD using two separate sets of siRNAs against *SMPD3* or the combinations thereof similarly reduced sEV secretion (Fig. 1L). Overall, these results further confirm the role of nSMase2 in sEV secretion in HeLa cells.

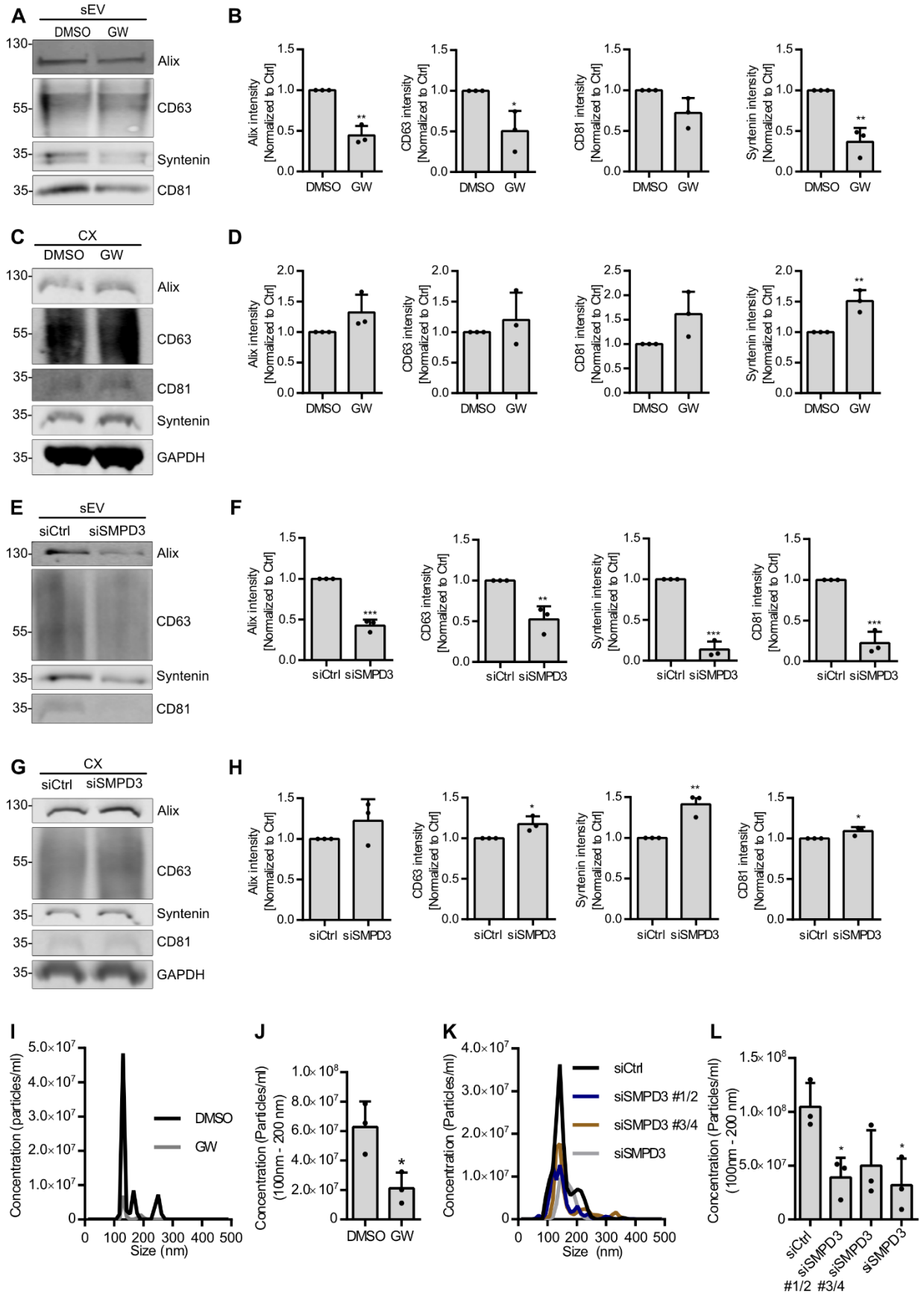
A
sEV
DMSO GW
130
Alix
55
CD63
35
Syntenin
35
CD81
B
Alix intensity [Normalized to Ctrl]
CD63 intensity [Normalized to Ctrl]
CD81 intensity [Normalized to Ctrl]
Syntenin intensity [Normalized to Ctrl]
DMSO GW
C
CX
DMSO GW
130
Alix
55
CD63
35
CD81
35
Syntenin
35
GAPDH
D
Alix intensity [Normalized to Ctrl]
CD63 intensity [Normalized to Ctrl]
CD81 intensity [Normalized to Ctrl]
Syntenin intensity [Normalized to Ctrl]
DMSO GW
E
sEV
siCtrl siSMPD3
130
Alix
55
CD63
35
Syntenin
35
CD81
F
Alix intensity [Normalized to Ctrl]
CD63 intensity [Normalized to Ctrl]
Syntenin intensity [Normalized to Ctrl]
CD81 intensity [Normalized to Ctrl]
siCtrl siSMPD3
G
CX
siCtrl siSMPD3
130
Alix
55
CD63
35
Syntenin
35
CD81
35
GAPDH
H
Alix intensity [Normalized to Ctrl]
CD63 intensity [Normalized to Ctrl]
Syntenin intensity [Normalized to Ctrl]
CD81 intensity [Normalized to Ctrl]
siCtrl siSMPD3
I
Concentration (particles/ml)
DMSO
GW
Size (nm)
J
Concentration (Particles/ml) (100nm - 200 nm)
DMSO GW
K
Concentration (Particles/ml)
siCtrl
siSMPD3 #1/2
siSMPD3 #3/4
siSMPD3
Size (nm)
L
Concentration (Particles/ml) (100nm - 200 nm)
siCtrl
siSMPD3 #1/2
siSMPD3 #3/4
siSMPD3

Figure 1: NSMase2 regulates sEV secretion in HeLa cells. (A) Western blot analysis of sEV fractions prepared from equal amounts of overnight DMSO- or GW4869 (GW)-treated HeLa cells. Samples were probed for the exosomal markers Alix, CD63, syntenin, and CD81. **(B)** Signal intensity quantifications of Alix, CD63, syntenin, and CD81 in sEV fractions from (A) calculated by normalizing the signal to loading control GAPDH levels in the corresponding cell lysates in (C) before normalization to the respective control. **(C)** Western blot of the corresponding cell lysates (CX) from (A), probed for loading control GAPDH in addition to the exosomal markers from (A). **(D)** Quantifications of intracellular Alix, CD63, syntenin, and CD81 signal intensity from (C) normalized to loading control GAPDH before normalization to the respective control. **(E)** Western blot analysis of sEV fractions prepared from equal amounts of control (siCtrl) and *SMPD3* KD (si*SMPD3*) HeLa cells, and probed for the exosomal markers Alix, CD63, syntenin, and CD81. **(F)** Signal intensity quantifications of Alix, CD63, syntenin, and CD81 in sEV fractions from (E), calculated by normalizing the signal to loading control GAPDH levels in the corresponding cell lysates in (G) before normalization to their respective control. **(G)** Western blot of the corresponding cell lysates (CX) from (E), probed for loading control GAPDH in addition to the exosomal markers from (E). **(H**) Quantifications of intracellular Alix, CD63, syntenin, and CD81 signal intensity from (G) normalized to loading control GAPDH before normalization to the respective control. **(I)** Representative size distribution of sEVs prepared from DMSO- or GW4869-treated HeLa cells. **(J)** NTA quantification of sEV concentration from (I). **(K)** Representative size distribution of sEV isolated from control or *SMPD3* KD HeLa cells. *SMPD3* KD used either pairs of siRNAs (si*SMPD3* #1/2 and si*SMPD3* #3/4) or a pool of all four siRNAs (si*SMPD3*). (L) NTA quantification of sEV concentration from (K). Data are presented as mean±s.d. of three biological replicates. ***P<0.0001; **P<0.001; *P<0.01 (unpaired two-tailed Student's *t*-test in B, D, F, H, J; one-way ANOVA followed by Dunnett's comparisons test in L). Molecular masses are indicated in kDa.

SMPD3 KD results in intracellular accumulation of MVBs

We reasoned, that analyzing ceramide distribution in different organelles could shed light on the specific subcellular activity of nSMase2 and subsequent effects on MVB formation and exosomal biogenesis. As a readout for nSMase2 activity, we used an anti- ceramide antibody previously used for studies of sphingomyelin metabolism and ceramide signaling (Vielhaber *et al*, 2001; Parashuraman & D'Angelo, 2019; Yabu *et al*, 2015). Ceramide staining was analyzed in DMSO- and GW4869-treated HeLa cells using confocal microscopy. As expected, GW4869 treatment significantly reduced intracellular ceramide levels, suggesting reduced nSMase2 activity (Fig. 2A, B). As ceramide is also provided by *de novo* synthesis from the endoplasmic reticulum, where nSMase2 also localizes (Shamseddine *et al*, 2015), we co-stained ceramide with the endosomal ESCRT-0 component HRS (also known as HGS) to determine nSMase2 activity specifically at the endosomal membrane. GW4869 treatment significantly reduced the amount of ceramide

colocalizing with HRS, confirming reduced nSMase2 activity at the endosomal level (Fig. 2A, B).

To further dissect the role of nSMase2 in sEV secretion, we next analyzed the intracellular distribution of the selected exosomal markers in HeLa cells by confocal microscopy. Reduced staining of syntenin (encoded by SDCBP) upon gene KD confirmed specificity of the ant-syntenin antibody (Fig, S1E). In agreement with the western blot analysis (Fig. 1G, H), *SMPD3* KD noticeably induced the intracellular accumulation of CD63, syntenin, and lysobisphosphatidic acid (LBPA), an MVB-specific lipid marker (Fig. 2C, E, and G). Accordingly, the total intracellular signal and the number of puncta per cell for these three markers were significantly increased following *SMPD3* KD (Fig. 2D, F, and H). Collectively, these data suggest that inhibition of nSMase2 activity at the endosomal membrane accumulates MVBs intracellularly.

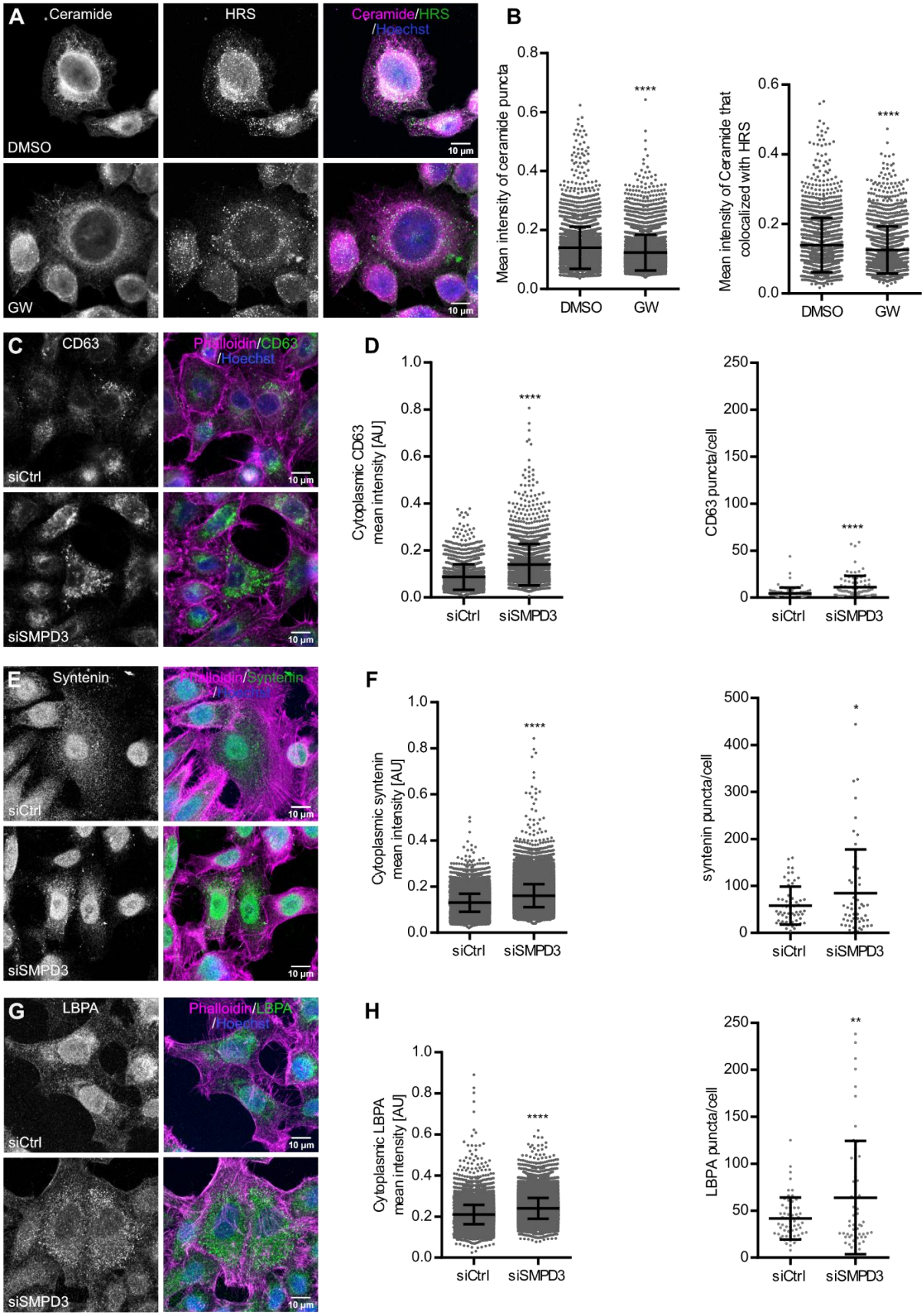
A
Ceramide
HRS
Ceramide/HRS
/Hoechst
DMSO
GW
10 µm
B
Mean intensity of ceramide puncta
0.0
0.2
0.4
0.6
0.8
****
DMSO
GW
Mean intensity of Ceramide that colocalized with HRS
0.0
0.2
0.4
0.6
****
DMSO
GW
C
CD63
Phalloidin/CD63
/Hoechst
siCtrl
siSMPD3
10 µm
D
Cytoplasmic CD63 mean intensity [AU]
0.0
0.2
0.4
0.6
0.8
1.0
****
siCtrl
siSMPD3
CD63 puncta/cell
0
50
100
150
200
250
****
siCtrl
siSMPD3
E
Syntenin
Phalloidin/Syntenin
/Hoechst
siCtrl
siSMPD3
10 µm
F
Cytoplasmic syntenin mean intensity [AU]
0.0
0.2
0.4
0.6
0.8
1.0
****
siCtrl
siSMPD3
syntenin puncta/cell
0
100
200
300
400
500
*
siCtrl
siSMPD3
G
LBPA
Phalloidin/LBPA
/Hoechst
siCtrl
siSMPD3
10 µm
H
Cytoplasmic LBPA mean intensity [AU]
0.0
0.2
0.4
0.6
0.8
1.0
****
siCtrl
siSMPD3
LBPA puncta/cell
0
50
100
150
200
250
**
siCtrl
siSMPD3

Figure 2: *SMPD3* KD results in intracellular accumulation of MVBs. (A) Confocal microscopy images of HeLa cells treated with DMSO or GW4869 (GW), stained for ceramide and HRS.Nuclei were stained with Hoechst 33342 **(B)** Dot plots of mean fluorescence intensity of ceramide puncta (left) and mean fluorescence intensity of ceramide puncta that colocalized with HRS (right) from (A). (C-H) Confocal microscopy images of control (siCtrl) and *SMPD3* KD (si*SMPD3*) HeLa cells stained for exosomal markers CD63 **(C)** and syntenin **(E)**, and the MVB marker LBPA **(G**), as well as actin (phalloidin). Nuclei were stain with Hoechst 33342. (**D**) Quantifications of cytoplasmic CD63 intensity (left) and CD63 puncta/cell (right) from (E). **(F)** Quantifications of cytoplasmic syntenin intensity (left) and syntenin puncta per cell (right) from E. **(H)** Quantifications of cytoplasmic LBPA intensity (left) and LBPA puncta per cell (right) from (G). The data in B, D, F, and H are presented as mean ± s.d.; $n > 50$ cells from two biological replicates for each staining. *p< 0.01; **p < 0,001; ****p < 0.0001. (Unpaired two-tailed Student's *t*-test). AU, arbitrary units.

nSMase2 regulates sEV secretion by modulating endolysosomal acidification

Recently, several studies have shown that endosomal acidification plays a role in regulating MVB sorting. MVBs with low pH are targeted for lysosomal degradation, whereas MVBs with relatively higher pH are transported towards the cell periphery for plasma membrane fusion to release sEVs (Guo *et al*, 2017; Latifkar *et al*, 2019). As expected, bafilomycin A1 (Baf), which increases endolysosomal acidification by inhibiting V-ATPase activity, significantly increased the secretion of CD63, syntenin, and CD81 in the sEV fraction (Fig. S1G, H) without significantly affecting the cell viability (Fig. S1F). NTA analysis further validated the increased sEV secretion upon Baf treatment (Fig. S1I, J). Based on these data, we next analyzed endolysosomal acidification upon *SMPD3* KD by staining with Lysotracker, a fluorescent dye that stains acidic cellular compartments (Robinson *et al*, 2012). We found that intracellular Lysotracker staining, as well as the number of acidic vesicles per cell, was significantly increased by *SMPD3* KD (Fig. 3A, B) or GW4869 treatment (Fig. S2A, B). Lysotracker staining was completely abolished by bafilomycin treatment (Fig. S2C), thus confirming the staining specificity.

To further investigate how increased endolysosomal acidification upon *SMPD3* KD affects lysosomes and the trafficking of MVBs towards the lysosome, we next analyzed the intracellular colocalization of LAMP1 and CD63. *SMPD3* KD led to an increased colocalization between CD63 and LAMP1 compared with that in control cells (Fig 3C, D). Interestingly, *SMPD3* KD significantly increased the LAMP1 signal intensity (Fig 3C, D), which was further confirmed by western blot (Fig 3E, F). The LAMP1 increase upon

SMPD3 KD was even more evident under a nutrient-depleted condition where cellular lysosomal activity peaks for autophagy (Levine, 2007) (Fig 3E, F). Overall, these results indicate that *SMPD3* regulates endolysosomal acidification and alters MVB trafficking.

The V-ATPase complex acidifies endosomes and lysosomes by translocating protons into their lumina in an ATP-dependent manner (Wang *et al*, 2021). As we found nSMase2 activity to be reduced at HRS-positive endosomes (Fig 2A, B) and acidification increased upon *SMPD3* KD (Fig 3A, B), we next tested whether nSMase2 and V-ATPase reside on the same endosomes. Indeed, a small fraction of nSmase2 colocalized with ATP6V0A1, a V0 transmembrane subunit of V-ATPase, in punctate structures in immunostaining (Fig. 3G, H). This is in line with an affinity-purification-based mass spectrometry study that showed nSMase2 interaction with ATP6VV0A1 (Huttlin *et al*, 2017). Moreover, the mean intensity of ceramide puncta colocalizing with transmembrane ATP6AP2, a core V-ATPase V0 subunit, was significantly reduced by GW4869 treatment, confirming nSMase2 activity on V-ATPase-positive membranes (Fig. 4A, B). Therefore, these data indicate that nSMase2 and V-ATPase activity could be interlinked on MVBs to regulate their acidification for sEV secretion.

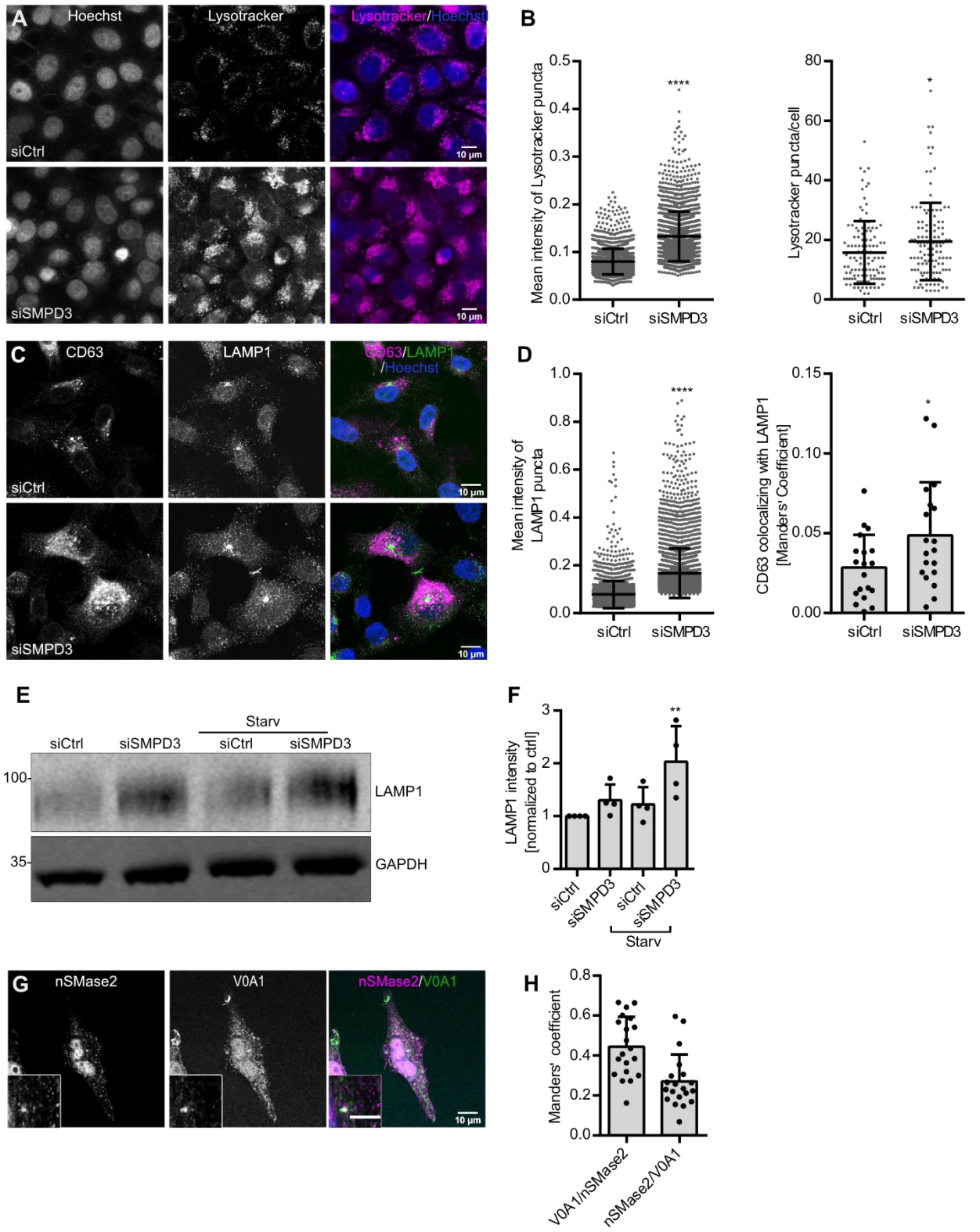

Figure 3: nSMase2 regulates sEV secretion by modulating endosomal acidification. (A) Confocal microscopy images of control (siCtrl) and *SMPD3* KD (si*SMPD3*) HeLa cells with intracellular acidic compartments labeled by Lysotracker. Nuclei were stained with Hoechst 33342. **(B)** Quantifications of mean intensity of Lysotracker puncta (left) and Lysotracker puncta

per cell (right) from (A). Data are presented as mean ± s.d.; n > 50 cells from three biological replicates. ****p < 0.0001 (Unpaired two-tailed Student's *t*-test). **(C)** Confocal microscopy images of control and *SMPD3* KD HeLa cells costained for the exosomal and MVB marker CD63 and the lysosomal marker LAMP1. Nuclei were stained with Hoechst 33342. **(D)** Quantifications of mean fluorescence intensity of LAMP1 puncta (left) and colocalization analysis of CD63 with LAMP1 (right) from (C). (Data are presented as mean ± s.d.; *n* = 20 cells from two biological replicates. *p< 0.01; ****p < 0.0001 (Unpaired two-tailed Student's *t*-test). **(E)** Western blot analysis of LAMP1 and GAPDH from control and *SMPD3* KD HeLa cells under normal and starvation (serum-depleted) conditions (Starv). Molecular masses are indicated in KDa. **(F)** Quantifications of LAMP1 signal normalized to loading control GAPDH before normalization to the control condition from (E). The data shown in (F) represent the mean ± s.d. of four biological replicates. **p < 0,001 (One-way ANOVA followed by Dunnett's comparisons test). **(G)** Representative confocal microscopy of HeLa cells co-stained for nSMase2 and ATP6V0A1. The scale bar in the magnified inset represents 5 µm. **(H)** Pixel-based colocalization between nSMase2 and ATP6V0A1 from (G). Strong nSMase2 nuclear signal was excluded from quantification by masking based on Hoechst 33342 staining. Data are presented as mean ± s.d. of n > 20 cells from two biological replicates.

NSMase2 regulates endolysosomal acidification by modulating V-ATPase assembly

V-ATPase complexes on endosomal membranes are partitioned into raft-like domains, enriched in sphingomyelin and cholesterol (Lafourcade *et al*, 2008), and their activity is regulated by the reversible assembly of the complex. For example, detachment of the cytoplasmic V1 domain, ATP6V1E1 subunit, from the V-ATPase complex has been shown to decrease its activity in yeast and mammalian cells (Sautin *et al*, 2005; Toei *et al*, 2010) A recent study has unraveled that ATG5 detaches ATP6V1E1 from the complex to deacidify the MVB lumen, thereby resulting in increased exosome secretion (Guo *et al*, 2017). We found that ATP6V1E1 localization changed from a diffuse pattern in the cytoplasm in control cells to a more punctate vesicular structure in *SMPD3* KD cells (Fig. 4C). Parallel to the findings of the study mentioned above, this could indicate an increase in ATP6V1E1 localization to endosomes, for example to MVBs. To analyze whether *SMPD3* KD increases endolysosomal acidification by inducing V-ATPase complex assembly, we analyzed the colocalization between ATP6V0A1 and ATP6V1A. Indeed, *SMPD3* KD significantly increased the colocalization between ATP6V0A1 and ATP6V1A, indicating increased V-ATPase assembly (Fig. 4D, E). Therefore, we next analyzed whether V-ATPase was internalized into ILVs during MVB maturation and subsequently secreted on sEVs. Indeed, under control conditions, we found the transmembrane subunit

ATP6V0A1 secreted in the sEV fraction, possibly confirming that it can be internalized into ILVs and released into sEVs. Interestingly, *SMPD3* KD reduced this secretion. ATP6V1A and ATP6V1E1, two cytosolic subunits of the V-ATPase complex, were absent from the sEV fraction under both conditions (Fig. 4F, G). The total intracellular levels of ATP6V0A1, ATP6V1E1, and ATP6V1A in total RIPA lysates were unaffected by *SMPD3* KD (Fig. S2D, E). These data show that ATP6V0A1 is secreted on sEVs in a nSMase2-dependent manner. To further confirm that *SMPD3* KD stabilizes the V-ATPase complex on the endosomal membrane, we next performed a biochemical cell fractionation. This assay yielded a cytosolic and an organelle fraction, the latter containing the membrane proteins (Itzhak *et al*, 2016). *SMPD3* KD indeed enriched ATP6V1E1 and ATP6V0A1 in the organelle fraction in comparison to control cells (Fig. 4H, I), suggesting increased assembly of V-ATPase complex at the membrane. Taken together, our data show that nSMase2 regulates sEV secretion by modulating V-ATPase assembly and activity on MVBs.

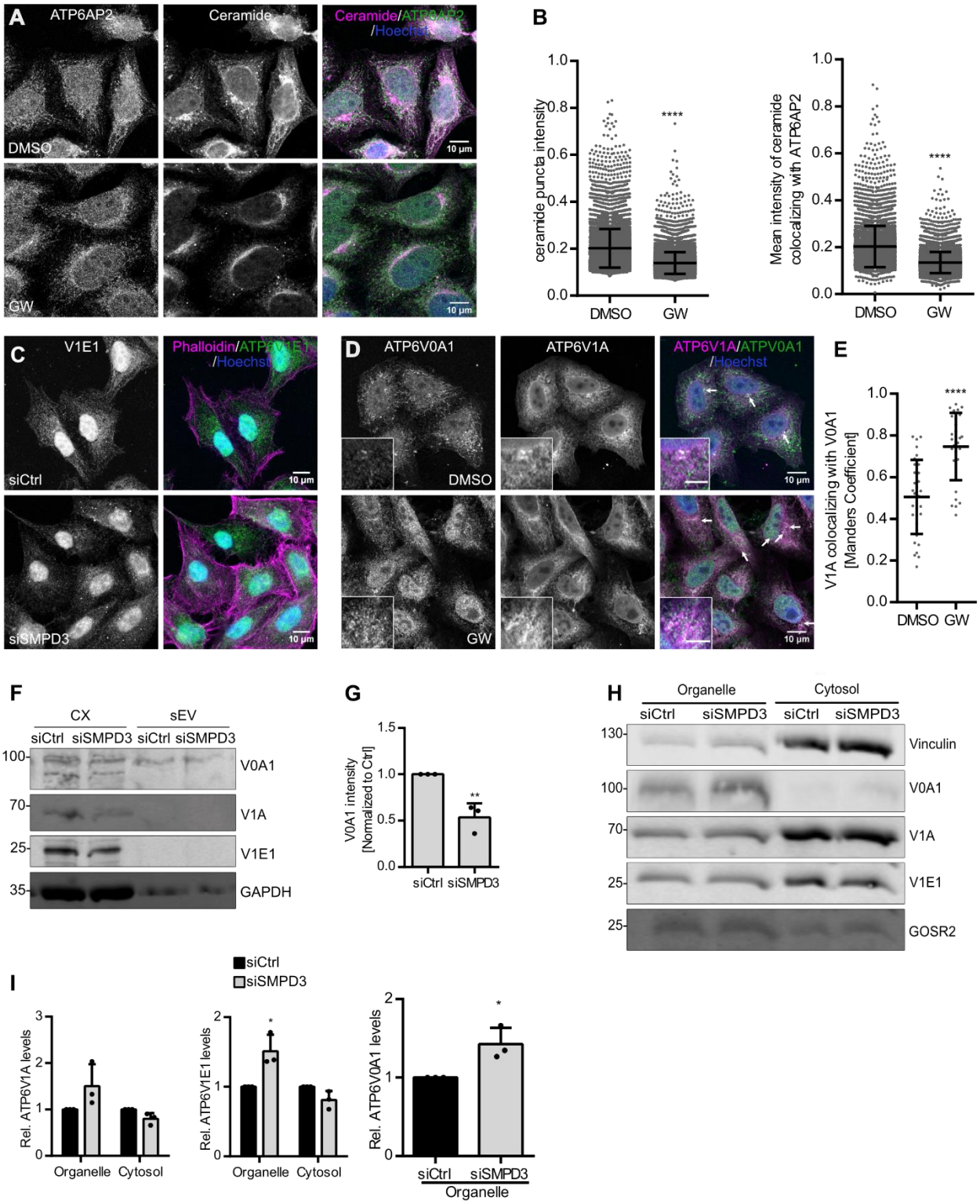

Figure 4: NSMase2 regulates endolysosomal acidification by modulating VATPase assembly. (A) Confocal microscopy images of HeLa cells treated with DMSO or GW4869 (GW), co-stained for ceramide and ATP6AP2. Nuclei were stained with Hoechst 33342. **(B)** Dot plots of mean fluorescence intensity of ceramide puncta (left) and mean fluorescence intensity of ceramide that colocalized with ATP6AP2 (right) from A. Data are presented as mean±s.d.; *n* > 50

cells from two biological replicates. ****P<0.0001 (unpaired two-tailed Student's t-test). **(C)** Confocal microscopy images of the cytoplasmic distribution of ATP6V1E1 (V1E1) in HeLa cells upon *SMPD3* KD (si*SMPD3*) compared with that of control cells (siCtrl). Actin was stained using phalloidin, and nuclei were stained using Hoechst 33342. Images are representative of three experiments. **(D)** Confocal microscopy images of DMSO- and GW4869-treated HeLa cells co-stained for ATP6V0A1 and ATP6V1A. Nuclei were stained with Hoechst. Arrows indicate ATP6V0A1 and ATPV1A colocalization. The scale bar in the magnified inset represents 5 µm. **(E)** Dot plots showing colocalization analysis of ATP6V1A with ATP6V0A1 from E. Data are presented as mean±s.d.; n>20 from two biological replicates. ****P<0.0001 (unpaired two-tailed Student's t-test). **(F)** Western blot analysis of ATP6V0A1 (V0A1), ATP6V1A (V1A), and ATP6V1E1 (V1E1), as well as GAPDH as loading control, in total cell lysates (CX) and sEV fractions prepared from control (siCtrl) and *SMPD3* KD (si*SMPD3*) HeLa cells. **(G)** Quantification of signal intensity of V0A1 in sEV fractions from F normalized to the corresponding loading control GAPDH in the CX before normalization to the respective control. Data are presented as mean ± s.d. of three biological replicates. **P<0.001 (unpaired two-tailed Student's t-test). **(H)** Western blot analysis of V0A1, V1A and V1E1 levels in organelle or cytosolic fractions upon *SMPD3* KD in HeLa cells. Vinculin and GOSR2 were used as cytosolic or organelle markers, respectively. **(I)** Quantifications of signal intensity of V1A and V1E1 in organelle and cytosolic fractions, and V0A1 in the organelle fraction from H. Cytosolic and organelle signals for each subunit were normalized to their respective loading control, vinculin or GOSR2, before normalization to the control condition. Molecular masses in D and H are indicated in kDa. The data shown in E represent mean ± s.d. of three biological replicates. *P<0.01 (Right and middle graphs; one-way ANOVA followed by Sidak's multiple comparisons test, left graph; *P<0.01, unpaired two-tailed Student's t-test).

MVB cholesterol levels regulate sEV secretion by modulating V-ATPase assembly

As nSMase2 hydrolyzes sphingomyelin into ceramide and phosphorylcholine, and ceramide triggers ILV formation, we reasoned that the enrichment of sphingomyelin on endosomal membranes upon *SMPD3* KD could support the assembly of V-ATPase complexes for acidification. Sphingomyelin forms lipid-ordered microdomains with cholesterol in model and cellular membrane systems (Hullin-Matsuda *et al*, 2014). Different transmembrane protein complexes, such as V-ATPases, are preferentially sorted into these microdomains, allowing their structural and functional regulation (Sezgin *et al*, 2017). A recent study reported the complete cryo-EM structure of the human V-ATPase complex and revealed that ordered lipid molecules including cholesterol are an integral part of the V0 complex (Wang *et al*, 2020). Hence, we hypothesized that sphingomyelin and cholesterol levels at MVBs could modulate V-ATPase assembly and thereby regulate MVB fate and sEV secretion. Therefore, similar to the enrichment of the sphingomyelin upon *SMPD3* KD, enrichment of cholesterol should increase endosomal acidification through supporting V-ATPase complex assembly, and at the same time

reduce sEV secretion. To specifically modulate cholesterol at the MVB level, we used U18666A (U18), which accumulates cholesterol in MVBs by inhibiting the cholesterol transporter Nieman-Pick C1 (NPC1) (Lu *et al*, 2015). As expected, U18 treatment, with a mild (<5%) cell viability reduction (Fig. S2F), significantly increased mean Lysotracker staining as well as Lysotracker puncta per cell (Fig. 5A, B), indicating increased V-ATPase activity upon MVB cholesterol accumulation. Additionally, U18 enriched both the transmembrane subunit ATP6V0A1 and the cytoplasmic subunit AT6V1E1 in the membrane fraction similar to *SMPD3* KD (Fig. 5C, D). Accordingly, cholesterol accumulation also reduced the secretion of the exosomal markers Alix and syntenin in the sEV fraction (Fig. 5E, F) with a concomitant slight increase in the intracellular levels of these proteins (Fig. 5G, H). NTA analysis further validated the reduction of sEV secretion upon U18 treatment (Fig. 5I, J). These data demonstrate that, in addition to ceramide and sphingomyelin, endosomal cholesterol levels also modulate both V-ATPase activity and sEV secretion. This strengthens the idea that the endosomal lipid environment governs secretory versus degradative MVB sorting by modulating endosomal acidification via V-ATPase recruitment, thereby exerting control over sEV secretion levels.

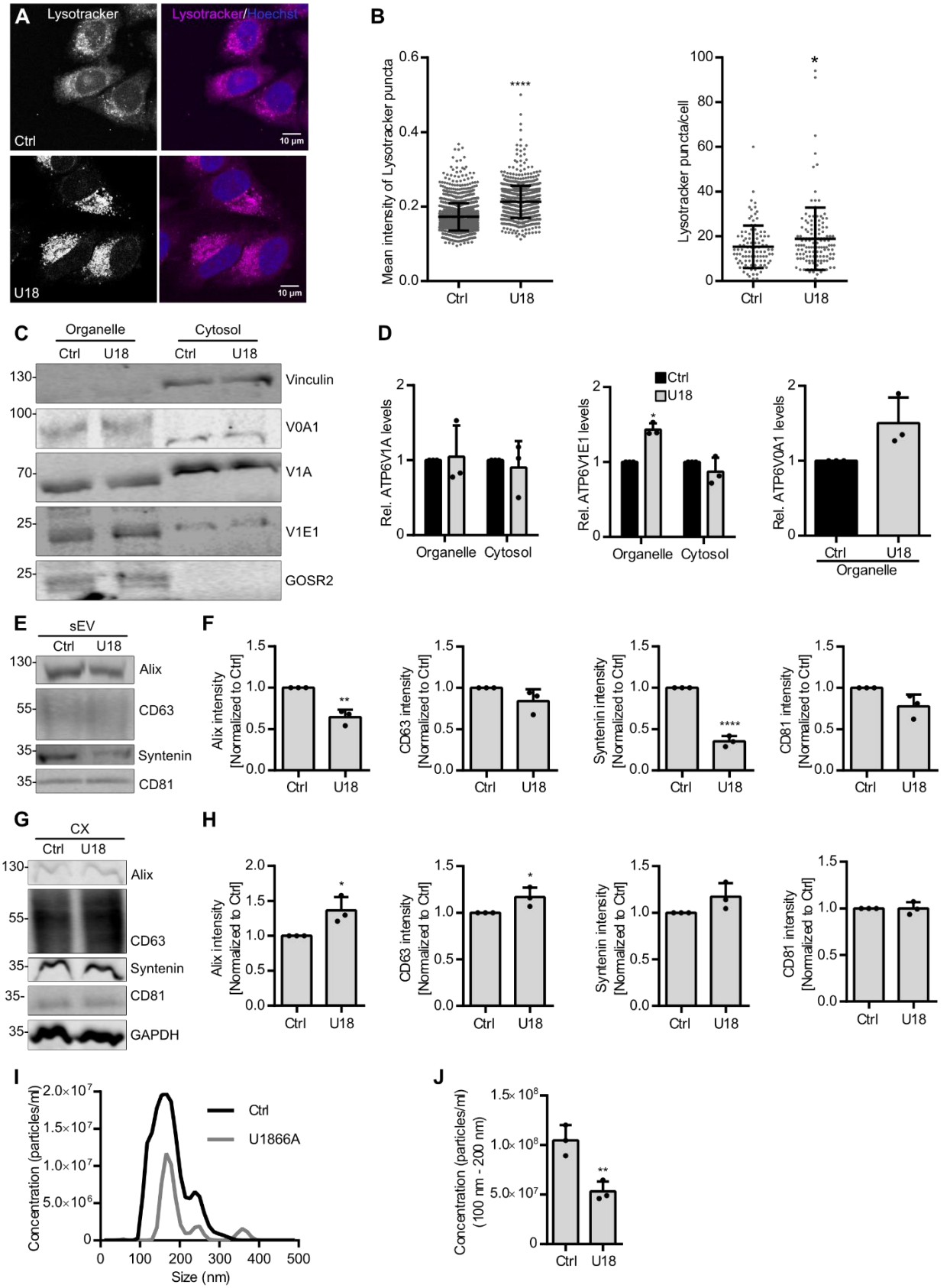

Figure 5: MVB cholesterol levels regulate sEV secretion by modulating V-ATPase

assembly. (A) Confocal microscopy images of control (Ctrl) and U18666A (U18)-treated HeLa cells with intracellular acidic compartments labeled by Lysotracker. Nuclei were stained by Hoechst 33342 **(B)** Quantifications of mean intensity of Lysotracker puncta (left) and Lysotracker staining puncta per cell from A. Data are presented as mean ± s.d.; *n* > 50 cells from three biological replicates. *P<0.01, ****p < 0.0001 (Unpaired two-tailed Student's *t*-test). **(C)** Western blot analysis of ATP6V0A1 (V0A1), ATP6V1A (V1A), and ATP6V1E1 (V1E1) levels in organelle or cytosolic fractions upon U18 treatment in HeLa cells. Vinculin and GOSR2 were used as the cytosolic and the organelle markers, respectively. **(D)** Quantifications of signal intensity of V1A and V1E1 in organelle and cytosolic fractions, and V0A1 in the organelle fraction from (C). Cytosolic and organelle signals for each subunit were normalized to their respective loading control, vinculin or GOSR2, before normalization to the control condition. **(E)** Western blot analysis of Alix, CD63, syntenin, and CD81 in sEV fractions prepared from equal amounts of control or U18-treated HeLa cells. **(F)** Signal intensity quantifications of Alix, CD63, syntenin, and CD81 in sEV fractions from E, calculated by normalizing the signal to loading control GAPDH levels in the corresponding cell lysates in G before normalization to their respective control. **(G)** Western blot analysis of the indicated exosomal markers in corresponding cell lysates (CX) from E. GAPDH was probed as a loading control. **(H)** Quantifications of intracellular Alix, CD63, syntenin, and CD81 signal intensity from G normalized to loading control GAPDH before normalization to the respective control. **(I)** Representative size distribution of sEVs isolated from control and U18-treated HeLa cells. **(J)** NTA quantification of sEV concentration from I. The data shown in D, F, H, and J represent the mean ± s.d. of three biological replicates. *p < 0.01, **p < 0,001, ****p < 0,0001 (Unpaired two-tailed Student's *t*-test). Molecular masses in C, E, and G are indicated in KDa.

TNFα regulates sEV secretion through nSMase2 activation

To investigate the functional implication of nSMase2 counteracting V-ATPase activity on endosomes, we investigated the possible role of TNFα upstream of nSMase2. TNFα is a critical pro-inflammatory cytokine implicated in the pathogenesis of various diseases such as cancer (reviewed in Balkwill, 2006). In addition to its role in the regulation of immunogenic reactions, TNFα mediates different cellular processes including cellular proliferation, differentiation, and migration (Balkwill, 2006). Among its pleiotropic actions, TNFα activates nSmase2 by translocating polycomb group protein EED from the nucleus. This translocation of the EED allows the recruitment of nSMase2 to the TNF receptor-1 (TFN-R1)-FAN-RACK1-complex for its activation (Philipp *et al*, 2010). In line with these data, we found increased ceramide staining upon TNFα treatment compared with that in the control cells, as well as increased ceramide puncta intensity colocalizing with HRS (Fig. 6A, B), these data indicate that TNFα activates nSMase2 on the endosomal membranes. Even though the number of acidic puncta per cell was increased, TNFα treatment, with less than 10% reduction of cell viability (Fig. S2G), significantly decreased

the total Lysotracker signal intensity, thereby indicating reduced V-ATPase activity (Fig. S2H, I).

Following the idea that TNFα might redirect MVBs towards secretion through its effect on nSMase2 and V-ATPase activity, we next investigated the effects of TNFα on sEV secretion directly. TNFα treatment indeed significantly increased the secretion of the exosomal markers Alix, CD63, and syntenin in the sEV fraction (Fig. 6C, D). While intracellular syntenin levels were significantly upregulated by TNFα treatment, no effect was observed for the intracellular levels of the exosomal markers CD63, Alix, and CD81 (Fig. 6E, F). Importantly, the increased secretion of Alix, CD63 (quantification in S2J), and syntenin in the sEV fraction induced by TNFα in control cells were rescued by *SMPD3* KD (Fig. 6G, H). NTA analysis of sEV samples further confirmed that increased sEV secretion by TNFα was rescued by *SMPD3* KD (Fig. 6I, J). confirming that TNFα stimulation affects sEV secretion via nSMase2 activity.

In alignment with our hypothesis that TNFα acts through nSMase2 activation at the MVB membrane and subsequently promotes V-ATPase sequestration into the ILV, TNFα furthermore increased ATP&V0A1 levels in the sEV fraction (Fig. 6K, L). Concordantly, *SMPD3* KD partially rescued the increased ATP6V0A1 secretion on sEVs (Fig. 6K, L). Collectively, these results indicate that TNFα activates nSMase2 on endosomes, which in turn counteracts V-ATPase activity on the MVB membrane and reduces endosomal acidification to promote sEV secretion (Fig. 7).

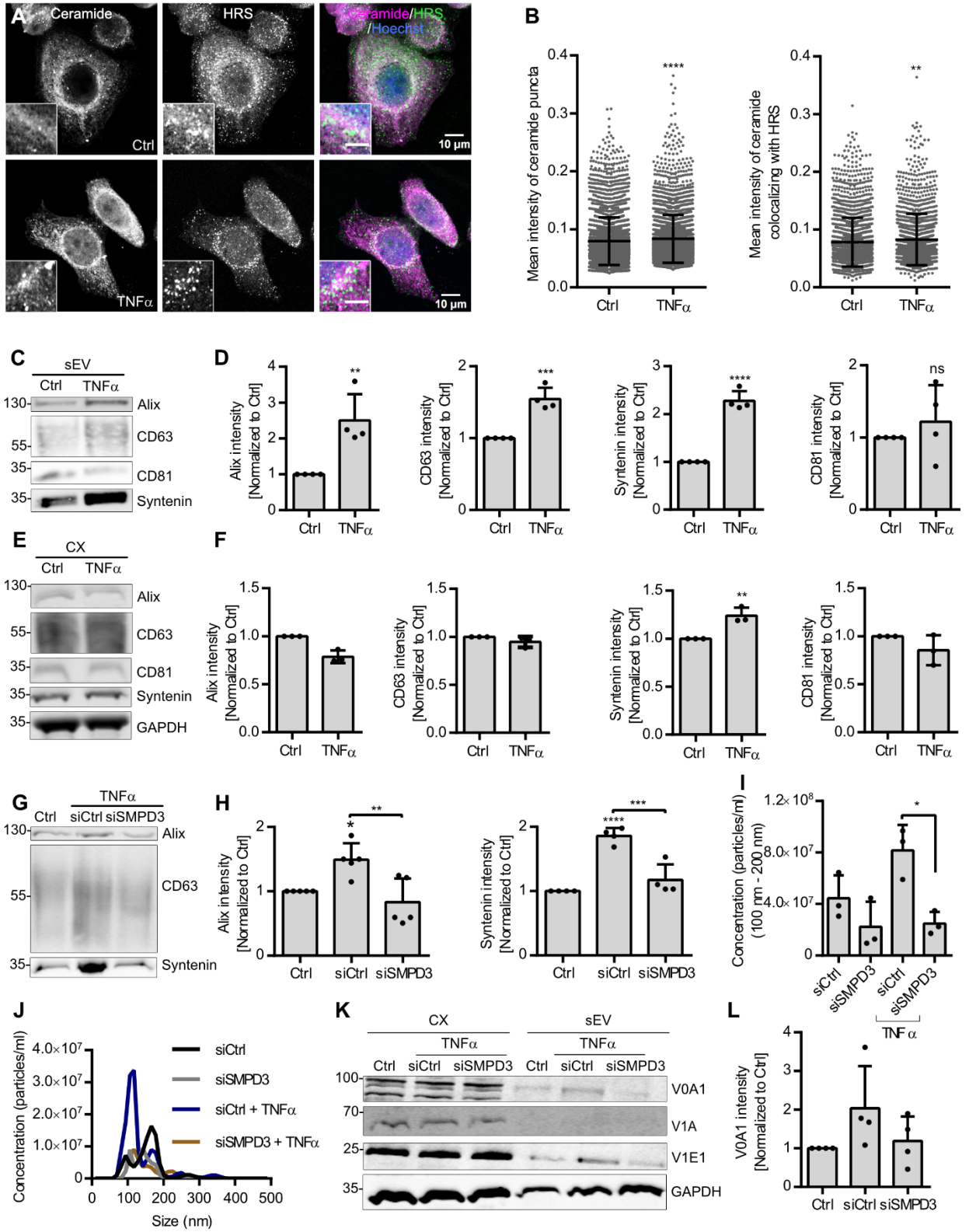

Figure 6: TNFα regulates sEV secretion through nSMase2 activation. **(A)** Confocal microscopy images of control (Ctrl) and TNFα-treated HeLa cells co-stained for ceramide and HRS. Nuclei were stained with Hoechst 33342. The scale bar in the magnified inset represents 5 µm. **(B)** Dot plots of mean fluorescence intensity of ceramide puncta (left) and mean fluorescence

intensity of ceramide that colocalized with HRS (right) from A. Data are presented as mean ± s.d.; n>50 cells from two biological replicates. **P<0.001; ****P<0.0001 (unpaired two-tailed Student's t-test). **(C)** Western blot analysis of Alix, CD63, syntenin and CD81 in sEV fractions prepared from equal amounts of control or TNFα-treated HeLa cells. **(D)** Signal intensity quantifications of Alix, CD63, syntenin and CD81 in sEV fractions from C, calculated by normalizing the signal to loading control GAPDH levels in the corresponding cell lysates in E before normalization to their respective control. Data are presented as mean ± s.d. of four biological replicates. *P<0.01, **P<0.001, ****P<0.0001 (unpaired two-tailed Student's t-test). **(E)** Western blot analysis of the indicated exosomal markers and GAPDH in the corresponding cell lysates (CX) from C. GAPDH was probed as a loading control. **(F)** Quantifications of intracellular Alix, CD63, syntenin and CD81 signal intensity from E normalized to loading control GAPDH before normalization to the respective control. Data are presented as mean ± s.d. of three biological replicates. **P<0.001 (unpaired two-tailed Student's t-test). **(G)** Western blot analysis of Alix, CD63 and syntenin in an sEV fraction prepared from an equal amount of control untreated cells (Ctrl) or control siRNA-treated (siCtrl) and *SMPD3* KD (si*SMPD3*) HeLa cells treated with TNFα. **(H)** Signal intensity quantifications of Alix and syntenin in sEV fractions from G, calculated by normalizing the signal to loading control GAPDH levels in the corresponding cell lysates before normalization to their respective control. Data are presented as mean ± s.d. of five (Alix) and four (Syntenin) biological replicates. ***P<0,0004 (one-way ANOVA followed by Tukey's multiple comparisons test). **(I)** NTA quantification of sEV concentration isolated from control and *SMPD3* KD HeLa cells with or without TNFα treatment. Data are presented as mean ± s.d. of three biological replicates. *P<0.01 (one-way ANOVA followed by Tukey's multiple comparisons test). **(J)** Representative size distribution of sEV analyzed by NTA from I. **(K)** Western blot analysis of ATPV0A1 (V0A1), ATP6V1A (V1A) and ATP6V1E1 (V1E1), as well as GAPDH as loading control, in the total cell lysates (CX) and corresponding sEV fractions prepared from untreated HeLa cells (Ctrl) and from control and *SMPD3* KD HeLa cells treated with TNFα. **(L)** Quantifications of signal intensity of V0A1 in the sEV fraction from K normalized to the corresponding loading control GAPDH in the CX before normalization to the respective control. Data are presented as mean ± s.d. of four biological replicates. (one-way ANOVA followed by Tukey's multiple comparisons test).

Discussion

Here, we demonstrate that nSMase2 controls exosome secretion by counteracting V-ATPase activity on endosomal membranes. We show a previously unknown mechanism by which nSMase2 regulates sEV secretion and provide evidence that the lipid environment at MVBs and specifically the levels of ceramide, sphingomyelin, and cholesterol regulate sEV secretion by modulating endosomal acidification. Importantly, we show that TNFα, a prominent pro-inflammatory cytokine known to activate nSMase2, promotes sEV secretion by modulating endosomal acidification via changes in V-ATPase complex assembly. These findings for the first time establish a molecular connection between TNFα-induced nSMase2 activation and sEV secretion.

Owing to its biophysical properties, ceramide generated by nSMase2 at the MVB membrane drives inward membrane budding to form ILVs (Trajkovic, 2008). We show that this impaired MVB membrane invagination affects sEV secretion by increasing V-ATPase activity through stabilizing it on the endosomal membrane. We propose that V-ATPases are selectively sequestered into MVBs under normal conditions to attenuate their lumen acidification activity and promote secretory MVB trafficking. We found that nSMase2 depletion reduces the sequestration of V-ATPase subunits into ILVs and instead renders them active on the MVB membrane for continued acidification. This consequently deregulates secretory MVB sorting and therefore reduces sEV secretion. Sequestration of growth factor receptors bound to their ligands into ILVs has been shown to attenuates their signaling by targeting them for lysosomal degradation (Piper & Katzmann, 2010). Conversely, ILV sequestration of glycogen synthase kinase β (GSKβ, encoded by *GSK3B*), triggered by WNT signaling, stabilizes many GSKβ protein substrates which are otherwise targeted for degradation (Taelman *et al*, 2010). We show that V-ATPase sequestration into ILVs occurs in a ceramide-dependent manner that significantly affects MVB trafficking fate and sEV secretion.

Recent studies have highlighted the role of MVB lumen acidification as a sorting signal – MVBs with less acidic lumen are sorted as secretory MVBs for exosome release. For example, ATG5 and LC3, independent of canonical macroautophagy, coordinately deacidify MVBs to promote sEV secretion (Guo *et al*, 2017). Additionally, numerous studies have reported that exosome secretion is controlled by endolysosomal acidification (Villarroya-Beltri *et al*, 2016; Edgar *et al*, 2016). Our findings on how changes in nSMase2-mediated endosomal acidification affect sEV secretion further substantiate these findings.

In addition to ceramide and sphingomyelin, we find MVB cholesterol levels to regulate sEV secretion through modulation of V-ATPase-mediated endosomal acidification. Cholesterol, in association with sphingomyelin, forms lipid-ordered microdomains on the membrane, providing an assembly platform for different protein complexes. This establishes a functional and structural connection between lipids and proteins, possibly allowing for a reciprocal regulation. The complete cryo-EM structure of the human V-ATPase complex has revealed that ordered lipid molecules including cholesterol are indeed an integral part of the V0 complex (Wang *et al*, 2020). Cholesterol, together with

ceramide generated by nSMase2 activity on the MVB membrane, may invaginate with V-ATPase subunits to form ILVs, which are known to harbor the highest cholesterol content in the endocytic pathway (Möbius *et al*, 2003).

The reported cell type-specific effects of nSMase2 inhibition on sEV secretion may be explained by the differences in cellular endosomal acidification levels, which in turn could be affected by different cellular and physiological factors. The ESCRT components drive ILV biogenesis at the MVB (Saksena *et al*, 2007) and the knockdown of the ESCRT components HRS, STAM1, and TSG101 reduces the secretion of CD63-positive EVs (Colombo *et al*, 2013). However, the role of the ESCRT- complexes in cargo loading and ILV generation for exosome secretion is increasingly challenged by other studies. For example, a recent study has shown that knockdown of individual ESCRT subunits counterintuitively increases exosome secretion by causing lysosomal dysfunction (Matsui *et al*, 2021). These findings are also in line with studies showing that the lysosomal degradation of several endocytosed receptors requires the ESCRT machinery for proper internalization of these receptors into ILVs (Futter *et al*, 1996; Haglund *et al*, 2003; Yamashita *et al*, 2008). Therefore, based on these studies and our results, it is tempting to speculate that ESCRT complexes support ILV generation for degradative MVBs that are targeted for lysosomes. On the other hand, ceramide generated by nSMase2 drives membrane invagination on the MVB to package V-ATPases into ILVs, thereby attenuating their lumen acidification activity and favoring secretory MVB transport for sEV release. These two pathways involving ceramide or the ESCRT machinery provide two mechanisms of ILV formation that have different outcomes for the fate of their endosomal compartment.

TNFα, a pro-inflammatory cytokine, activates nSMase2. TNFα activates TNF receptor-1 (TNF-R1), which translocates EED from the nucleus. EED then simultaneously interacts with RACK1 and nSMase2. This interaction couples EED and nSMase2 to the TFN-R1-FAN-RACK1-complex and activates nSMase2 (Philipp *et al*, 2010). However, the exact downstream effect of the TNFα-induced nSMase2 pathway on cellular processes is not fully understood. Our findings elucidate the mechanism by which TNFα-induced nSMase2 activation promotes sEV secretion by modulating endosomal acidification. TNFα stimulation has been shown to compromise lysosome integrity by either compromising

lysosomal acidification or by permeabilizing the lysosomal membrane. This in turn affects the cellular degradative capacity and reduces the autophagy flux (Wang *et al*, 2015; Werneburg *et al*, 2002). The exact molecular mechanism underlying this process remains unknown. Based on our findings, it would be worthwhile to investigate whether this occurs via nSMase2 activation.

In addition to the proposed role of nSMase2 in the initial ILV generation (Trajkovic *et al*, 2008), we show that nSMase2 activity controls later MVB trafficking by counteracting V-ATPase-mediated lumen acidification, thereby promoting a secretory rather than a degradative fate. With increased lysosome biogenesis upon *SMPD3* KD under starvation conditions (Fig. 3 C-F), how nSMase2-mediated endosomal acidification regulation affects autophagy remains an interesting question to explore. Furthermore, how nSMase2-dependent MVB deacidification affects recruitment of further MVB secretory machinery including Rab27a, Rab27b (Ostrowski *et al*, 2010) and SNARE proteins such as YKT6 (Gross *et al*, 2012) remains to be investigated. Further study on TNFα-induced nSMase2 activation in cancer cells may shed light on the role of TNFα and sEV in cancer progression.

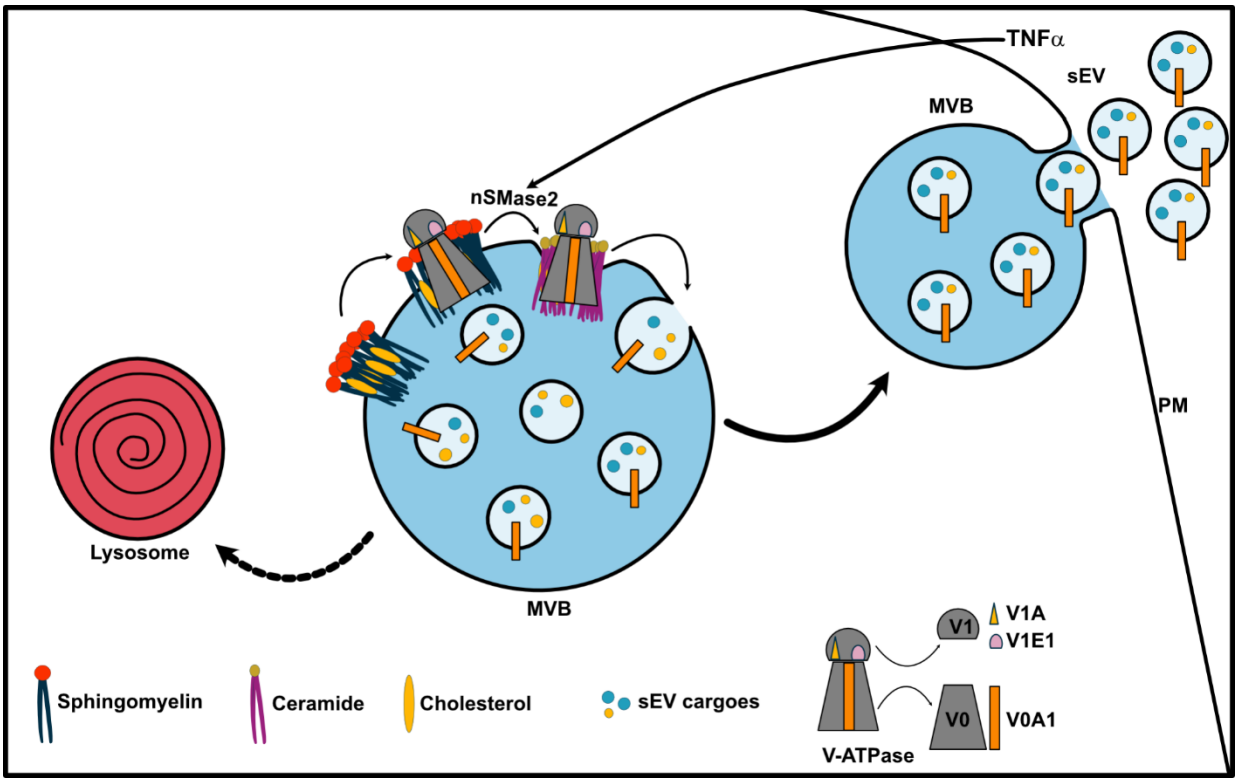

Figure 7: nSMase2 regulates sEV secretion by counteracting V-ATPase-mediated endosomal acidification. Working model showing how nSMase2 regulates sEV secretion via counteracting V-ATPase-mediated endosome acidification. Ceramide generated by nSMase2 activity on the MVB drives inward membrane invagination to selectively incorporate the V-ATPase subunit ATP6V0A1 (V0A1) and other sEV *cargos* into ILVs targeted for secretion. The sequestration of V0A1 into ILVs attenuates MVB lumen acidification to favor secretory MVB trafficking for sEV release. V1A, ATP6V1A; V1E1, ATP6V1E1.

Materials and Methods

Cell culture and Transfection

HeLa cells (kindly provided by Holger Bastians, Goettingen) were maintained in DMEM (Thermo Fischer Scientific Life technologies, 52100021) supplemented with 10% fetal calf serum (Biochrom) and 10 µg/ml Penicillin/Streptomycin (Sigma Aldrich, P4333) at 37 °C in a humidified atmosphere with 5% CO_2. Cells were transiently transfected with ScreenFect-siRNA (Screenfect) for 72 h according to the manufacturer's instructions and routinely checked for mycoplasma contamination. Cells were treated with the following drugs for 16 h: GW4869 (5 µM, Sigma Aldrich, D1692), Bafilomycin (100 ng/ml, Sigma

Aldrich, B1793), TNFα (5 ng/ml, Peprotech, 300-01A) and U18666A (10 µM, Sigma Aldrich, U3633).

Table 1: Dharmacon siRNA SMARTpools were used against:

Gene	Catalog number	Sequence
SMPD3	D-006678-01	5'-CAAAGCGGCCUCCUCUUU-3'
	D-006678-04	5'-CAAGCGAGCAGCCACCAAA-3'
	D-006678-17	5'-ACC AAAGAAUCGUCGGGUA-3'
	D-006678-18	5'-CGAACGGCCUGUACGAUGA-3'
UBC	D-19408-01	5'-GUGAAGACCCUGACUGGUA-3'
Non-targeting	D-001210-03	5-AUGUAUUGGCCUGUAUUAG-3'

Antibodies

The following antibodies and dilutions were used for Western blotting (WB) or for immunofluorescence staining (IF): Alix (WB 1:1000; Santa Cruz, sc53540), CD63/H5C6 (WB 1:100; IF 1:10; DSHB, AB_528158), syntenin (WB 1:1000; IF 1:100; Abcam, ab133267), GAPDH (WB 1:1000; Millipore, CB1001), HRS (IF 1:100; ProteinTech, 1039-1-AP), ceramide (IF 1:100; Enzo, ALX-804-196), LBPA (IF 1:100; Millipore, MABT837), nSMase2 (IF 1:100; Santa Cruz, sc-166637), ATP6V0A1 (WB 1:1000; IF 1:100; Novus Bio, NB1-89342), vinculin (WB 1:1000; ProteinTech, 66305-1-Ig), ATP6V1E1 (WB 1:1000; IF 1:100; ProteinTech, 15280-1-AP), ATP6V1A (WB 1:1000; Abnova, H00000523-M02), GOSR2 (WB 1:1000 ProteinTech, 66134-1-Ig).

Small extracellular vesicles Isolation

For sEV isolation, 400 000 cells (siRNA transfection) or 500 000 cells (inhibitor treatment) were seeded. SEVs were purified by differential centrifugation as previously described (Menck *et al*, 2017). In short, cells were incubated with an sEV-free growth medium for

defined periods. Subsequently, the conditioned medium was collected and subjected to sequential centrifugation steps at 750 g, 1500 g, and 14,000 g, before pelleting sEVs at 100,000 g. The sEV pellet was lysed with RIPA lysis buffer (50 mM Tris-HCl (pH 7.5), 150 mM NaCl, 1% (v/v) Igepal, 0.5% (w/v) SDS, 1 x Roche protease inhibitor) diluted at 1:1 with Phosphate-buffered saline (PBS).

Western blot analysis

Cell and sEV lysates, in SDS-PAGE sample buffer (300 mM Tris-HCl pH 6.8,12 % SDS, β-mercaptoethanol), were boiled for 5 min before the proteins were separated on 4-12% gradient gels (Bolt Bis-Tris Plus Gels, Thermo Fischer Scientific). Proteins were then transferred to PVDF membranes (Merck) and blocked with 5% (wt/vol) milk in Tris-buffered saline containing 0.2% Tween 20 (TBST) for 30 min. Membranes were incubated with primary antibodies overnight at 4°C. After washing, membranes were incubated with fluorescently labeled secondary antibodies at room temperature in the dark and detected using the Li-COR Odyssey system. Quantitative measurements were done with Fiji/ImageJ (NIH, Bethesda, MD).

Nanoparticles tracking analysis

A Malvern Panalytical Nanosight NS300 instrument was used to measure sEV particles diluted in PBS (1:100) using the parameters camera level 14, screen gain 10.8, detection threshold 5). For each sample, a total of three videos of 30-60 s was measured. The videos were analyzed using the NanoSight NTA 2.3 Analytical Software and the particles concentration, size distribution, and the general mean and mode of the samples were obtained.

Immunostainings, microscopy, and image analysis

Cells were grown in 8-well microscopic coverslips (Sarstedt, 94.6170.802), reverse transfected with siRNAs or treated as indicated, were fixed and permeabilized with 4% paraformaldehyde and 0.2% Triton-X-100. The slides were then blocked in 3 % bovine serum albumin diluted in PBS, followed by 90 min incubation with primary antibodies. After washing three times, cells were incubated with secondary antibodies conjugated to Alexa-Fluor-488 or 546. Nuclei and actin were labeled by Hoechst 33342 (Thermo Fischer Scientific, 62249) and conjugated phalloidin respectively. Live cells were incubated with 200 nM Lysotracker DND-red-99 (Thermo Fischer Scientific, L7528) for 45 min to label acidic compartments and fixed with 4% paraformaldehyde after washing three times with PBS. The cells were visualized with a Zeiss LSM780 confocal microscope (Plan Neofluor 63X/oil NA 1.4 objective). Staining and microscopy conditions were kept identical for comparisons. Mean fluorescence intensity of puncta, the number of puncta per cell, and colocalization quantifications were performed using available pipelines with some modifications in CellProfiler (Broad Institute of MIT and Harvard).

Viability assay

Cell viability was measured by performing a CellTiter-Glo assay (Promega, G8461). Cells were seeded in a 96-well plate. After the indicated treatment, 100 μl of the cell titer glow reagent (Promega) was added to each well (1:1). The plate was incubated on a shaker for 2 min at room temperature to allow cell lysis and then incubated without shaking for 10 min to allow luminescence signal stabilization. The signal was measured using a luminometer and data were analyzed using MikroWin 2000 lite Version 4.43.

Real-time qPCR

Total RNA was isolated from cells using Trizol (Thermo Fischer Scientific Invitrogen, 15596026). Equal amounts of RNA (2 µg) were reverse transcribed into cDNA by treatment with M-MLV reverse transcriptase (Thermo Fischer Scientific Invitrogen,

28025013). The resulting cDNA product was analyzed by real-time quantitative PCR using iTaq Universal SYBRgreen Supermix (Bio-Rad, 172-5125) and gene-specific primers (β-Actin; forward, 5'-GAGCACAGAGCCTCGCCTTT-3', reverse, 5'-ACATGCCGGAGCCGTTGTC-3'). (*SMPD3*; forward, 5'-CAACAAGTGTAACGACGATGCC, reverse, 5'- CGATTCTTTGGTCCTGAGGTGT-3'). Transcript Ct-values were converted to fold change expression changes ($2^{-\Delta\Delta Ct}$ values) after normalization to the housekeeping gene β-actin. Quantitative real-time PCR was performed using the CFX system (Bio-Rad).

Organelle and membrane fractionation

Cells were fractionated into organelle and cytosolic fractions based on a published protocol (Itzhak *et al*, 2016). Briefly, all steps were performed on ice with pre-chilled ice-cold buffer. Cells were incubated in hypotonic lysis buffer (25 mM Tris HCl, pH 7.5, 50 mM sucrose, 0.5 mM $MgCl_2$, 0.2 mM EGTA) for 5 min after washing once with PBS and once with hypotonic lysis buffer. Cells were then scraped in fresh hypotonic lysis buffer and transferred to a Dounce homogenizer (B.Braun) and homogenized with 15 strokes with the tight pestles (B.Braun). Sucrose concentration was immediately restored to 250 mM with hypertonic sucrose buffer (2.5 M sucrose, 25 mM Tris-HCl pH 7.5, 0.5 mM $MgCl_2$, 0.2 mM EGTA) after homogenization. Homogenized crude cell lysates were centrifuged at 1000 g for 10 min to separate nuclear material. The organelle fraction was obtained by centrifuging the post-nuclear supernatant at 78400 g for 30 min and the resulting supernatant was collected as the cytosolic fraction. The organelle pellet was dissolved in SDS buffer (2.5% SDS, 50 mM Tris-HCl pH 8.1) and heated for 5 min at 72 °C.

Protein concentration determination

Protein concentration was determined by using the Pierce BCA Protein Assay Kit (Thermo Scientific, 23225) according to the manufacturer's protocol. Protein lysates diluted with PBS were added to 500 µL of a 1:50 mixture of Buffer B and Buffer A. The

mixture was incubated at 60°C for 30 min and transferred to cuvettes for analysis with NanoDrop. A standard curve for protein BCA analysis and PBS as blank were used.

Statistics

Data were analyzed using GraphPad Prism 6 built-in tests. All data are presented as means±S.D.s. Details about the significance test, the number of replicates, and the *P* values are reported in the respective figure legends.

Acknowledgments

The authors would like to thank Prof. Dr. Bastians (University of Goettingen) for HeLa cells and Dr. Christian Westendorf (MPI, Goettingen) for the NTA facility. We thank Dr. Karen Linnenmannstöns, Dr. Leonie Witte, and Dr. Pradhipa Karuna M for critically reading the manuscript and Mona Honemann-Capito for her excellent technical and scientific support.

Author Contribution

D.C.: Conceptualization, Investigation, Formal analysis, Writing - Original Draft, Review & Editing J.C.G.: Conceptualization, Writing - Review & Editing, Funding acquisition

Conflict of interest

The authors declare that they have no conflict of interest

Funding

Research in the lab of J.C.G. is supported by the Deutsche Forschungsgemeinschaft Research Center grant GR4810/2-1. Open access funding provided by Health and Medical University Potsdam. Deposited in PMC for immediate release.

References

Baietti MF, Zhang Z, Mortier E, Melchior A, Degeest G, Geeraerts A, Ivarsson Y, Depoortere F, Coomans C, Vermeiren E, *et al* (2012) Syndecan-syntenin-ALIX regulates the biogenesis of exosomes. *Nat Cell Biol* 14: 677–685

Balkwill F (2006) TNF-α in promotion and progression of cancer. *Cancer Metastasis Rev* 25: 409–416

Bebelman MP, Smit MJ, Pegtel DM & Baglio SR (2018) Biogenesis and function of extracellular vesicles in cancer. *Pharmacol Ther* 188: 1–11

Ciardiello C, Cavallini L, Spinelli C, Yang J, Reis-Sobreiro M, Candia P De, Minciacchi VR & Di Vizio D (2016) Focus on extracellular vesicles: New frontiers of cell-to-cell communication in cancer. *Int J Mol Sci* 17: 1–17

Colombo M, Moita C, Van Niel G, Kowal J, Vigneron J, Benaroch P, Manel N, Moita LF, Théry C & Raposo G (2013) Analysis of ESCRT functions in exosome biogenesis, composition and secretion highlights the heterogeneity of extracellular vesicles. *J Cell Sci* 126: 5553–5565

Danzer KM, Kranich LR, Ruf WP, Cagsal-Getkin O, Winslow AR, Zhu L, Vanderburg CR & McLean PJ (2012) Exosomal cell-to-cell transmission of alpha synuclein oligomers. *Mol Neurodegener* 7: 1–18

Edgar JR, Manna PT, Nishimura S, Banting G & Robinson MS (2016) Tetherin is an exosomal tether. *Elife* 5: 1–19

Forgac M (2007) Vacuolar ATPases: Rotary proton pumps in physiology and pathophysiology. *Nat Rev Mol Cell Biol* 8: 917–929

Futter CE, Pearse A, Hewlett LJ & Hopkins CR (1996) Multivesicular endosomes containing internalized EGF-EGF receptor complexes mature and then fuse directly with lysosomes. *J Cell Biol* 132: 1011–1023

Gross JC, Chaudhary V, Bartscherer K & Boutros M (2012) Active Wnt proteins are secreted on exosomes. *Nat Cell Biol* 14: 1036–1045

Guo H, Chitiprolu M, Roncevic L, Javalet C, Hemming FJ, Trung MT, Meng L, Latreille E, Tanese de Souza C, McCulloch D, *et al* (2017) Atg5 Disassociates the V1V0-ATPase

to Promote Exosome Production and Tumor Metastasis Independent of Canonical Macroautophagy. *Dev Cell* 43: 716-730.e7

Haglund K, Sigismund S, Polo S, Szymkiewicz I, Di Fiore PP & Dikic I (2003) Multiple monoubiquitination of RTKs is sufficient for their endocytosis and degradation. *Nat Cell Biol* 5: 461–466

Hofmann K, Tomiuk S, Wolff G & Stoffel W (2000) Cloning and characterization of the mammalian brain-specific, Mg2+-dependent neutral sphingomyelinase. *Proc Natl Acad Sci U S A* 97: 5895–900

Hu H-Y, Yu C-H, Zhang H-H, Zhang S-Z, Yu W-Y, Yang Y & Chen Q (2019) Exosomal miR-1229 derived from colorectal cancer cells promotes angiogenesis by targeting HIPK2. *Int J Biol Macromol*

Hullin-Matsuda F, Taguchi T, Greimel P & Kobayashi T (2014) Lipid compartmentalization in the endosome system. *Semin Cell Dev Biol* 31: 48–56

Huttlin EL, Bruckner RJ, Paulo JA, Cannon JR, Ting L, Baltier K, Colby G, Gebreab F, Gygi MP, Parzen H, *et al* (2017) Architecture of the human interactome defines protein communities and disease networks. *Nature* 545: 505–509

Itzhak DN, Tyanova S, Cox J & Borner GHH (2016) Global, quantitative and dynamic mapping of protein subcellular localization. *Elife* 5: 1–36

Kajimoto T, Okada T, Miya S, Zhang L & Nakamura SI (2013) Ongoing activation of sphingosine 1-phosphate receptors mediates maturation of exosomal multivesicular endosomes. *Nat Commun* 4

Kanada M, Bachmann MH & Contag CH (2016) Signaling by Extracellular Vesicles Advances Cancer Hallmarks. *Trends in Cancer* 2: 84–94

Lafourcade C, Sobo K, Kieffer-Jaquinod S, Garin J & van der Goot FG (2008) Regulation of the V-ATPase along the endocytic pathway occurs through reversible subunit association and membrane localization. *PLoS One* 3

Latifkar A, Ling L, Hingorani A, Johansen E, Clement A, Zhang X, Hartman J, Fischbach C, Lin H, Cerione RA, *et al* (2019) Loss of Sirtuin 1 Alters the Secretome of Breast Cancer Cells by Impairing Lysosomal Integrity. *Dev Cell* 49: 393-408.e7

Leidal AM, Huang HH, Marsh T, Solvik T, Zhang D, Ye J, Kai FB, Goldsmith J, Liu JY,

Huang YH, *et al* (2020) The LC3-conjugation machinery specifies the loading of RNA-binding proteins into extracellular vesicles. *Nat Cell Biol* 22

Levine B (2007) Cell biology: Autophagy and cancer. *Nature* 446: 745–747

Li XQ, Liu JT, Fan LL, Liu Y, Cheng L, Wang F, Yu HQ, Gao J, Wei W, Wang H, *et al* (2016) Exosomes derived from gefitinib-treated EGFR-mutant lung cancer cells alter cisplatin sensitivity via up-regulating autophagy. *Oncotarget* 7: 24585–24595

Lu F, Liang Q, Abi-Mosleh L, Das A, de Brabander JK, Goldstein JL & Brown MS (2015) Identification of NPC1 as the target of U18666A, an inhibitor of lysosomal cholesterol export and Ebola infection. *Elife* 4: 1–16

Matsui T, Osaki F, Hiragi S, Sakamaki Y & Fukuda M (2021) ALIX and ceramide differentially control polarized small extracellular vesicle release from epithelial cells. *EMBO Rep*: 1–11

Menck K, Sönmezer C, Worst TS, Schulz M, Dihazi GH, Streit F, Erdmann G, Kling S, Boutros M, Binder C, *et al* (2017) Neutral sphingomyelinases control extracellular vesicles budding from the plasma membrane. *J Extracell Vesicles* 6: 1378056

Möbius W, van Donselaar E, Ohno-Iwashita Y, Shimada Y, Heijnen HFG, Slot JW & Geuze HJ (2003) Recycling compartments and the internal vesicles of multivesicular bodies harbor most of the cholesterol found in the endocytic pathway. *Traffic* 4: 222–231

van Niel G, D'Angelo G & Raposo G (2018) Shedding light on the cell biology of extracellular vesicles. *Nat Rev Mol Cell Biol* 19: 213–228

Ostrowski M, Carmo NB, Krumeich S, Fanget I, Raposo G, Savina A, Moita CF, Schauer K, Hume AN, Freitas RP, *et al* (2010) Rab27a and Rab27b control different steps of the exosome secretion pathway. *Nat Cell Biol* 12: 19–30

Panigrahi GK, Praharaj PP, Peak TC, Long J, Singh R, Rhim JS, Elmageed ZYA & Deep G (2018) Hypoxia-induced exosome secretion promotes survival of African-American and Caucasian prostate cancer cells. *Sci Rep* 8: 1–13

Parashuraman S & D'Angelo G (2019) Visualizing sphingolipid biosynthesis in cells. *Chem Phys Lipids* 218: 103–111

Philipp S, Puchert M, Adam-Klages S, Tchikov V, Winoto-Morbach S, Mathieu S,

Deerberg A, Kolker L, Marchesini N, Kabelitz D, *et al* (2010) The Polycomb group protein EED couples TNF receptor 1 to neutral sphingomyelinase. *Proc Natl Acad Sci U S A* 107: 1112–1117

Piper RC & Katzmann DJ (2010) Biogenesis and function of MVBs. *Annu Rev Cell Dev Biol* 23: 519–547

Raiborg C & Stenmark H (2009) The ESCRT machinery in endosomal sorting of ubiquitylated membrane proteins. *Nature* 458: 445–452

Robinson MW, Alvarado R, To J, Hutchinson AT, Dowdell SN, Lund M, Turnbull L, Whitchurch CB, O'Brien BA, Dalton JP, *et al* (2012) A helminth cathelicidin-like protein suppresses antigen processing and presentation in macrophages via inhibition of lysosomal vATPase. *FASEB J* 26: 4614–4627

Roxrud I, Raiborg C, Pedersen NM, Stang E & Stenmark H (2008) An endosomally localized isoform of Eps15 interacts with Hrs to mediate degradation of epidermal growth factor receptor. *J Cell Biol* 180: 1205–1218

Saksena S, Sun J, Chu T & Emr SD (2007) ESCRTing proteins in the endocytic pathway. *Trends Biochem Sci* 32: 561–573

Sautin YY, Lu M, Gaugler A, Zhang L & Gluck SL (2005) Phosphatidylinositol 3-Kinase-Mediated Effects of Glucose on Vacuolar H+-ATPase Assembly, Translocation, and Acidification of Intracellular Compartments in Renal Epithelial Cells. *Mol Cell Biol* 25: 575–589

Sezgin E, Levental I, Mayor S & Eggeling C (2017) The mystery of membrane organization: Composition, regulation and roles of lipid rafts. *Nat Rev Mol Cell Biol* 18: 361–374

Shamseddine AA, Airola M V. & Hannun YA (2015) Roles and regulation of neutral sphingomyelinase-2 in cellular and pathological processes. *Adv Biol Regul* 57: 24–41

Taelman VF, Dobrowolski R, Plouhinec JL, Fuentealba LC, Vorwald PP, Gumper I, Sabatini DD & De Robertis EM (2010) Wnt signaling requires sequestration of Glycogen Synthase Kinase 3 inside multivesicular endosomes. *Cell* 143: 1136–1148

Théry C, Witwer KW, Aikawa E, Alcaraz MJ, Anderson JD, Andriantsitohaina R, Antoniou

A, Arab T, Archer F, Atkin-Smith GK, *et al* (2018) Minimal information for studies of extracellular vesicles 2018 (MISEV2018): a position statement of the International Society for Extracellular Vesicles and update of the MISEV2014 guidelines. *J Extracell Vesicles* 7

Toei M, Saum R & Forgac M (2010) Regulation and isoform function of the V-ATPases. *Biochemistry* 49: 4715–4723

Trajkovic K (2008) Ceramide triggers budding of exosome vesicles into multivesicular endosomes (Science (1244)). *Science (80-)* 320: 179

Trajkovic K, Hsu C, Chiantia S, Rajendran L, Wenzel D, Wieland F, Schwille P, Brügger B & Simons M (2008) Ceramide triggers budding of exosome vesicles into multivesicular endosomes. *Science (80-)* 319: 1244–1247

Vielhaber G, Brade L, Lindner B, Pfeiffer S, Wepf R, Hintze U, Wittern KP & Brade H (2001) Mouse anti-ceramide antiserum: A specific tool for the detection of endogenous ceramide. *Glycobiology* 11: 451–457

Villarroya-Beltri C, Baixauli F, Mittelbrunn M, Fernández-Delgado I, Torralba D, Moreno-Gonzalo O, Baldanta S, Enrich C, Guerra S & Sánchez-Madrid F (2016) ISGylation controls exosome secretion by promoting lysosomal degradation of MVB proteins. *Nat Commun* 7

Wang L, Wu D, Robinson C V., Wu H & Fu T-M (2020) Structures of a Complete Human V-ATPase Reveal Mechanisms of Its Assembly. *Mol Cell*: 1–11

Wang MX, Cheng XY, Jin M, Cao YL, Yang YP, Wang J Da, Li Q, Wang F, Hu LF & Liu CF (2015) TNF compromises lysosome acidification and reduces α-synuclein degradation via autophagy in dopaminergic cells. *Exp Neurol* 271: 112–121

Wang R, Wang J, Hassan A, Lee CH, Xie XS & Li X (2021) Molecular basis of V-ATPase inhibition by bafilomycin A1. *Nat Commun* 12

Werneburg NW, Guicciardi ME, Bronk SF & Gores GJ (2002) Tumor necrosis factor-α-associated lysosomal permeabilization is cathepsin B dependent. *Am J Physiol - Gastrointest Liver Physiol* 283: 947–956

Yabu T, Shiba H, Shibasaki Y, Nakanishi T, Imamura S, Touhata K & Yamashita M (2015) Stress-induced ceramide generation and apoptosis via the phosphorylation and

activation of nSMase1 by JNK signaling. *Cell Death Differ* 22: 258–273

Yamashita Y, Kojima K, Tsukahara T, Agawa H, Yamada K, Amano Y, Kurotori N, Tanaka N, Sugamura K & Takeshita T (2008) Ubiquitin-independent binding of Hrs mediates endosomal sorting of the interleukin-2 receptor β-chain. *J Cell Sci* 121: 1727–1738

Supplementary Figures

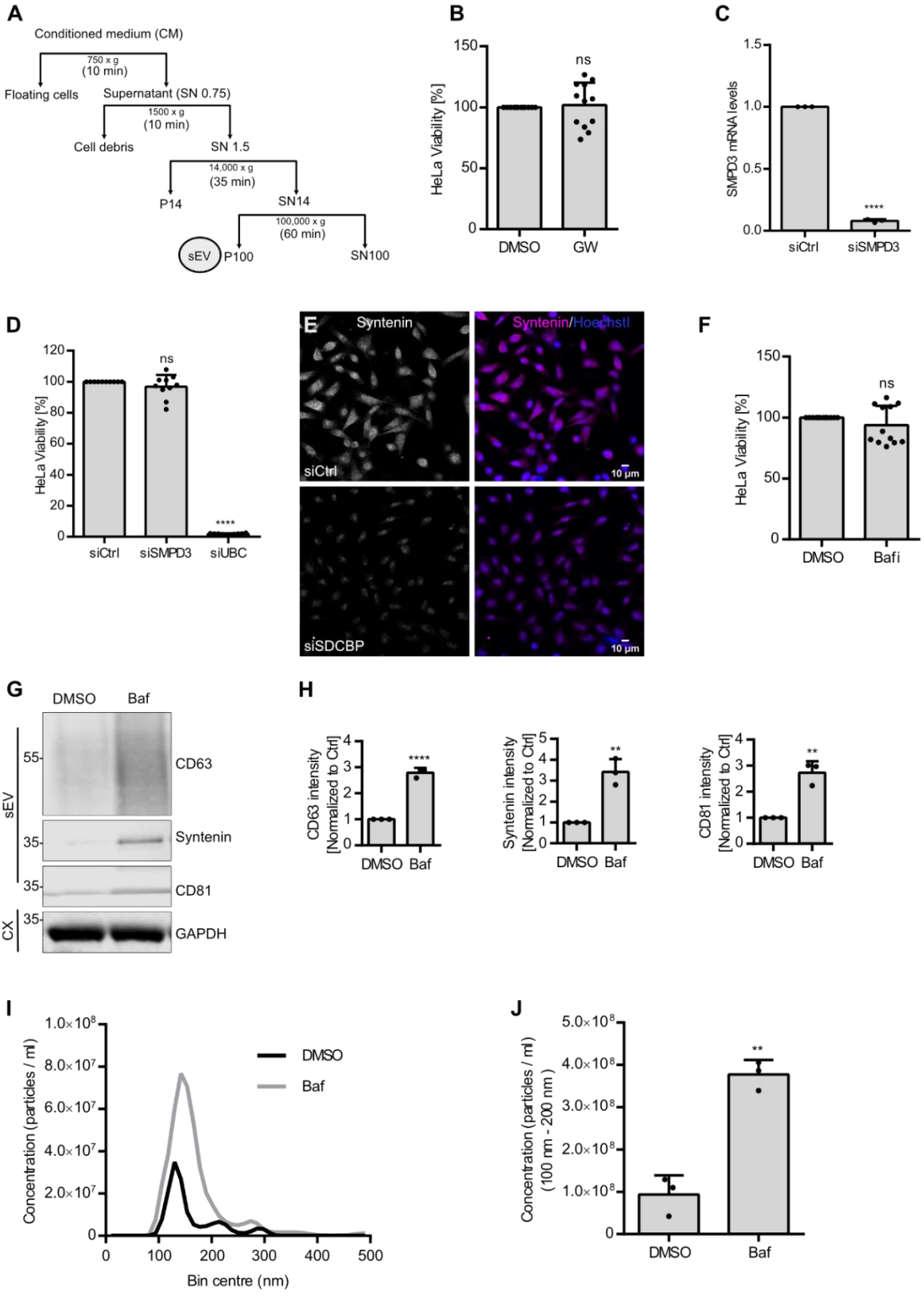

Figure S1: (A) Scheme of sEV isolation from cell culture conditioned medium (CM) through

stepwise serial centrifugation with duration (min) of each step indicated. The pellet (P) obtained after 100 000 g centrifugation corresponds to the sEV fraction. **(B)** HeLa cell viability assay upon GW4869 treatment. **(C)** *SMPD3* KD efficiency validated by real-time qPCR. **(D)** HeLa cell viability assay upon *SMPD3* KD, *UBC* KD was used as a negative control. **(E)** Confocal microscopy images of control and syntenin (*SDCBP*) KD HeLa stained for syntenin and Hoechst. **(F)** HeLa cell viability assay upon bafilomycin A1 treatment. **(G)** Western blot analysis of CD63, Syntenin, and CD81 in sEV fractions prepared from equal amounts of DMSO- and Bafilomycin A1 (Baf)-treated HeLa cells and GAPDH in cell lysate (CX). **(H)** Signal intensity quantifications of CD63, syntenin, and CD81 in sEV fractions from G calculated by normalizing to loading control GAPDH signal in the corresponding cell lysates before normalization to their respective control. **(I)** Representative size distribution of sEVs analyzed by NTA. **(J)** NTA quantification of sEV concentration. The data shown in B, C, D, F, H, and J represent mean ± s.d. of three biological replicates. ****p < 0,0001, **p < 0,001, *p < 0.01 (Unpaired two-tailed student's *t* test).

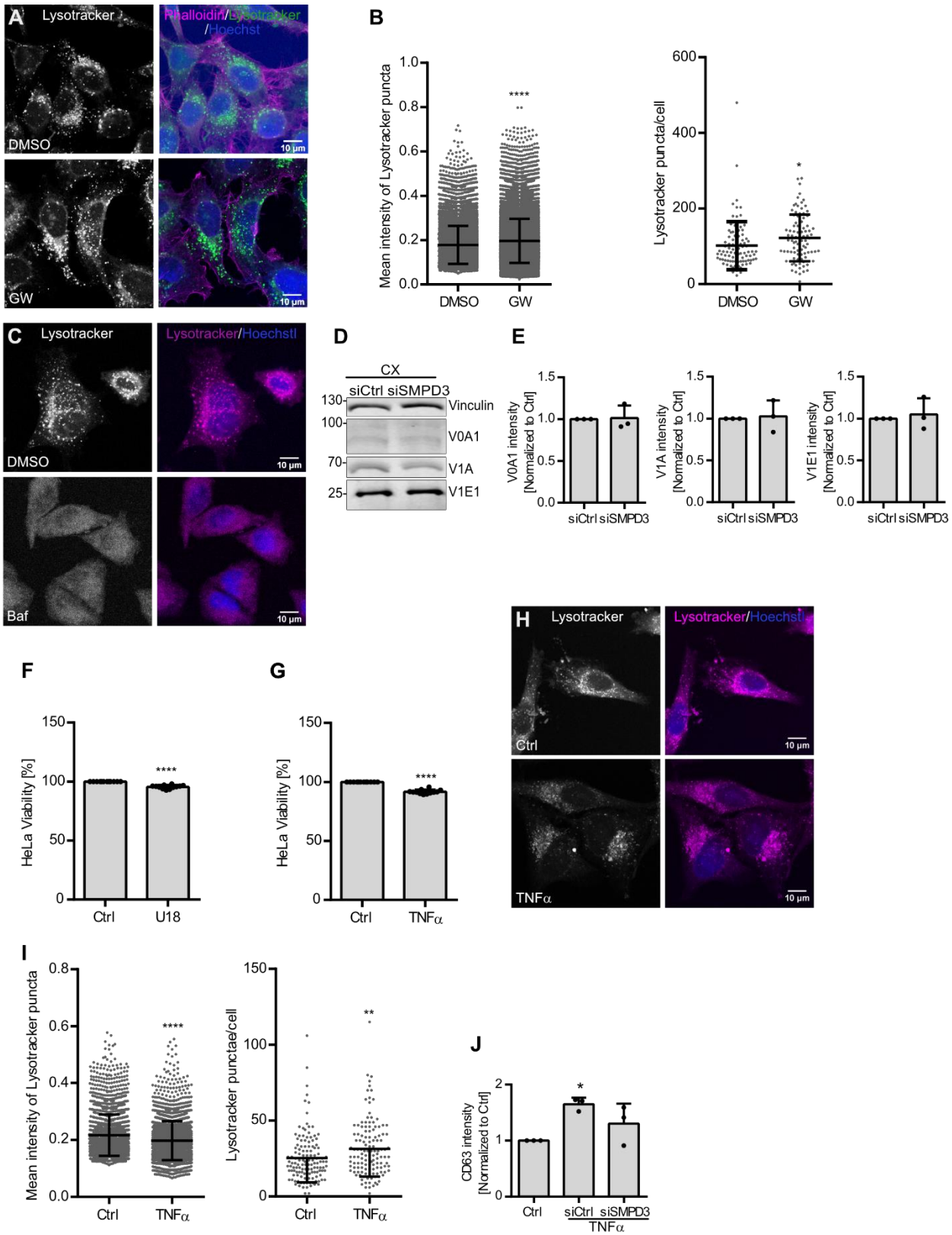

Figure S2: (A) Confocal microscopy images of DMSO- and GW4869-treated HeLa cells with intracellular acidic compartments labeled by Lysotracker (B) Quantifications of mean intensity of Lysotracker punctae (left) and lysotracker staining puncta per cell (right) from A. (mean ± s.d.;

n > 50 cells from three biological replicates. ****p < 0.0001 (Unpaired two-tailed Student's t-test). (C) Confocal microscopy images of DMSO- and Baf-treated HeLa cells with intracellular acidic compartments labeled by Lysotracker. (D) Western blot analysis of intracellular V0A1, V1A, and V1E1 in RIPA-cell lysates of HeLa cells. Vinculin was probed as a loading control. (E) Quantifications of intracellular ATP6V0A1 (V0A1), ATP6V1A (V1A), and ATP6V1E1 (V1E1) in signal intensity from D calculated by normalizing to loading control GAPDH before normalization to the respective control. (F) HeLa cell viability assay upon U18 treatment. (G) HeLa cell viability assay upon TNFα treatment. (H) Confocal microscopy images of control and TNFα treated HeLa cells with intracellular acidic compartments labeled by Lysotracker (I) Quantifications of mean intensity of Lysotracker puncta (left) and lysotracker puncta per cell (right) from H. data shown as mean ± s.d.; n > 50 cells from 3 biological replicates. ****p < 0.0001 (Unpaired two-tailed Student t-test). (J) Signal intensity quantifications of CD63 in sEV fractions from Fig. 6G calculated by normalizing the signal to loading control GAPDH levels in the corresponding cell lysates before normalization to their respective control. The data shown in E, F, G, and J represent means ± s.d. of three biological replicates; ****p < 0,0001, **p < 0,001, *p < 0.01 (Unpaired two-tailed student's t test and one-way ANOVA followed by Dunnett's multiple comparison's test for J).

2.2 Manuscript II: Neutral Sphingomyelinase 1 regulates cellular fitness at the level of ER stress and cell cycle

This manuscript is available on the preprint server bio-archive (bioRxiv) and is submitted to Review Commons for peer-review publication.

BioRxiv link:

https://biorxiv.org/cgi/content/short/2022.02.23.481585v1

Neutral Sphingomyelinase 1 regulates cellular fitness at the level of ER stress and cell cycle

Dolma Choezom[1], and Julia Christina Groß[1,2,3]

Affiliations:

[1]Developmental Biochemistry, University Medical Center Goettingen, Goettingen, Germany

[2]Hematology and Oncology, University Medical Center Goettingen, Goettingen, Germany

[3]Health and Medical University, Potsdam, Germany

***Correspondence:**

Julia Christina Gross, Health and Medical University Potsdam, Potsdam, Germany

Julia.gross@health-and-medical-university.de

Abstract

Neutral sphingomyelinase 1 (nSMase1, encoded by *SMPD2*) belongs to the sphingomyelinase enzyme family that hydrolyzes sphingomyelin to produce signaling active lipid ceramide and phosphorylcholine. The molecular characterization and biological function of nSMase1 remain poorly studied. Here, we report that *SMPD2* knockdown (KD) reduces LAMP1 at the mRNA levels and is required for initiating a full-potential unfolded protein response under ER stress. Additionally, *SMPD2* KD dramatically reduces the global protein translation rate. We further show that *SMPD2* KD cells are arrested in the G1 phase of the cell cycle and that two important cell cycle regulating processes - PI3K/Akt pathway and Wnt signaling pathway are altered. Taken together, we propose a role for nSMase1 in buffering ER stress and modulating cellular fitness via cell cycle regulation.

Keywords

Cell cycle arrest, Wnt-signaling, Ceramide, PI3K/AKT, ER stress, LAMP1, translation

Introduction

Sphingomyelin, a major lipid constituent of the plasma membrane, through its catabolic metabolism generates several bioactive signaling lipids: ceramide, sphingosine, and sphingosine1-phosphate (Hannun & Obeid, 2008). Sphingomyelindiesterases (SMPDs) or sphingomyelinases (SMases) are a family of enzymes that hydrolyze the phosphodiester bond of the sphingomyelin to produce ceramide and phosphorylcholine (Airola & Hannun, 2013). The sphingomyelinases are broadly divided into three major classes: acid sphingomyelinases, alkaline sphingomyelinases, and neutral sphingomyelinases based on their pH optima (Airola & Hannun, 2013). In mammals, four neutral sphingomyelinase members have been identified, nSMase1 (encoded by *SMPD2*) ((Tomiuk *et al*, 1998)), nSMase2 (*SMPD3*) , nSMase3 (*SMPD4*) , and mitochondrial associated nSMase (MA-nSMase; *SMPD5*) (Yabu *et al*, 2009; Wu *et al*, 2010).

We have previously shown that nSMase2 activity at the endosomal membrane regulates exosome secretion by counteracting V-ATPase-mediated endosomal acidification (Choezom & Gross, 2022). The number and different cellular localization of the neutral sphingomyelinase family members suggest distinct functions for each enzyme. NSMase1 shares identical domain architecture to ISC1, the yeast homolog to neutral sphingomyelinases (Tomiuk *et al*, 1998; Hofmann *et al*, 2000). In contrast to the overexpressed nSMase1 which localizes to the endoplasmic reticulum (Fensome *et al*, 2000; Rodrigues-Lima *et al*, 2000; Hofmann *et al*, 2000), endogenous nSMase1 exclusively localizes to the nuclear matrix (Mizutani *et al*, 2001). Although nSMase1 hydrolyzes sphingomyelin *in-vitro*, sphingomyelin metabolism remains unaffected upon its overexpression in cells (Tomiuk *et al*, 1998; Sawai *et al*, 1999). Likewise, nSMase1 mouse knockout showed no obvious phenotype with no detectable changes in

sphingomyelin metabolism (Zumbansen & Stoffel, 2002). Instead of sphingomyelin, a study has shown that nSMase1 hydrolyzes lyso-platelet-activating factor (lyso-PAF) *in-vitro* and in cells (Sawai *et al*, 1999). This indicates the putative nSMase1 could be a lyso-PAF phospholipase C with lyso-PAF as its biological substrate (Sawai *et al*, 1999). Despite being the first neutral sphingomyelinase in mammals to get cloned and identified, the biochemical and molecular characterization of nSMase1 remains poorly studied.

In contrast to the above biochemical studies, several studies have shown that ceramide generated by nSMase1 activity induces cellular death via different pathways under different stress conditions (Tonnetti *et al*, 1999; Jaffrézou *et al*, 1996; Jana & Pahan, 2004; Lee *et al*, 2004). JNK-signaling activates nSMase1 by phosphorylation to generate ceramide for apoptosis induction upon different environmental stresses such as heat shock and UV irradiation (Yabu *et al*, 2015). Given the insufficient and contrasting results on the role of nSMase1, we aimed to ascertain the biological role of nSMase1 by using siRNA-mediated gene knockdown (KD) in two human cell lines: HCT116, a human colorectal cancer cell line, and HeLa, a cervical cancer line.

Here, we discover that nSMase1 plays an important role in maintaining overall cellular homeostasis. *SMPD2* KD reduces LAMP1 (lysosomal-associated membrane protein 1) proteins levels by downregulating its mRNA. And this dramatic reduction in LAMP1 protein has no apparent effect on the function of lysosomes as autophagy remained unaffected. Interestingly, *SMPD2* KD cells are not only inefficient in activating a full-potential unfolded protein response (UPR) signaling upon ER stress but are arrested in the G1 phase of the cell cycle. We further show that two important cell cycle regulating processes - PI3K/Akt pathway and Wnt signaling pathway- are altered by *SMPD2* KD. Specifically, *SMPD2* KD affects PI3K/Akt signaling by significantly reducing the level of phosphorylated Akt. Most importantly, *SMPD2* KD significantly reduces the Wnt signaling activity by reducing β-catenin protein levels in HeLa cells and Wnt3a in HCT116 at both protein and mRNA levels. Additionally, *SMPD2* KD dramatically reduces the overall protein translation rate. These findings prove an important biological role for nSMase1 and provide strong foundations for further studies on dissecting its molecular function and pathway.

Results

SMPD2 Knockdown downregulates LAMP1 mRNA

Sphinghomylinases are active at different cellular membranes (Airola & Hannun, 2013). We have previously shown that nSMase2 (gene name: *SMPD3*) activity at the endosomal membrane regulates exosome secretion by counteracting V-ATPase-mediated endosomal acidification (Choezom & Gross, 2022). Here, we analyzed the potential role of nSMase1, a less well-understood member of the neutral sphingomyelinase family, in the regulation of endosomal trafficking decisions. *SMPD2* knockdown (KD) significantly reduced HeLa cell viability when compared with control cells. In comparison, KD of *SMPD3*, NSMAF, an activating factor of nSMase2 (Philipp *et al*, 2010), and syntenin (gene name: SDCBP), an adaptor protein involved in exosome biogenesis (Baietti *et al*, 2012), did not affect cell viability (Fig. S1A). These data indicate that *SMPD2* is a vital gene for cellular survival. Upon *SMPD3* KD, endosomal markers and acidified compartments accumulate intracellularly (Choezom & Gross, 2022). *SMPD3* KD also slightly increased lysosomal protein LAMP1 levels, in contrast, *SMPD2* KD strongly downregulated LAMP1 in both HeLa (Fig. 1A, Fig. S1B) and HCT116 (Fig. S1C). NSMAF and syntenin (encoded by *SDCBP*) KD did not alter LAMP1 protein levels (Fig. 1A). Interestingly, *SMPD2* KD did not affect lysosomal acidification as the total Lysotracker puncta per cell remained unaffected by *SMPD2* KD (Fig. 1B, C). To directly determine whether the downregulation of LAMP1 protein upon *SMPD2* KD affects lysosomal activity, we analyzed autophagy flux with two known markers – LC3B-II and P62 - by measuring their lysosomal turnover under both serum-fed and serum-starvation conditions with and without lysosomal inhibition with Bafilomycin-A (BAF) (Tanida *et al*, 2005). We found that P62 and LC3B-II flux remained unchanged upon *SMPD2* KD under both basal and serum starvation conditions (Fig. 1D-F). These data allow two conclusions: Firstly, upon SMPD2 KD, downregulated LAMP1 does not affect lysosomal function. Secondly, as LAMP1 protein levels remained downregulated even upon lysosomal inhibition (Fig. 1D), we concluded that *SMPD2* KD does not downregulate LAMP1 proteins through lysosomal degradation.

We next analyzed whether *SMPD2* KD downregulates LAMP1 through proteasomal degradation by using proteasomal inhibitor MG132. Efficient proteasomal inhibition was demonstrated by accumulation of β-catenin and ER-resident protein BiP compared with control cells (Fig. 1G), but MG132 did not affect *SMPD2* KD-induced LAMP1 downregulation, indicating that *SMPD2* KD does not downregulate LAMP1 by proteasomal degradation (Fig. 1G, Fig. S1D). As LAMP1 protein was targeted for neither lysosomal nor proteasomal degradation in *SMPD2* KD cells, we next analyzed LAMP1 mRNA levels by qPCR (Fig. 1H). Indeed, the LAMP1 mRNA level was significantly reduced by *SMPD2* KD in both HeLa (Fig. 1H) and HCT116 (Fig. S1E) cell lines. In contrast, the mRNA level of LAMP2, another closely related lysosomal membrane protein, remained unchanged upon *SMPD2* KD (Fig. S1F). Overall, these data confirm that *SMPD2* KD specifically downregulates LAMP1 not via protein degradation pathways but at the mRNA level.

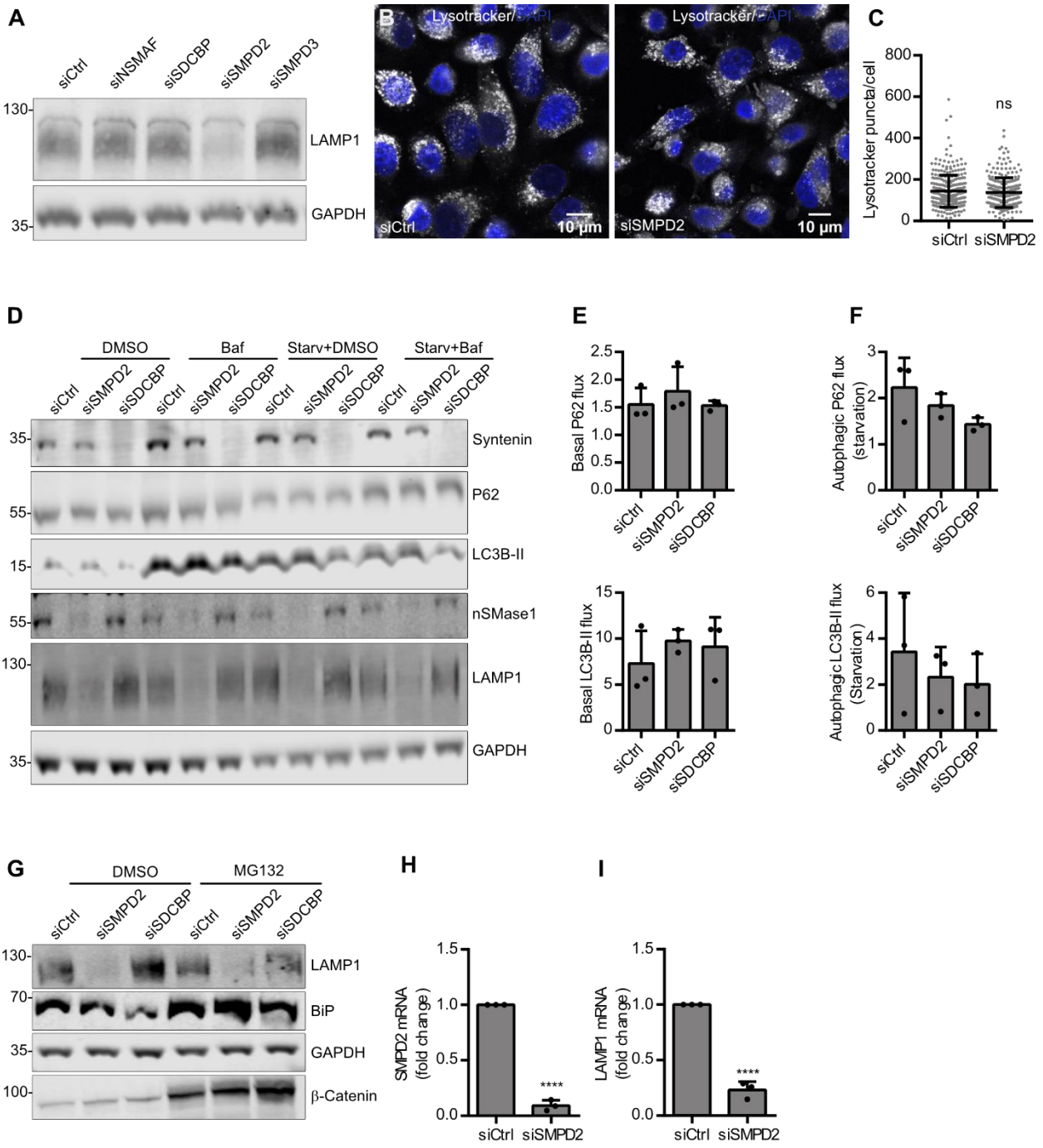

Figure 1: ***SMPD2* KD downregulates LAMP1 mRNA**. **(A)** HeLa cells were transfected with the indicated siRNAs for 48 h and lysates were immunoblotted against LAMP1 and loading control GAPDH. **(B)** HeLa cells transfected with control (Ctrl) and *SMPD2* siRNA for 48 h were stained with Lysotracker and DAPI and analyzed by confocal microscopy. **(C)** Quantifications of Lysotracker puncta per cell from (B). Unpaired Student's two-tailed *t-test*. **(D)** HeLa cells transfected with the indicated siRNAs for 48 h were then grown in FBS containing medium or serum-starved (starv) with or without Bafilomycin A (Baf) for 16 h. **(E)** Quantifications of lysosomal turnover of P62 and LC3B-II under basal conditions from (D). Ordinary one-way ANOVA followed by Dunnett's multiple comparisons test, not significant. **(F)** Quantifications of lysosomal turnover of P62 and LC3B-II under serum starvation conditions from (D). Ordinary one-way ANOVA

followed by Dunnett's multiple comparisons test. **(G)** HeLa cells transfected with the indicated siRNA for 48 h were then treated with DMSO or MG132 for 16 h. Lysates were immunoblotted against LAMP1, BiP, β-Catenin, and loading control GAPDH. **(H)** Real-time qPCR analysis of *SMPD2* mRNA in HeLa cells after 48 h of *SMPD2* KD. Unpaired Student's two-tailed *t-test*, ****p < 0.0001. **(I)** Real-time qPCR analysis of LAMP1 mRNA in HeLa cells after 48 h of SMPD2 KD. Unpaired Student's two-tailed *t-test*, ****p < 0.0001. All the experiments from (A)-(I) were done in at least three biological replicates.

SMPD2 KD causes inefficient activation of UPR upon ER stress induction

As a readout for nSMase1 activity, we used a ceramide antibody previously used for sphingomyelin metabolism and ceramide signaling studies (Vielhaber *et al*, 2001; Parashuraman & D'Angelo, 2019; Yabu *et al*, 2015). Confocal microscopy analysis upon *SMPD2* KD showed a significant reduction of staining in both mean intensity of the intracellular ceramide puncta and mean intensity of ceramide puncta that colocalize with the ER marker Calnexin (Fig. S1G, H). These data suggest that *SMPD2* KD affects cellular ceramide levels specifically at the ER. In addition to the reduced ceramide levels at the ER upon *SMPD2* KD (Fig. S1G, H), overexpressed nSMase1 localizes to the ER (Rodrigues-Lima *et al*, 2000; Fensome *et al*, 2000; Tomiuk *et al*, 2000), where transmembrane proteins such as LAMP1 are translated (Schwarz & Blower, 2016). In line with this, we found nSMase1 protein levels significantly increased upon ER stress induction with tunicamycin (Tuni) or thapsigargin (Thapsig) in HeLa cells (Fig. 2A, B). As nSMase1 protein level was increased by ER stress, we next investigated if *SMPD2* KD induces ER stress and therefore activates unfolded protein response (UPR) pathways. ER morphology appeared unchanged upon *SMPD2* KD (Fig. S1I). We analyzed three ER stress markers, BiP, Calnexin, and PDI (protein disulfide-isomerase) which are usually upregulated through UPR pathways upon ER stress induction (Oslowski & Urano, 2011) (Fig. 2C-F). We found BiP to be upregulated at the protein level by both inhibitors, which was slightly impaired by *SMPD2* KD after 4 h of treatment (Fig. 2C, D). We next analyzed different markers that are upregulated through UPR activation upon ER stress at the mRNA level. Although *SMPD2* KD alone did not activate UPR, *SMPD2* KD cells failed to upregulate several ER stress markers (sXBP-1, ATF4, and EDEM) to the same levels as their control counterparts upon stress induction (Fig. 2G-K). Furthermore, under ER stress conditions the LAMP1 mRNA remained significantly downregulated by *SMPD2* KD

(Fig. 2L). And in alignment with the increased nSMase1 protein levels (Fig. 2A, B), *SMPD2* mRNA levels were slightly increased by tunicamycin and thapsigargin treatment (Fig. 2M).

The UPR activation upon ER stress results in mRNA degradation through IRE-1 RNase activity (the RIDD pathway) to relieve stress by reducing protein translation burden in the ER (Hollien *et al*, 2009). LAMP1 mRNA was identified as a substrate of IRE-1-dependent decay of mRNAs (Maurel *et al*, 2014). If LAMP1 mRNA is degraded through the RIDD pathway upon *SMPD2* KD, we hypothesized that IRE-1 RNase activity inhibitor 4μ8C (Cross *et al*, 2012) should restore LAMP1 mRNA and protein levels. IRE-1 cleaves XBP-1 (X-box binding protein) mRNA into two transcripts, known as spliced XBP1 and 2 (sXPB1 and 2) (Maurel *et al*, 2014). The efficient inhibition of the IRE-1 RNase activity by 4μ8C was confirmed by the absence of spliced XBP-1 (sXBP-1) mRNA (Fig. S1J). However, LAMP1 mRNA, as well as protein levels, remained downregulated, when cells were treated with 4μ8C overnight after 48 h of *SMPD2* KD (Fig. S1K, L). Surprisingly, even under ER stress conditions induced by Tunicamycin treatment (Fig. S1L) *SMPD2* KD-downregulated LAMP1 protein level did not recover under 4μ8C treatment. These data indicate that reduced mRNA level upon *SMPD2* KD is not caused by degradation through the RIDD pathway.

Since *SMPD2* KD cells failed to activate an efficient UPR signaling upon ER stress induction and are less viable under normal conditions, we next analyzed how SMPD2 KD affects cellular fitness under ER stress. Indeed, *SMPD2* KD cells are less viable upon ER stress than their control counterparts; especially, *SMPD2* KD cells treated with thapsigargin are significantly less viable than *SMPD2* KD treated with DMSO. Surprisingly, 4μ8C significantly increased viability in both control and *SMPD2* KD cells (Fig. 2N). In summary, the above data suggest that although *SMPD2* KD does not downregulate LAMP1 mRNA through the RIDD pathway and does not induce ER stress, a full-potential UPR signaling activation upon ER stress is not achieved in *SMPD2 KD* cells, and consequently their cellular fitness is impaired under ER stress conditions.

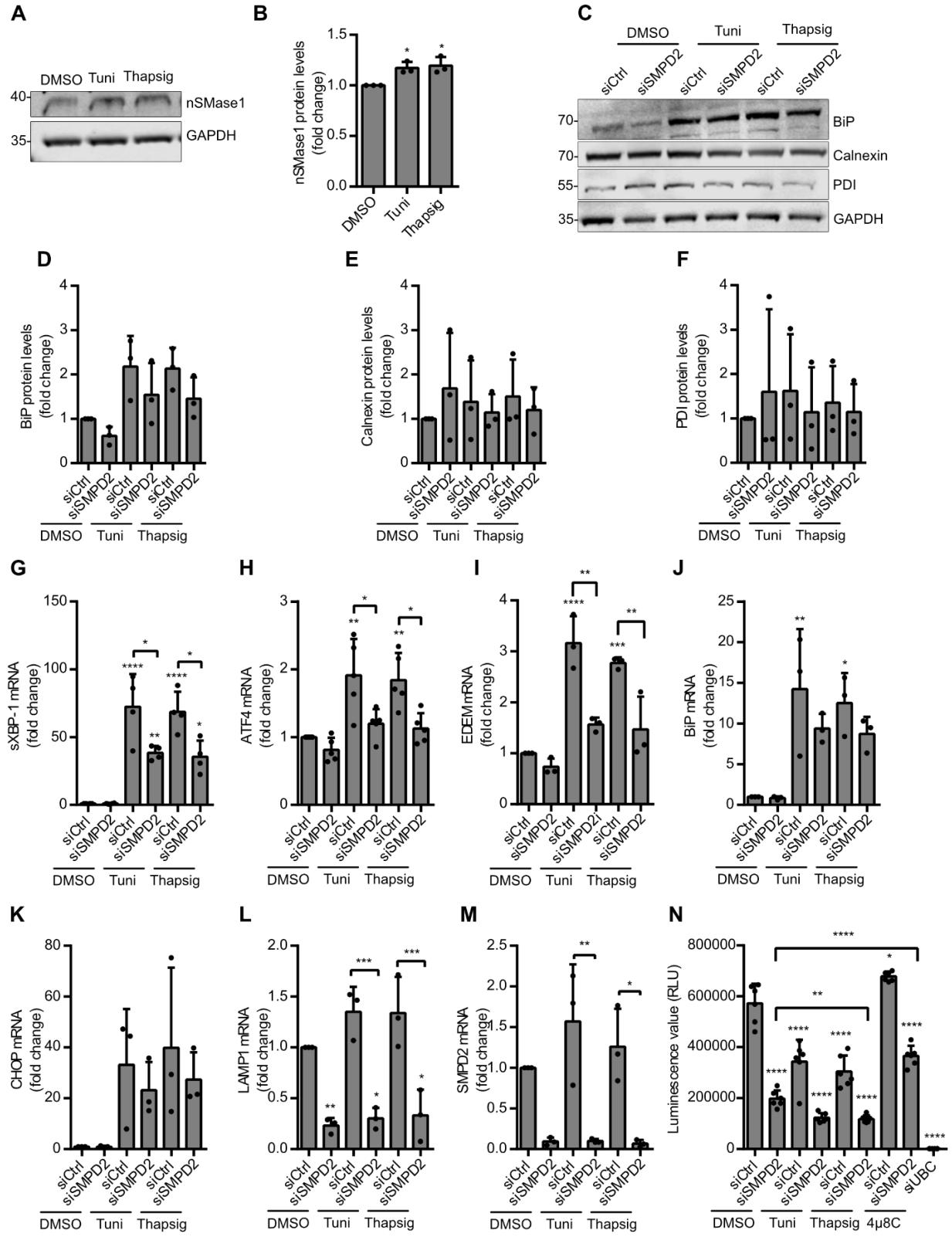

Figure 2: *SMPD2* KD causes inefficient activation of ER stress signaling. (A) HeLa cells treated with tunicamycin (Tuni) and Thapsigargin for 4 h and cell lysates were immunoblotted against nSMase1 and loading control GAPDH. **(B)** Western blot quantifications of nSMase1 from

(A) normalized to the corresponding loading control GAPDH before normalization to the control. Ordinary one-way ANOVA followed by Dunnett's multiple comparisons test, *p < 0.01 **(C)** HeLa cells transfected with Ctrl or SMP2 siRNA for 48 h were treated with tunicamycin or Thapsigargin for 4 h. Cell lysates were immunoblotted against BiP, Calnexin, PDI, and loading control GAPDH. (D-E) Western blot quantifications of BiP **(D)**, Calnexin **(E)**, and PDI **(F)** normalized to the corresponding loading control GAPDH before normalization to the control. Ordinary one-way Anova followed by Tukey's multiple comparisons test. (G-M) Real-time qPCR analysis of spliced XBP-1 (sXBP-1) **(G)**, ATF4 **(H)**, EDEM **(I)**, BiP **(J)**, CHOP **(K)**, LAMP1 **(L)**, and *SMPD2* **(M)** mRNA in HeLa cells transfected with Ctrl and *SMPD2* siRNA for 48 h and treated with tunicamycin or thapsigargin for 4 h. Ordinary one-way Anova followed by Tukey's multiple comparisons test, ****p < 0.0001, ***p < 0.0009 **p < 0.001, *p < 0.01. **(N**) Viability assay of HeLa cells transfected with Ctrl, *SMPD2*, and *UBC* siRNA for 48 h and then treated with 4μ8C (16 h) or tunicamycin or thapsigargin for 4 h. Ordinary one-way Anova followed by Tukey's multiple comparisons test, ****p < 0.0001, ***p < 0.0009 **p < 0.001, *p < 0.01. siRNA against UBC was used as a negative control for the viability assay. All experiments above, unless otherwise stated, are done in three biological replicates.

SMPD2 KD arrests cells in the G1 phase

As *SMPD2* KD significantly decreased cell viability (Fig. S1A, 2N), and JNK signaling was shown to induce apoptosis via nSMase1-induced ceramide generation under various stress conditions (Yabu *et al*, 2015), we next investigated whether *SMPD2* KD induces apoptosis using flow cytometry (Fig. S2A). In alignment with the previous results (Fig. S1A, 2N), *SMPD2* KD significantly reduced viable cells in an Annexin/PI assay (Fig. 3A). Although early apoptosis was significantly increased (A^-/PI^+), no significant change in late apoptosis (A^+/PI^+) and necrosis levels (A^-/PI^+) were observed upon *SMPD2* KD (Fig. 3A). Concordantly, *SMPD2* KD did not induce the cleavage of different apoptosis marker proteins as determined by western blot analysis of Caspase-3, -7, and PARP (Fig. 3B, Fig.S2B-E).

Since the reduced cell viability upon *SMPD2* KD is not caused by apoptosis, we next analyzed the cell proliferation rate by incucyte imaging. Indeed, the cell proliferation rate was significantly lowered by *SMPD2* KD (Fig. 3C). Additionally, *SMPD2* KD cells are significantly bigger when compared to the control cells (Fig. 3D, Fig. S2F), suggesting an *SMPD2* KD-induced cell cycle delay. Cell cycle progression analysis by flow cytometry (Fig. S2G) revealed *SMPD2* KD to significantly increase the percentage of cells in G1 (Fig. 3E). The percentage of cells in G1 was furthermore increased (by around 20%) when *SMPD2* KD duration was increased from 48 h to 72 h (Fig. 3F) and reduced slightly after

96 h when compared to the 72 h *SMPD2* KD (Fig. S2H). Overall, these data indicate that a significant number of *SMPD2* KD cells show a delay in cell cycle progression. To test whether *SMPD2* KD causes a transient G1 arrest, we analyzed the protein expression of two G1 cell cycle arrest markers – P21 and P27, along with P53 which regulate these two proteins (Chen, 2016). *SMPD2 KD* significantly upregulated the protein expression of both P21 and P27 (Fig. 3G, H), while P53 protein levels remained unchanged upon *SMPD2* KD (Fig. S3A). In agreement with the FACS data (Fig. 3F), both P21 and P27 protein expression reached a maximum after 72 h of *SMPD2* KD (Fig. 3G, H) when compared to 96 h *SMPD2* KD (Fig. S3B, C). In summary, these data indicate that *SMPD2* KD cells are bigger and proliferate slower than the control cells, as they are arrested in the G1 phase of the cell cycle at the peak of the transient *SMPD2* KD.

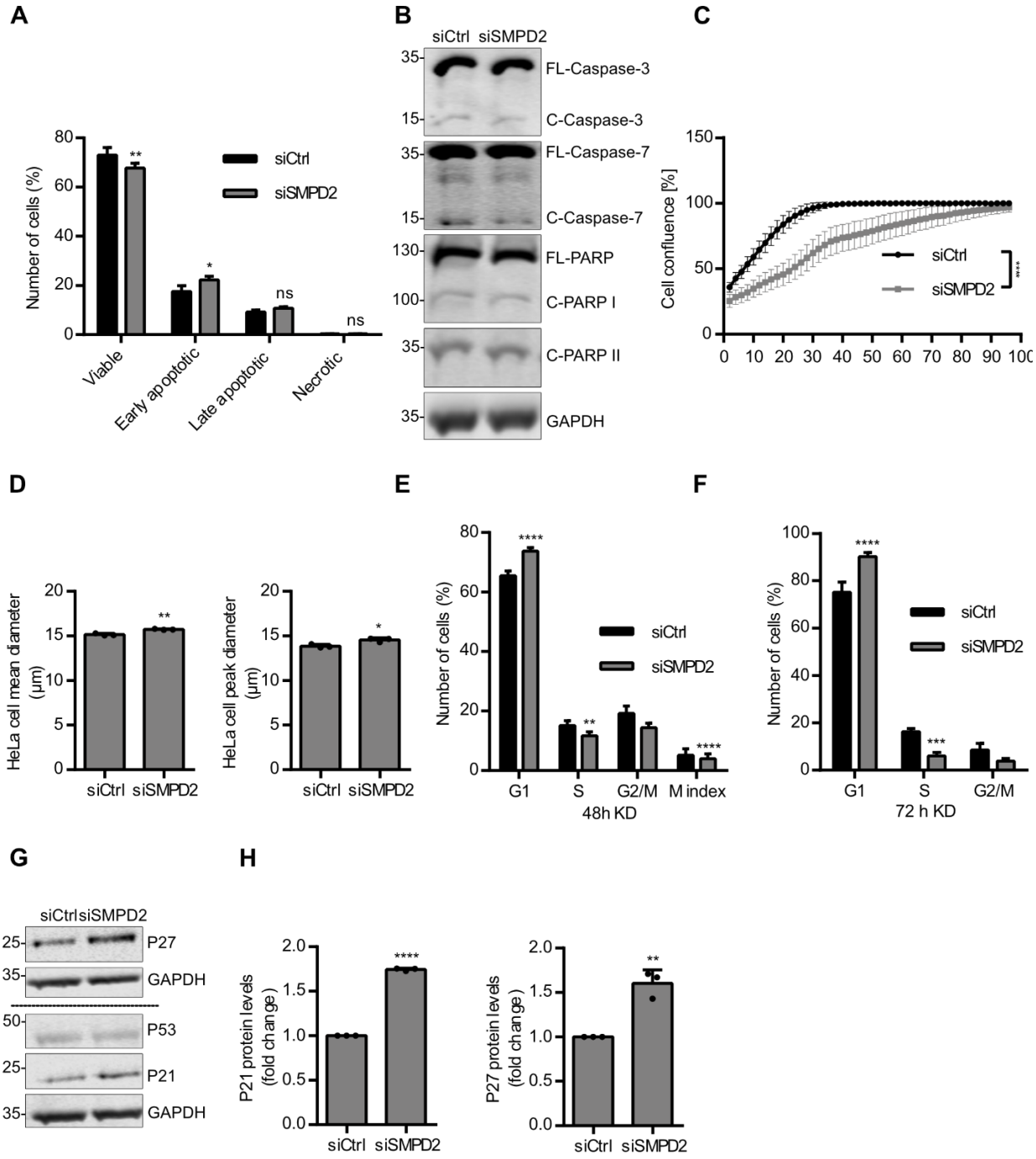

Figure 3: *SMPD2* KD arrests cells in the G1 phase. (A) Percentage of HeLa cells transfected with Ctrl or *SMPD2* siRNA for 48 h were analyzed by flow cytometry and sorted into Viable (Annexin-V^-/PI^-), Early apoptotic (Annexin-V^+/PI^-), Late apoptotic (Annexin-V^+/PI^+), and Necrotic (Annexin-V^-/PI^+). Two-way ANOVA followed by Sidak's multiple comparisons test, **p < 0.001, *p < 0.01. **(B)** HeLa cells were transfected with Ctrl or *SMPD2* siRNA for 48 h and then cell lysates were immunoblotted against different apoptosis markers and loading control GAPDH. **(C)** HeLa cells transfected with Ctrl or SMPD siRNA for 48 h were replated and seeded into a 96-well plate for Incucyte proliferation analysis. Proliferation rate was measured by cell confluence percent versus time by taking images of the wells at 2 h intervals for the indicated duration. Paired Student's two-tailed *t-test*, ****p < 0.0001. **(D)** HeLa cell mean diameter (Left) and peak diameter

(Right) determined with Casy cell counter after 72 h of Ctrl or *SMPD2* siRNA transfection. Unpaired Student's two-tailed *t-test*, *p < 0.01. (E-F) Percentage of HeLa cells transfected with Ctrl or SMPD2 siRNA for 48 h **(E)** and 72 h **(F)** were gated for G1, S, and G2/M. Mitotic index in (E) was determined from the G2/M population positive for p-Mpm-2 staining. Two-way ANOVA followed by Sidak's multiple comparisons test, ****p < 0.0001, ***p < 0.0009 **p < 0.001. **(G)** Lysates from HeLa cells transfected with Ctrl or SMPD2 siRNA for 72 h were immunoblotted against P27, P53, P21, and loading control GAPDH. **(H)** Western blot quantifications of P21 (Left) and P27 (Right) normalized to the corresponding loading control GAPDH before normalization to the control. Unpaired Student's two-tailed *t-test*, ****p < 0.0001, **p < 0.001. All experiments from (A) to (H) are done in three biological replicates.

SMPD2 KD downregulates the Wnt signaling pathway

Next, we investigated the molecular pathway through which *SMPD2* KD causes G1 cell cycle arrest. Since various lipids in the nucleus are indicated to regulate many processes including gene transcription (Martelli *et al*, 2004), we analyzed if *SMPD2* KD upregulates P21 and P27 for G1 arrest through the P53-dependent DNA damage response pathway. DNA damage, through ataxia telangiectasia mutated (ATM) or Rad3-related protein (ATR), phosphorylates two checkpoint kinases (Chk1 and Chk2) which then activates P53 by phosphorylation (Chen, 2016) (Fig. 4A). Activated P53 upregulates, among many of its target genes, two cell cycle inhibitory proteins P21 and P27. Therefore, an increase in phosphorylated Chk1 and Chk2 could indicate activation of the DNA damage response pathway upon *SMPD2* KD. The expression level of the phosphorylated Chk1 and phosphorylated Rb (Retinoblastoma protein), another cell cycle inhibitory protein, was not changed by *SMPD2* KD (Fig. 4B, C; Fig. S3D). However, *SMPD2* KD significantly decreased the phosphorylated Chk2 level (Fig. 4B, C), in line with a role of Chk2 at the crossroad of DNA damage and metabolic fitness (Ajazi *et al*, 2021).

Extracellular growth signals are integrated into intracellular signals by pathways such as PI3K/Akt to drive cell cycle progression (Vivanco & Sawyers, 2002) (Fig. 4D). *SMPD2* was shown to exhibit a negative gene interaction with PTEN (phosphatase and tensin Homolog), a tumor suppressor gene that inhibits G1-S transition by antagonizing PI3k/Akt pathway activation (Fig. 4D) (Vizeacoumar *et al*, 2013). Therefore, we analyzed the level of phosphorylated PTEN and AKT upon *SMPD2* KD. Although phosphorylated PTEN levels remained unchanged, *SMPD2* KD significantly reduced the level of phosphorylated Akt (Fig. 4E, F). This suggests that *SMPD2* KD could affect PI3K/Akt pathway.

Wnt signaling is another major pathway that drives cell proliferation (Freese *et al*, 2010). Interestingly, *SMPD2* KD not only reduced Wnt activity but also reduced the APC KD-stabilized Wnt activity (Fig. 4G). Reduction of APC KD-stabilized wnt activity by *SMPD2* KD indicates that the KD affects the Wnt signaling at the level or downstream of β-catenin. Indeed, β-catenin protein levels were downregulated by *SMPD2* KD in HeLa cells (Fig. S3E, F). Surprisingly, in HCT116 cells, although β-catenin protein levels remained unchanged upon *SMPD3*, Wnt3a protein levels were significantly reduced by *SMPD2* KD (Fig. 4H, I). We furthermore analyzed Wnt signaling components upon *SMPD2* KD by qPCR in HCT116. In alignment with the reduction in Wnt3a protein levels, *SMPD2* KD dramatically reduced Wnt3a mRNA (Fig. 4J). Surprisingly, *SMPD2* KD significantly upregulated AXIN2 mRNA (Fig. 4J), which is involved in the negative feedback loop of Wnt signaling (Lustig *et al*, 2001). The mRNA levels of the other Wnt signaling components CTNNB-1, EVI, and WNT7B remained unchanged upon *SMPD2* KD (Fig. S3G). Additionally, SMPD4, another member of nSMases, showed no compensatory increase in mRNA levels upon *SMPD2* KD (Fig. S3H).

Since many proteins and mRNA are downregulated upon *SMPD2* KD, we next analyzed the overall protein translation upon *SMPD2* KD by puromycin assay (Goodman & Hornberger, 2013) and using protein translation inhibitor cycloheximide (CHX) as a negative control. Indeed, *SMPD2* KD significantly reduced the overall protein translation (Fig. 4K, L).

In summary, the data above indicate that *SMPD2* KD seems to affect many cellular processes by downregulating their signaling components including Wnt signaling – which could explain the reduction in global protein translation and G1 cell cycle arrest.

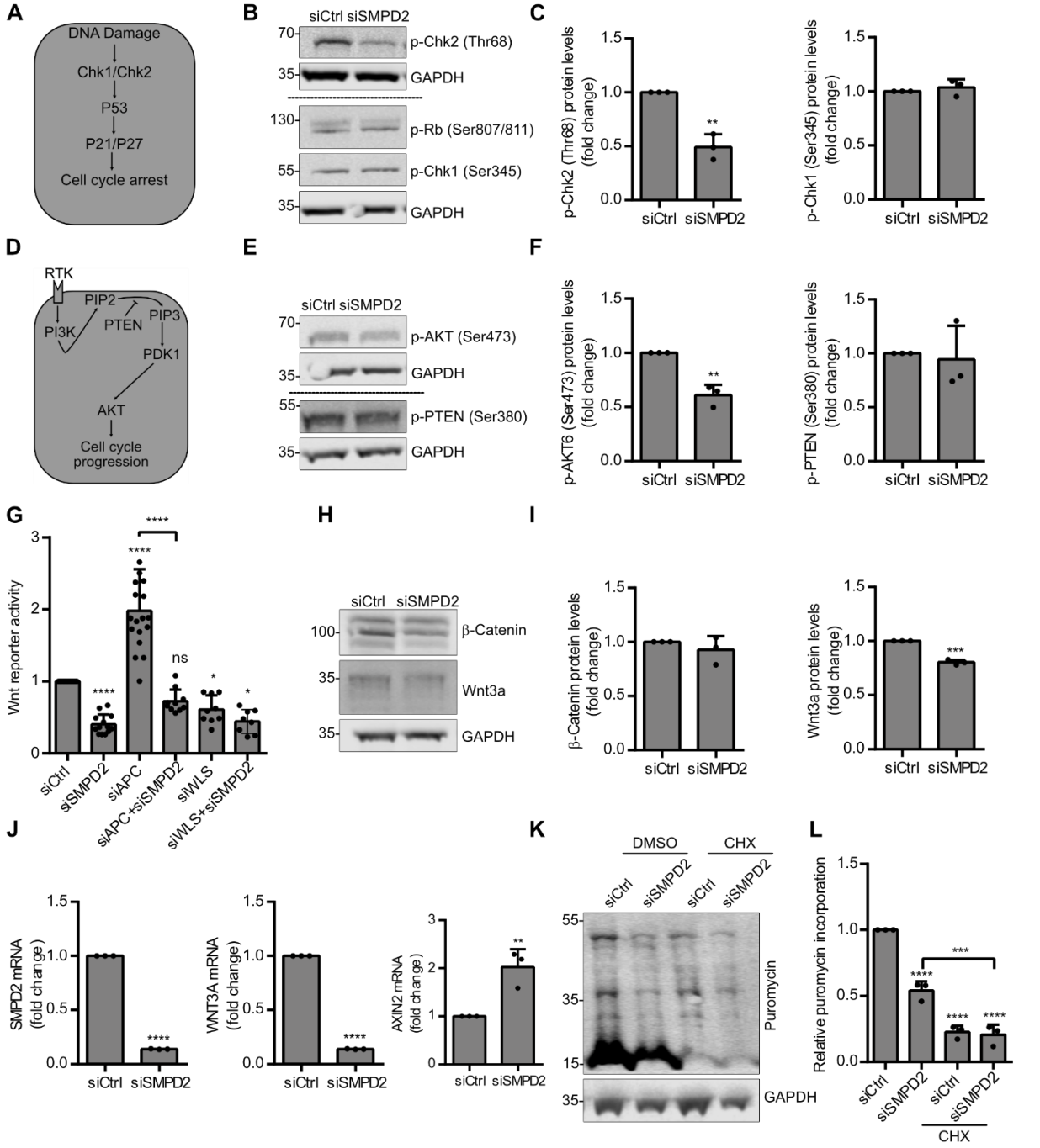

Figure 4: Wnt signaling is downregulated in *SMPD2* KD cells. **(A)** Scheme showing P53-dependent DNA damage response pathway that mediates G1 cell cycle arrest. **(B)** Lysates from HeLa cells transfected with Ctrl or *SMPD2* siRNA for 48 h were immunoblotted against the p-Chk2, p-Chk1, p-Rb, and loading control GAPDH. **(C)** Western blot quantifications of p-Chk1 and p-Ch2 from (B) normalized to the corresponding loading control GAPDH before normalization to the control. Unpaired Student's two-tailed *t-test*, **p < 0.001. **(D)** Scheme showing PI3K/Akt signaling pathway. **(E)** Lysates from HeLa cells transfected with Ctrl or *SMPD2* siRNA for 48 h were immunoblotted against the p-Akt, p-PTEN, and loading control GAPDH. **(F)** Western blot quantifications of p-Akt and p-PTEN from (E) normalized to the corresponding loading control GAPDH before normalization to the control. Unpaired Student's two-tailed *t-test*, **p < 0.001. **(G)**

Wnt reporter activity analysis in HCT116 cells transfected with the indicated siRNAs for 72 h measured using TCF/LEF luciferase reporter assay. The reporter vectors were transected 24 h after siRNA reverse transfection. Ordinary one-way Anova followed by Tukey's multiple comparisons test, ****p < 0.0001, *p< 0.01. **(H)** HCT116 cells were transfected with Ctrl or *SMPD2* siRNAs for 72 h and lysates were immunoblotted against β-catenin, Wnt3a, and loading control GAPDH. **(I)** Western blot quantifications from (I) normalized to the corresponding loading control GAPDH before normalization to the control. Unpaired Student's two-tailed *t-test*, ***p < 0.0009. **(J)** Real-time qPCR analysis of *SMPD2*, WNT3A, and AXIN2 mRNA in HCT116 cells transfected with Ctrl and *SMPD2* siRNA for 72 h. Unpaired Student's two-tailed *t-test*, ****p < 0.0001. **(K)** HeLa cells were transfected with Ctrl or *SMPD2* siRNA for 48 h and treated with or without Cycloheximide (CHX) for 16 h. Lysates, after labeling with puromycin for 1 h, were immunoblotted against puromycinylated proteins with puromycin antibody. **(L)** Western blot quantifications from (K) normalized to the corresponding loading control GAPDH before normalization to the control. Ordinary one-way Anova followed by Tukey's multiple comparisons test, ****p < 0.0001, ***p < 0.009. All experiments from (A)-(L) are done in three biological replicates.

Discussion

We found that nSMase1 plays an important role in maintaining cellular fitness. NSMase1 is required for activating a full-potential adaptive UPR upon ER stress induction with tunicamycin and thapsigargin- two inhibitors that cause ER stress through distinct mechanisms. *SMPD2* KD cells failed to upregulate multiple genes that are usually upregulated through UPR pathways upon ER stress to the same levels as their control counterparts. Furthermore, we show that nSMase1 is necessary for proper cell cycle progression during the G1 phase as *SMPD2* KD led to a significant G1 arrest. Moreover, the overall protein translation at the ribosome was reduced by SMPD2 KD. These data, for the first time, establish an important biological role for *SMPD2* at the level of UPR activation upon ER stress and cell cycle progression.

We further show that nSMase1 regulates LAMP1 protein expression at the level of its mRNA but not LAMP2. LAMP1 and LAMP2 are the major glycoproteins localized on the lysosomal membrane and thought to contribute to lysosomal integrity, catabolism, and pH maintenance (Sawada *et al*, 1993). *SMPD2* KD downregulated LAMP1 mRNA and thereby reduced its protein expression. Interestingly, lysosomal acidification and function remain unaffected by this significant reduction in the LAMP1 protein levels as both lysotracker staining and the autophagy flux remained unchanged. Therefore, the downstream biological implication of this dramatic LAMP1 downregulation upon *SMPD2* KD would be of great interest for future studies.

ER stress is sensed by three ER membrane proteins – IRE1α, PERK, and ATF6α – which initiate UPR through three distinct pathways by upregulating different proteins (Hetz *et al*, 2020). Although nSMase1 expression was increased by ER stress, *SMPD2* KD alone did not induce an ER stress condition as no UPR activation was observed. Upon ER stress induction, *SMPD2* KD cells failed to upregulate multiple genes under the control of all three master regulators. These data indicate that *SMPD2* KD affects all the three UPR pathways in the ER. Indeed, several early studies have shown that overexpressed nSMase1 resides in the ER (Fensome *et al*, 2000; Rodrigues-Lima *et al*, 2000; Tomiuk *et al*, 2000) and recent affinity-based mass spectrometry studies have shown that nSMase1 interacts with multiple ER-resident proteins including reticulon 3 and reticulon 4 (Huttlin *et al*, 2017, 2021). Therefore, based on the observations from our study, it is clear that nSMase1 plays a functional role in restoring ER function and homeostasis under ER stress conditions. The UPR signaling activation persists until an adaptive response to the ER stress is achieved, in the case of unresolvable stress, the UPR turns pro-apoptotic to induce cell death (Hetz *et al*, 2020). Indeed, due to their inability to mount a full-potential UPR signaling, *SMPD2* KD cells are less viable upon ER stress induction.

Additionally, *SMPD2* KD significantly downregulated LAMP1 and Wnt3a mRNAs – both of which are translated and subsequently modified in the ER as an integral membrane and a secretory protein respectively. NSMase1 could affect signaling recognition particle (SRP)-dependent targeting of these proteins to the ER for translation as nSMase1 was shown to interact with both signal recognition particle receptor B (SRPRB) and the translocon-associated signal sequence receptor 2 (SSR2). These two proteins are ER membrane proteins required for proper docking of the whole mRNA:ribosome:polypeptide:SRP complex to the ER for efficient translation (Akopian *et al*, 2013). It is therefore conceivable that nSMase1 plays an important role in the translation of these proteins possibly by providing specific lipids to establish membrane nanodomains for efficient docking of this co-translation machinery to the ER. In this way, downregulation of LAMP1 and Wnt3a could be due to a disrupted SRP-dependent targeting of these mRNAs to the ER for translation upon *SMPD2* KD. In line with its ER localization and potential functions, nSMase1 also interacts with several GPI (Glycosylphosphatidylinositol) anchor attaching proteins such as

glycosylphosphatidylinositol anchor attachment 1 (GPAA1) and Phosphatidylinositol glycan anchor biosynthesis, class S (PIG-S) (Huttlin *et al*, 2021).

Overall, the data from others and our study demonstrate that nSMase1 at the ER plays an important role in activating an efficient adaptive UPR upon ER stress and could also regulate other aspects of ER function such as translation and post-translational modifications.

Since *SMPD2* KD cells are arrested in the G1 phase with both P21 and P27 upregulated, it is possible that nSMase1 activity, by generating required structural lipids, might drive the remodeling of the nuclear envelope, chromatin, and nuclear matrix during cell cycle progression (Mizutani *et al*, 2001). Alternatively, since nSMase1 belongs to the superfamily of endo/exonucleases (Bill X.Wu, Christopher J.Clarke, 2010) that cleave the phosphodiester bond between the successive nucleotides, it may hydrolyze the phosphodiesterase bond of the DNA. As described for many endo/exonucleases (Nishino & Morikawa, 2002), it, therefore, could be involved in DNA repair and cell cycle progression. In this way, inefficient DNA repair upon *SMPD2* KD might induce a DNA-damage-like response that upregulates P21 and P27 to induce G1 cell cycle arrest. Therefore, it is noteworthy to further investigate the activation of tumor suppressor gene P53 upon *SMPD2* KD. P53 senses DNA damage and mediates cell cycle arrest by upregulating P21 and P27 (Chen, 2016).

Duplication of not only cellular DNA content but also of membranes and organelles is a prerequisite for cellular growth and division. Lipids – both storage and membrane – play an important role in cell cycle regulation (Storck *et al*, 2018). For example, two triacylglycerol lipases Tgl3 and Tgl4 are required for efficient cell cycle progression during the G1/S transition in yeast cells (Chauhan *et al*, 2015). Specifically, lipolysis-derived sphingolipids activate PP2A, a major cell cycle regulating protein phosphatase, to dephosphorylate SWE1 (human ortholog WEE1) for efficient cell cycle progression (Chauhan *et al*, 2015). Therefore, it is conceivable that ceramide generated by nSMase1 acts as a second messenger targeting proteins involved in cell-cycle regulation such as PP2A. Indeed, several studies proposed PP1 and PP2A as the potential intracellular protein target of ceramide. PP2A dephosphorylates over 300 substrates involved in the cell cycle, thereby regulating almost all the major pathways including the Wnt pathway

and the cell cycle checkpoints (Wlodarchak & Xing, 2016). Therefore, reduced Wnt-signaling could be also due to deregulated PP2A activity upon *SMPD2* KD. Collectively, these data suggest that nSMase1 plays an important role in overall cellular fitness and proliferation without which cells enter a transient G1 arrest with reduced global protein translation.

So far, the biological role as well the physiological substrate for nSMase1 is unknown. Our study shows that nSMase1 plays a vital role in overall cellular fitness and survival as *SMPD2* KD induced transient G1 arrest. Additionally, nSMase1 activity is essential for activating an efficient UPR upon ER stress induction. The observations and data described herein would serve as a strong foothold for further studies in unraveling not only the molecular function but also the molecular pathways through which nSMase1 contributes to maintaining cellular homeostasis.

Materials and methods

Cell culture and transfection (siRNA and plasmids)

HeLa (kindly provided by Holger Bastians, Goettingen) and HCT116 cells (DSMZ) were maintained in DMEM (Thermo Fischer Scientific Life technologies, 52100021) supplemented with 10% fetal calf serum (Biochrom) and 10 µg/ml Penicillin/Streptomycin (Sigma-Aldrich, P4333) at 37 °C in a humidified atmosphere with 5% CO_2. Cells were transiently transfected with ScreenFect-siRNA (Screenfect) for indicated duration according to the manufacturer's instructions. The cells were authenticated and routinely checked for mycoplasma contamination. Cells were treated with the drugs in the following concentrations for indicated durations. Bafilomycin (Sigma-Aldrich, 100ng/ml, 16 h); MG132 (Sigma-Aldrich, 100 ng/ml, 16 h); 4µ8C (Millipore Merck, 49 µM, Duration as indicated); Cycloheximide (Carlroth, 20 µg/ml, 16 h).

Table 2: Dharmacon siRNA SMARTpools against the indicated genes used in the study

Target Gene	Catalog Number	Sequence
SMPD2	D-006677-01	5’-GCAGAGAGGUCGCCGUUGA-3’
	D-006677-02	5’-GGAGGUCAAUGGCUUAUAU-3'
	D-006677-03	5’-CAAGGCAGUUUCUGGGUUU-3'
	D-006677-04	5’-UGAAACCACUACAGGCUUU-3'
APC	D-003869-05	5’-GAUGAUAUGUCGCGAACUU-3'
	D-003869-06	5’-GAGAAUACGUCCACACCUU-3'
	D-003869-07	5’-GAACUAGAUACACCAAUAA-3'
EVI/ WLS	D-018728-01	5’-ACGAAUCCCUUCUACAGUA-3'
	D-018728-02	5’-UAACGGAAGGCCAUUGGAA-3'
	D-018728-03	5’-UAAAGGAUAUCCGGUUGGU-3'
	D-018728-04	5’-GAACCACAUCGCAGGGUAU-3'
SDCBP	D-008270-01	5’-GCAAGACCUUCCAGUAUAA-3'
	D-008270-02	5’-UAACAUCCAUAGUGAAAGA-3'
	D-008270-03	5’-GAAGGACUCUCAAAUUGCA-3'
	D-008270-04	5’-GGAUGGAGCUCUGAUAAAG-3'
NSMAF	D-017920-01	5’-CGAGUGGAUUGAUCUAAUA-3'
	D-017920-02	5’-UUACGCAAAUCUUGGAAUU-3'
	D-017920-03	5’-CGCAAUGGAUCUUCAGUAU-3'
	D-017920-04	5’-CGACAUCUACCAAAAGUUC-3'

SMPD3	D-006678-01	5’-CAAAGCGGCCUCCUCUUU-3’
	D-006678-04	5’-CAAGCGAGCAGCCACCAAA-3’
	D-006678-17	5’-ACCAAAGAAUCGUCGGGUA-3’
	D-006678-18	5’-CGAACGGCCUGUACGAUGA-3’
UBC	D-19408-01	5'-GUGAAGACCCUGACUGGUA-3'
Non-targeting	D-001210-03	5’-AUGUAUUGGCCUGUAUUAG-3'

Antibodies

The following antibodies and dilutions were used for western blot (WB) or for immunofluorescence staining (IF): LAMP1 (WB 1:1000, Abcam, ab24170); Syntenin (WB 1:1000, Abcam, ab133267); GAPDH (WB 1:1000, Millipore, CB1001); Calnexin (WB 1:1000, Abcam, ab75801), P62/SQSTM1 (WB 1:1000, Abnova,H00008878-M01); MAP LC3B (WB 1:1000, Santa Cruz, sc-376404); Ceramide (IF 1:100, Enzo, ALX-804-196); BiP (WB 1:1000, CST, 3177T), nSMase1 (WB 1:1000, Sigma, SAB1404383); β-Catenin (WB 1:1000, BD Transduction, 610154), PDI (WB 1:1000, CST,3501T), FL-Caspase 3 (WB 1:1000, CST, 14220T); C-Caspase-3 (WB 1:100, CST, 9664T), FL-Caspase 7 (WB 1:1000, CST, 12827T); C-Caspase-7 (WB 1:1000, CST, 8438T); FL-PARP (WB 1:1000, CST, 9542T), C-PARP (WB 1:1000, CST, 5625T), p-Chk2 (Thr68) (WB 1:1000, CST, 2197T); p-Rb (Ser807/811) (WB 1:1000, CST, 8516T); p-Chk1 (Ser345) (WB 1:1000, CST, 2348T); p-AKT (Ser473) (WB 1:1000, CST, 4060T); Puromycin (WB 1:1000, Millipore, MABE343); pPTEN (Ser380) (WB 1:1000, CST, 9551T); p27 Kip1 (WB 1:1000, CST, 3686T), p21 Waf1/Cip1 (WB 1:1000, CST, 2947T)

Western blot analysis

Cell lysates in the SDS-PAGE sample buffer were boiled for 5 min before separating the protein on 4-12% gradient gels (Bolt Bis-Tris Plus Gels, Thermo Scientific). Proteins were

then transferred onto PVDF membranes (Merck) and blocked with 5% (wt/vol) milk-TBST for 30 min before incubating with primary antibodies overnight at 4°C. After washing, membranes were incubated with fluorescently labeled secondary antibodies at room temperature in the dark and detected using the Li-COR Odyssey system. Western blot quantifications were done with Odyssey Infrared Image Studio Lite Ver 5.2

Autophagy flux measurement

Densitometric analysis of the LC3B-II, P62, and GAPDH bands was performed using Odyssey Infrared Image Studio Lite Ver 5.2. To determine autophagy flux, under both basal and serum-starvation autophagy induced conditions, lysosomal turnover of endogenous LC3B-II and P62 were determined. LC3B-II and P62 bands were normalized to GAPDH (LC3B-II/GAPDH, P62/GAPDH). Autophagy flux was then determined by dividing the normalized value of the Bafilomycin-treated lysate by the normalized value of the control-treated lysate of the same sample(Tanida *et al*, 2005).

Immunostaining, microscopy, and image analysis

Cells were grown in 8-well microscopic coverslips (Sarstedt and IBIDI for live imaging), reverse transfected with indicated siRNAs, and were fixed and permeabilized with 4% paraformaldehyde and 0.2% Triton-X-100. The slides were then blocked in 3% bovine serum albumin diluted in PBS, followed by 90 min incubation with primary antibodies. After washing three times, cells were incubated with secondary antibodies conjugated to Alexa-Fluor-488 or 546. Nuclei and actin were labeled by Hoechst and conjugated phalloidin respectively. 200 nM ER tracker (Thermo Scientific Life technologies, E34250) were added to live cells. The cells were visualized with a Zeiss LSM780 confocal microscope (Plan Neofluor 63X/oil NA 1.4 objective). Staining and microscopy conditions were kept identical for comparisons. The number of puncta/cell quantifications were performed using available pipelines with some modifications in CellProfiler (Broad Institute of MIT and Harvard).

CellTiter-Glo® luminescent viability assay

Cell viability was measured by performing a CellTiter-Glo assay (Promega, G8461). Cells were seeded in a 96-well plate. After reverse siRNA transfection or drug treatment for the indicated duration, 100 μl of the cell titer glow reagent (Promega) diluted to 1:5 with PBS were added to each well. The plate was incubated on a shaker for 2 min at RT to allow cell lysis and then incubated without shaking for 10 min at RT to allow luminescence signal stabilization. The signal was measured using a Centro LB 960 microplate luminometer (Berthold Technologies) and data were analyzed using MikroWin 2000 lite Version 4.43.

Incucyte proliferation assay

HeLa cells transfected with control or *SMPD2* siRNA for 48 h were replated and 6000 transfected cells per well were seeded into Incucyte® Imagelock 96-well plates. The real-time proliferation of the cells was detected by the Incucyte® S2 Live Cell Analysis System (Sartorious) by imaging each well at 2 h intervals.

RNA isolation and real-time qPCR

Total cellular RNA was isolated using Trizol (Thermo Scientific Invitrogen). The reverse transcription was carried out with 2 µg of RNA. The resulting cDNA product was analyzed by real-time quantitative PCR using Taq Universal SYBRgreen Supermix (Bio-Rad). Transcript Ct-values were converted to fold change expression changes (2-$\Delta\Delta$Ct values) after normalization to the housekeeping gene β-actin. Quantitative real-time PCR was performed using a CFX system (Bio-Rad).

Table 3: List of primers with their respective sequences used in the study

Gene	Company	Sequence (5'-3')
SMPD2	Merck Millipore	FP: TTTGCTGGAGGAGGTGTGGAG
		RP: AAGCTCCTGGATTGGATGTTTGG
LAMP1	Merck Millipore	FP: CAGTTCGGGATGAATGCAAG
		RP: TGCACTTGTAGGAATTGCCG
CHOP	Merck Millipore	FP: AGAACCAGGAAACGGAAACAGA
		RP: TCTCCTTCATGCGCTGCTTT
EDEM	Merck Millipore	FP: CAAGTGTGGGTACGCCACG
		RP: AAAGAAGCTCTCCATCCGGTC
BiP	Merck Millipore	FP: TGTTCAACCAATTATCAGCAAACTC
		RP: TTCTGCTGTATCCTCTTCACCAGT
Calnexin	Merck Millipore	FP: TTCACATAGGCACCACCACA
		RP: GGAAGTGGTTGCTGTGTATG
CTNNB-1	Merck Millipore	FP: AAGCGGCTGTTAGTCACTGG
		RP: CGAGTCATTGCATACTGTCCAT
sXBP-1	Merck Millipore	FP:C TGAGTCCGAATCAGGTGCAG
		RP: ATCCATGGGGAGATGTTCTGG
WNT3A	Merck Millipore	FP: AGCAGGACTCCCACCTAAAC RP
		RP: AGAGGAGACACTAGCTCCAGG
WNT7B	Merck Millipore	FP: CCCGGCAAGTTCTCTTTCTTC
		RP: GGCGTAGCTTTTCTGTGTCCAT
β-actin	Merck Millipore	FP: GAGCACAGAGCCTCGCCTTT
		RP: ACATGCCGGAGCCGTTGTC
ATF4	Merck Millipore	FP: GTTCTCCAGCGACAAGGCTA
		RP: ATCCTGCTTGCTGTTGTTGG
SMPD3	Merck Millipore	FP: GTGTAACGACGATGCCCTGG
		RP: GGATGGCGCTGTCCTCTTG

Wnt reporter activity assay

Endogenous Wnt signaling activity was assessed by employing a dual-luciferase β-catenin/TCF4 reporter assay. HCT116 cells were transfected with a TCF firefly reporter plasmid (pgGL4.1-6xKD FLuc) (Demir *et al*, 2013) and a constitutively β-catenin renilla reporter plasmid (pgGL4.1-RLuc) (Demir *et al*, 2013) 24 h after reverse transfection with the indicated siRNA. Relative Wnt reporter activity was determined by normalizing the firefly luminescence value to the renilla luminescence value after 48 h of the plasmid transfection.

Cell cycle analysis by flow cytometry

Flow cytometry was used to analyze cell cycle distribution. Trypsinized cells pelleted at 400 g for 5 min were fixed by adding cold 70% ethanol dropwise while vortexing. Fixed cells were incubated at -20 ˚C for 1 h before pelleting at 400 g for 5 min and washed once in PBS. Mitotic cells were labeled by staining with primary antibody against phospho-Mpm-2 (1:1600) for 1 hr followed by 30 min incubation in secondary antibody conjugated to Alexa Fluor 488 (1:2000). Cells were then centrifuged at 400 g for 5 min and resuspended in PBS with 0.5 µg/ml RNAseA and 10 µg/ml propidium iodide to stain for DNA content. Cell cycle distribution of 10 000 cells was analyzed by using a BD FACSCanto II (BD Biosciences) and BD FACSDiva 9.0.1 software.

Apoptosis analysis by flow cytometry

For apoptosis analysis, FITC Annexin V Apoptosis Detection Kit with PI (BioLegend) was used according to the manufacturer's instructions. Briefly, cells were stained with Annexin-FITC and propidium iodide for 15 min at RT after washing the cells once with PBS and then resuspending in Annexin V binding buffer. Dead and Floating cells were added to each sample for analysis by pelleting the conditioned medium at 1500 g for 5 min. Apoptosis of 10 000 cells from each sample was analyzed by using a BD FACSCanto II (BD Biosciences) and BD FACSDiva 9.0.1 software.

Puromycin assay

To analyze protein translation rate, 16 µg/ml of puromycin were added to siRNA reverse transfected or inhibitor-treated cells as indicated for 45 min (Goodman & Hornberger, 2013). Cell extracts were harvested in RIPA lysis buffer and puromycinylated proteins were detected by western blot using puromycin antibody.

Statistics

Data were analyzed using GraphPad Prism 6 built-in tests. All data are presented as mean ± s.d. Details about the significance test, the number of replicates, and the *P* values are reported in the respective figure legends.

Acknowledgments

The authors would like to thank Prof.Dr. Holger Bastians (University of Goettingen) for HeLa cells. We thank Dr. Karen Linnenmannstöns, Dr.Leonie Witte, and Dr. Pradhipa Karuna M for critically reading the manuscript and Mona Honemann-Capito for her excellent technical and scientific support. Research in the lab of JCG is supported by the DFG-funded Research Center, grant GR4810/2-1.

Author contribution

D.C.: Conceptualization, investigation, formal analysis, writing – original draft, review & editing J.C.G.: Conceptualization, Writing – review & editing, funding acquisition

Conflict of Interest

The authors declare no conflict of interests

References

Airola M V & Hannun YA (2013) Sphingolipid metabolism and neutral sphingomyelinases. *Handb Exp Pharmacol* (215): 57–

Ajazi A, Bruhn C, Shubassi G, Lucca C, Ferrari E, Cattaneo A, Bachi A, Manfrini N, Biffo S, Martini E, *et al* (2021) Endosomal trafficking and DNA damage checkpoint kinases dictate survival to replication stress by regulating amino acid uptake and protein synthesis. *Dev Cell* 56: 2607-2622.e6

Akopian D, Shen K, Zhang X & Shan SO (2013) Signal recognition particle: An essential protein-targeting machine

Baietti MF, Zhang Z, Mortier E, Melchior A, Degeest G, Geeraerts A, Ivarsson Y, Depoortere F, Coomans C, Vermeiren E, *et al* (2012) Syndecan-syntenin-ALIX regulates the biogenesis of exosomes. *Nat Cell Biol* 14: 677–685

Bill X.Wu, Christopher J.Clarke and YAH (2010) Mammalian Neutralsphingomyelinases: Regulation and Roles in Cell Signaling Responses. *Neuromolecular Med* 12: 320–330

Chauhan N, Visram M, Cristobal-Sarramian A, Sarkleti F & Kohlwein SD (2015) Morphogenesis checkpoint kinase Swe1 is the executor of lipolysis-dependent cell-cycle progression. *Proc Natl Acad Sci U S A* 112: E1077–E1085

Chen J (2016) The cell-cycle arrest and apoptotic and progression. *Cold Spring Harb Perspect Biol*: 1–16

Choezom D & Gross JC (2022) Neutral Sphingomyelinase 2 controls exosomes secretion via counteracting V-ATPase-mediated endosome acidification. *J Cell Sci*

Cross BCS, Bond PJ, Sadowski PG, Jha BK, Zak J, Goodman JM, Silverman RH, Neubert TA, Baxendale IR, Ron D, *et al* (2012) The molecular basis for selective inhibition of unconventional mRNA splicing by an IRE1-binding small molecule. *Proc Natl Acad Sci U S A* 109: 869–878

Demir K, Kirsch N, Beretta CA, Erdmann G, Ingelfinger D, Moro E, Argenton F, Carl M, Niehrs C & Boutros M (2013) RAB8B Is Required for Activity and Caveolar Endocytosis of LRP6. *Cell Rep* 4: 1224–1234

Fensome AC, Rodrigues-Lima F, Josephs M, Paterson HF & Katan M (2000) A neutral magnesium-dependent sphingomyelinase isoform associated with intracellular membranes and reversibly inhibited by reactive oxygen species. *J Biol Chem* 275: 1128–1136

Freese JL, Pino D & Pleasure SJ (2010) Wnt signaling in development and disease. *Neurobiol Dis* 38: 148–153

Goodman CA & Hornberger TA (2013) Measuring protein synthesis with SUnSET: A valid alternative to traditional techniques? *Exerc Sport Sci Rev* 41: 107–115

Hannun YA & Obeid LM (2008) Principles of bioactive lipid signalling : lessons from sphingolipids. *Nat Rev Mol Cell Biol* 9

Hetz C, Zhang K & Kaufman RJ (2020) Mechanisms, regulation and functions of the unfolded protein response. *Nat Rev Mol Cell Biol* 21: 421–438

Hofmann K, Tomiuk S, Wolff G & Stoffel W (2000) Cloning and characterization of the mammalian brain-specific, Mg2+-dependent neutral sphingomyelinase. *Proc Natl Acad Sci U S A* 97: 5895–900

Hollien J, Lin JH, Li H, Stevens N, Walter P & Weissman JS (2009) Regulated Ire1-dependent decay of messenger RNAs in mammalian cells. *J Cell Biol* 186: 323–331

Huttlin EL, Bruckner RJ, Navarrete-Perea J, Cannon JR, Baltier K, Gebreab F, Gygi MP, Thornock A, Zarraga G, Tam S, *et al* (2021) Dual proteome-scale networks reveal cell-specific remodeling of the human interactome. *Cell* 184: 3022-3040.e28

Huttlin EL, Bruckner RJ, Paulo JA, Cannon JR, Ting L, Baltier K, Colby G, Gebreab F, Gygi MP, Parzen H, *et al* (2017) Architecture of the human interactome defines protein communities and disease networks. *Nature* 545: 505–509

Jaffrézou JP, Levade T, Bettaïeb A, Andrieu N, Bezombes C, Maestre N, Vermeersch S, Rousse A & Laurent G (1996) Daunorubicin-induced apoptosis: Triggering of ceramide generation through sphingomyelin hydrolysis. *EMBO J* 15: 2417–2424

Jana A & Pahan K (2004) Fibrillar amyloid-β peptides kill human primary neurons via NADPH oxidase-mediated activation of neutral sphingomyelinase: Implications for Alzheimer's disease. *J Biol Chem* 279: 51451–51459

Lee JT, Xu J, Lee JM, Ku G, Han X, Yang DI, Chen S & Hsu CY (2004) Amyloid-β peptide

induces oligodendrocyte death by activating the neutral sphingomyelinase-ceramide pathway. *J Cell Biol* 164: 123–131

Lustig B, Jerchow B, Sachs M, Weiler S, Pietsch T, Rarsten U, Van De Wetering M, Clevers H, Schlag PM, Birchmeier W, *et al* (2001) Negative feedback loop of Wnt signaling through upregulation of conductin/axin2 in colorectal and liver tumors. *Langenbeck's Arch Surg* 386: 466

Martelli AM, Falà F, Faenza I, Billi AM, Cappellini A, Manzoli L & Cocco L (2004) Metabolism and signaling activities of nuclear lipids. *Cell Mol Life Sci* 61: 1143–1156

Maurel M, Chevet E, Tavernier J & Gerlo S (2014) Getting RIDD of RNA: IRE1 in cell fate regulation. *Trends Biochem Sci* 39: 245–254

Mizutani Y, Tamiya-Koizumi K, Nakamura N, Kobayashi M, Hirabayashi Y & Yoshida S (2001) Nuclear localization of neutral sphingomyelinase 1: biochemical and immunocytochemical analyses. *J Cell Sci* 114: 3727–3736

Nishino T & Morikawa K (2002) Structure and function of nucleases in DNA repair: Shape, grip and blade of the DNA scissors. *Oncogene* 21: 9022–9032

Oslowski CM & Urano F (2011) Measuring ER stress and the unfolded protein response using mammalian tissue culture system 1st ed. Elsevier Inc.

Parashuraman S & D'Angelo G (2019) Visualizing sphingolipid biosynthesis in cells. *Chem Phys Lipids* 218: 103–111

Philipp S, Puchert M, Adam-Klages S, Tchikov V, Winoto-Morbach S, Mathieu S, Deerberg A, Kolker L, Marchesini N, Kabelitz D, *et al* (2010) The Polycomb group protein EED couples TNF receptor 1 to neutral sphingomyelinase. *Proc Natl Acad Sci U S A* 107: 1112–1117

Rodrigues-Lima F, Fensome AC, Josephs M, Evans J, Veldman RJ & Katan M (2000) Structural requirements for catalysis and membrane targeting of mammalian enzymes with neutral sphingomyelinase and lysophospholipid phospholipase C activities: Analysis by chemical modification and site-directed mutagenesis. *J Biol Chem* 275: 28316–28325

Sawada R, Jardine KA & Fukuda M (1993) The genes of major lysosomal membrane glycoproteins, lamp-1 and lamp-2. 5'-Flanking sequence of lamp-2 gene and

comparison of exon organization in two genes. *J Biol Chem* 268: 9014–9022

Sawai H, Domae N, Nagan N & Hannun YA (1999) Function of the cloned putative neutral sphingomyelinase as lyso- platelet activating factor-phospholipase C. *J Biol Chem* 274: 38131–38139

Schwarz DS & Blower MD (2016) The endoplasmic reticulum: Structure, function and response to cellular signaling. *Cell Mol Life Sci* 73: 79–94

Storck EM, Özbalci C & Eggert US (2018) Lipid Cell Biology: A Focus on Lipids in Cell Division. *Annu Rev Biochem* 87: 839–869

Tanida I, Minematsu-Ikeguchi N, Ueno T & Kominami E (2005) Lysosomal turnover, but not a cellular level, of endogenous LC3 is a marker for autophagy. *Autophagy* 1: 84–91

Tomiuk S, Hofmann K, Nix M, Zumbansen M & Stoffel W (1998) Cloned mammalian neutral sphingomyelinase: Functions in sphingolipid signaling? *Proc Natl Acad Sci* 95: 3638–3643

Tomiuk S, Zumbansen M & Stoffel W (2000) Characterization and subcellular localization of murine and human magnesium-dependent neutral sphingomyelinase. *J Biol Chem* 275: 5710–5717

Tonnetti L, Verí MC, Bonvini E & D'Adamio L (1999) A role for neutral sphingomyelinase-mediated ceramide production in T cell receptor-induced apoptosis and mitogen-activated protein kinase-mediated signal transduction. *J Exp Med* 189: 1581–9

Vielhaber G, Brade L, Lindner B, Pfeiffer S, Wepf R, Hintze U, Wittern KP & Brade H (2001) Mouse anti-ceramide antiserum: A specific tool for the detection of endogenous ceramide. *Glycobiology* 11: 451–457

Vivanco I & Sawyers CL (2002) The phosphatidylinositol 3-kinase-AKT pathway in humancancer. *Nat Rev Cancer* 2: 489–501

Vizeacoumar FJ, Arnold R, Vizeacoumar FS, Chandrashekhar M, Buzina A, Young JTF, Kwan JHM, Sayad A, Mero P, Lawo S, *et al* (2013) A negative genetic interaction map in isogenic cancer cell lines reveals cancer cell vulnerabilities. *Mol Syst Biol* 9

Wlodarchak N & Xing Y (2016) PP2A as a master regulator of the cell cycleThe Impact of Pollution on Worker Productivity. *Crit Rev Biochem Mol Biol* 51: 162–184

Wu BX, Rajagopalan V, Roddy PL, Clarke CJ & Hannun YA (2010) Identification and characterization of murine mitochondria-associated neutral sphingomyelinase (MA-nSMase), the mammalian sphingomyelin phosphodiesterase 5. *J Biol Chem* 285: 17993–18002

Yabu T, Shiba H, Shibasaki Y, Nakanishi T, Imamura S, Touhata K & Yamashita M (2015) Stress-induced ceramide generation and apoptosis via the phosphorylation and activation of nSMase1 by JNK signaling. *Cell Death Differ* 22: 258–273

Yabu T, Shimuzu A & Yamashita M (2009) A novel mitochondrial sphingomyelinase in zebrafish cells. *J Biol Chem* 284: 20349–20363

Zumbansen M & Stoffel W (2002) Neutral sphingomyelinase 1 deficiency in the mouse causes no lipid storage disease. *Mol Cell Biol* 22: 3633–3638

Supplementary Figures

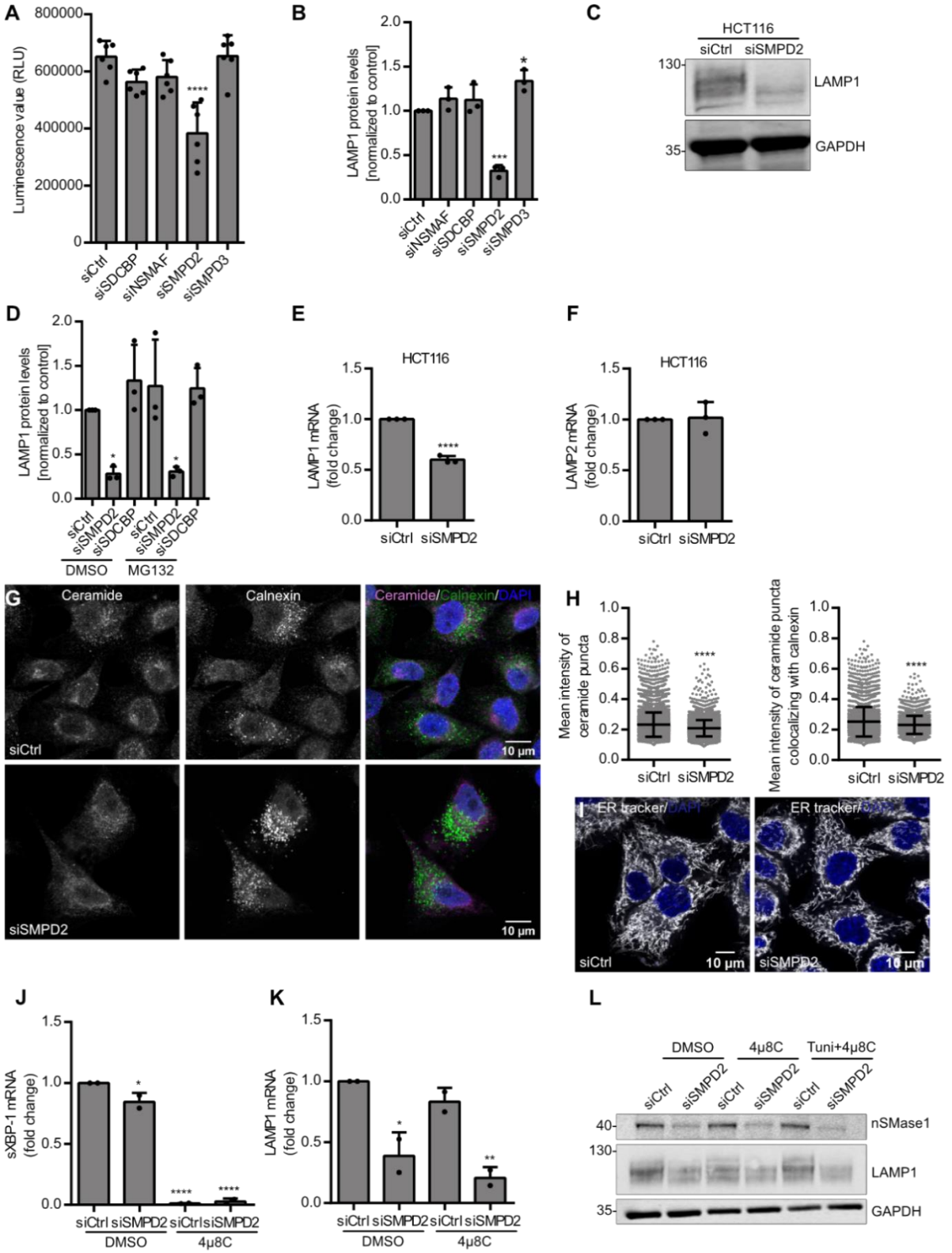

Figure S1: (A) Viability assay of HeLa cells transfected with Ctrl, *SDCBP*, *NSMAF*, *SMPD2*, and *SMPD3* siRNA for 48 h. Ordinary one-way ANOVA followed by Dunnett's multiple comparisons

test, ****p < 0.0001. **(B)** Western blot quantifications of LAMP1 from (Fig.1A) normalized to the corresponding loading control GAPDH before normalization to the control. Ordinary one-way ANOVA followed by Dunnett's multiple comparisons test, ***p < 0.0009. **(C)** HCT116 cells were transfected with the indicated siRNAs for 48 h and lysates were immunoblotted against LAMP1 and loading control GAPDH. **(D)** Western blot quantifications of LAMP1 from (Fig.1G) normalized to the corresponding loading control GAPDH before normalization to the control. Ordinary one-way ANOVA followed by Dunnett's multiple comparisons test, *p < 0.01. (E-F) Real-time qPCR analysis of LAMP1 **(E)** and LAMP2 **(F)** mRNA in HCT116 cells after 72 h of *SMPD2* KD. Unpaired Student's two-tailed t-test, ****p < 0.0001. **(G)** HeLa cells transfected with control (Ctrl) and *SMPD2* siRNA for 48 h were stained for ceramide and calnexin and analyzed by confocal microscopy. **(H)** Quantifications of mean intensity of ceramide puncta per cell from (G) (left) and mean intensity of ceramide puncta colocalizing with calnexin (right) from three independent experiments. Unpaired Student's two-tailed t-test, ****p < 0.0001. **(I)** HeLa cells transfected with Ctrl or *SMPD2* siRNA for 48 h were live imaged by staining with ER tracker and DAPI. **(J)** Real-time qPCR analysis of sXBP-1 mRNA in HeLa cells transfected with Ctrl and *SMPD2* siRNA and treated with 4μ8C for 48 h. Ordinary one-way ANOVA followed by Dunnett's multiple comparisons test, ****p < 0.0001, *p < 0.01, from two independent experiments. **(K)** Real-time qPCR analysis of LAMP1 mRNA in HeLa cells transfected with Ctrl or *SMPD2* siRNA and treated with 4μ8C for 48 h. Ordinary one-way ANOVA followed by Dunnett's multiple comparisons test, ****p < 0.0001, **p < 0.001, *p < 0.01, from two independent experiments. **(L)** HeLa cells reverse transfected with Ctrl and *SMPD2* siRNA were grown with DMSO or 4μ8C for 48 h and treated with tunicamycin for 4 h. Cell lysates were immunoblotted against nSMase1, LAMP1, and loading control GAPDH. All experiments from (A)-(L) are done in three biological replicates.

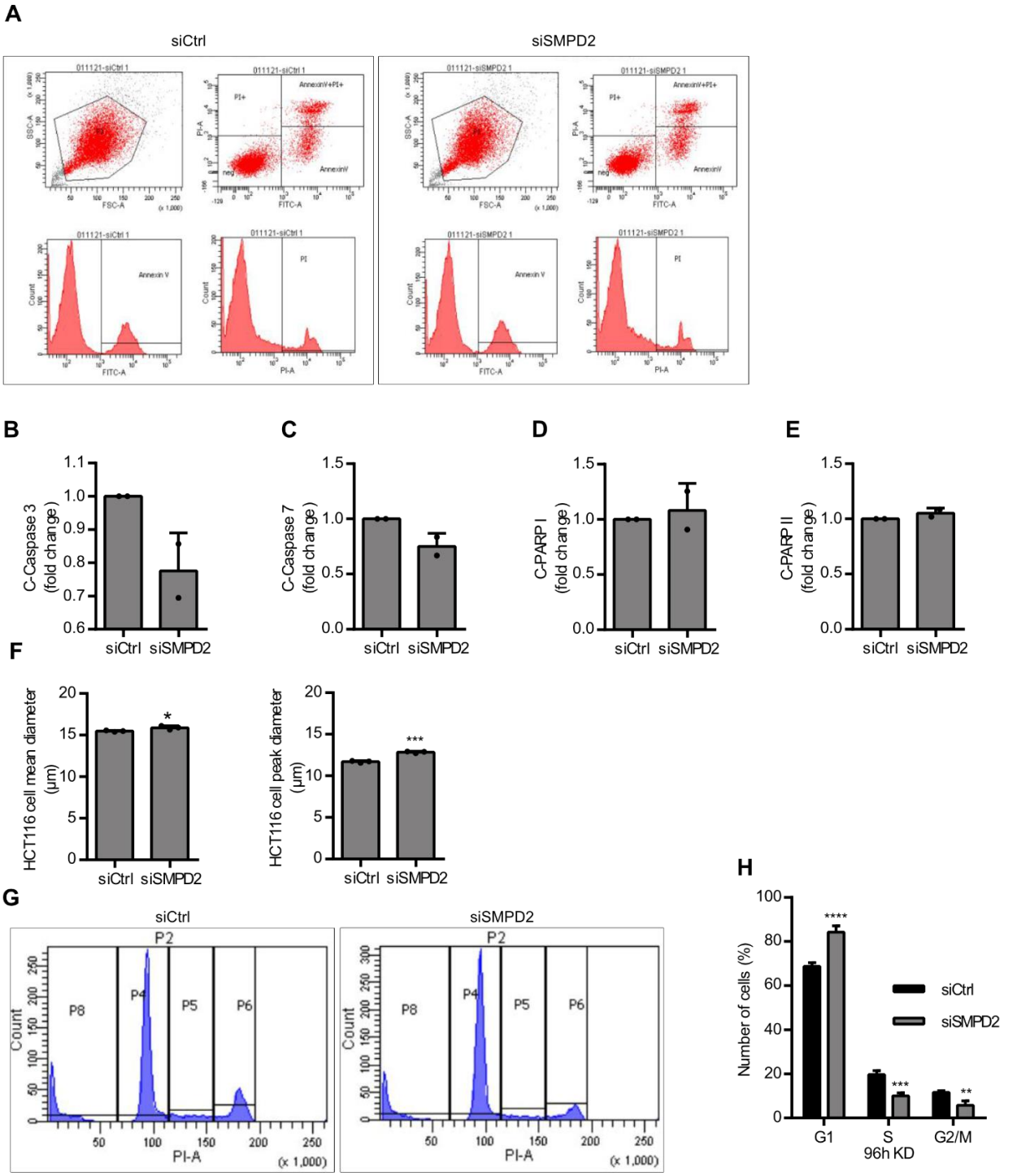

Figure S2: **(A)** Flow Cytometry analysis of FITC Annexin-V and PI staining of HeLa cells transfected with Ctrl (left) or *SMPD2* (right) siRNA for 48 h. Forward and side scatter plot (above left) of HeLa cells gated for the subsequent analysis, two-dimensional scatter plot gating cell populations into four quadrants based on PI versus FITC Annexin-V staining (above right), Populations of cells gated for only FITC Annexin-V (below left) and only PI (below right). (B-E) Western blot quantifications of cleaved caspase 3 **(B)**, caspase 7 **(C)**, PARP I **(D)**, and PARP II **(E)** in relative to the respective full length (FL) proteins from two independent experiments. **(F)** HCT116 cell mean diameter (above) and peak diameter (bottom) determined with Casy cell

counter after 72 h of Ctrl or *SMPD2* siRNA transfection. **(G)** Flow cytometry analysis HeLa cells transfected with Ctrl (left) or *SMPD2* (right) siRNA for 48 h were gated to distribute the cell population into G1, S, and G2/M phase of the cell cycle **(H)** Percentage of HeLa cells transfected with Ctrl or *SMPD2* siRNA for 96 h were gated for G1, S, and G2/M. Two-way ANOVA followed by Sidak's multiple comparisons test, ****p < 0.0001, ***p < 0.0009 **p < 0.001. All experiments from (A)-(H) are done in three biological replicates unless otherwise stated.

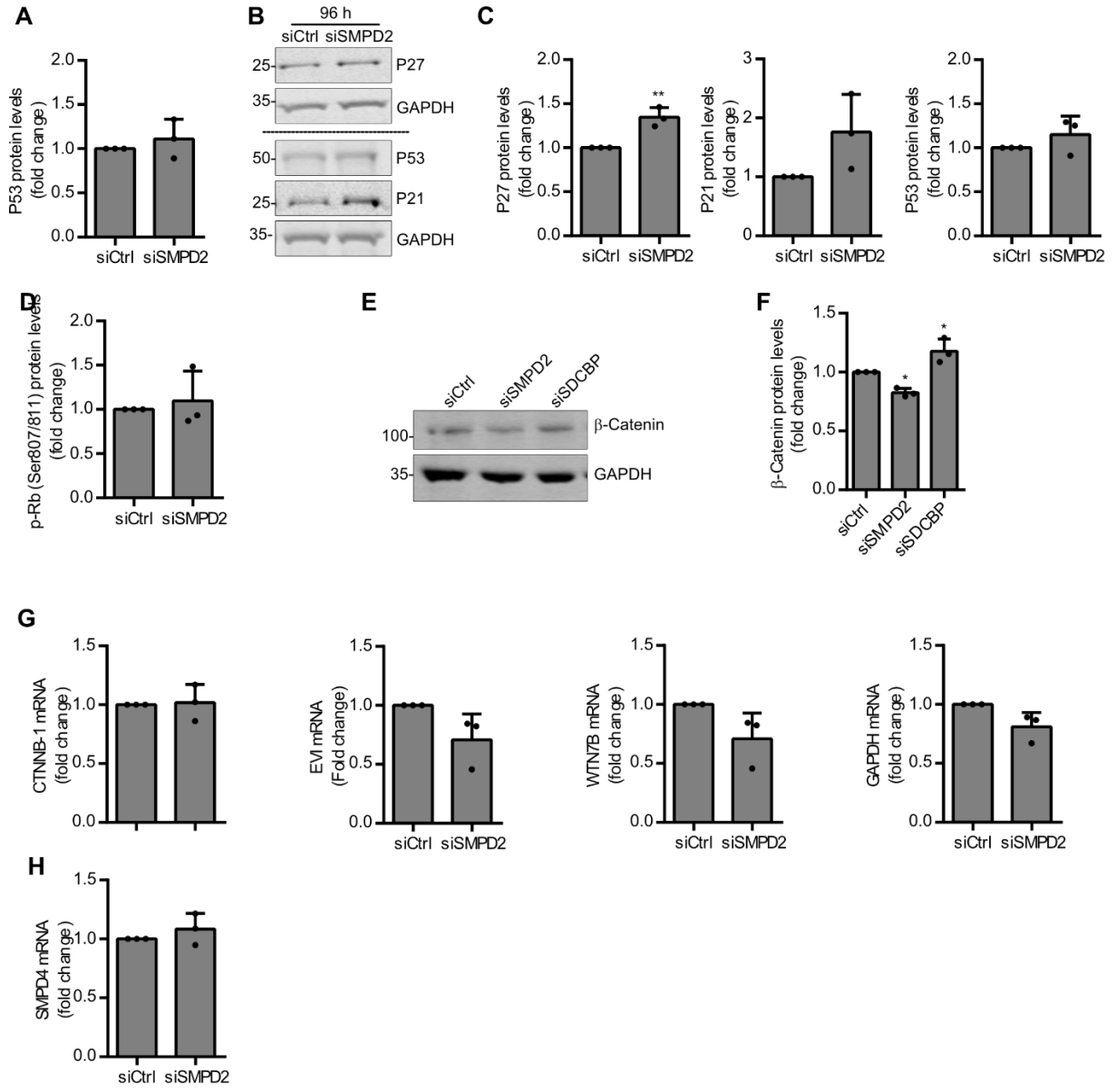

Figure S3: **(A)** Western blot quantifications of P53 protein levels from (Fig. 3G) normalized to the corresponding loading control GAPDH before normalization to the control. Unpaired Student's two-tailed *t-test*). **(B)** Lysates from HeLa cells transfected with Ctrl or *SMPD2* siRNA for 96 h were immunoblotted against P27, P53, P21, and loading control GAPDH. **(C)** Western blot quantifications from (B) of P27, P21, and P53 normalized to the corresponding loading control

GAPDH before normalization to the control. Unpaired Student's two-tailed *t-test*, ****p < 0.0001, **p < 0.001. **(D)** Western blot quantifications of p-Rb from (Fig. 4B) normalized to the corresponding loading control GAPDH before normalization to the control. Unpaired Student's two-tailed *t-test*, **p < 0.001. **(E)** HeLa cells were transfected with the indicated siRNAs for 48 h and lysates were immunoblotted against β-catenin and loading control GAPDH. **(F)** Western blot quantifications of β-catenin from (E) normalized to the corresponding loading control GAPDH before normalization to the control. Ordinary one-way ANOVA followed by Dunnett's multiple comparisons test, *p < 0.01. **(G)** Real-time qPCR analysis of CTNNB-1, EVI, WNT7B, and GAPDH mRNA in HCT116 cells transfected with Ctrl and *SMPD2* siRNA for 72 h. Unpaired Student's two-tailed *t-test*. **(H)** Real-time qPCR analysis of SMPD4 mRNA in HCT116 cells transfected with Ctrl and *SMPD2* siRNA for 72 h. Unpaired Student's two-tailed *t-test*, ****p < 0.0001. All experiments from (A)-(H) are done in three biological replicates.

3 Discussion

3.1 Neutral Sphingomyelinase 2 controls sEV secretion by counteracting V-ATPase-mediated endosome acidification

Our study demonstrates that nSMase2 regulates sEV secretion by counteracting V-ATPase activity on endosomal membranes. We delineate a so far unknown mechanism by which nSMase2 regulates sEV secretion and provide evidence that the local lipid environment at MVBs and specifically the levels of ceramide, sphingomyelin, and cholesterol regulate sEV secretion by modulating endosomal acidification. Importantly, we show that TNFα, a prominent pro-inflammatory cytokine and a known nSMase2 agonist, promotes sEV secretion by modulating endosomal acidification via inhibiting V-ATPase complex assembly. These findings for the first time establish a molecular link between TNFα-induced nSMase2 activation and sEV secretion.

3.1.1 Avoiding degradation and trafficking of MVBs for sEV secretion

Mature MVBs loaded with ILVs face two fates: lysosomal degradation or peripheral trafficking for sEV secretion. Although the molecular mechanisms underlying cargo sorting and subsequent ILV biogenesis at the MVB membrane are well studied (Cullen & Steinberg, 2018), the regulatory factors that actively sort MVBs for transport towards the plasma membrane for eventual sEV secretion are largely unknown. Cells establish a balance between these two fates. For example, impaired lysosomal degradation results in the elimination of defective neuro-toxic proteins such as amyloid through sEV secretion (Erez Eitan *et al*, 2016).

During MVB formation, cargos tagged with ubiquitylation are recognized and then sorted into ILVs in an ESCRT-machinery-dependent manner (Saksena *et al*, 2007). Although this ubiquitylation-based ESCRT machinery-dependent pathway is the major mechanism that drives ILV biogenesis at MVBs that are eventually sorted for lysosomal degradation (Cullen & Steinberg, 2018), studies have implicated the ESCRT machinery in ILV biogenesis for sEV secretion as well (Willms *et al*, 2016; Colombo *et al*, 2013). As

described for degradative ILV biogenesis (Dores *et al*, 2012, 2016), the ESCRT accessory protein ALG-2-interacting protein X (Alix), in concert with syndecan and syntenin, also drives ILV biogenesis for sEV secretion (Baietti *et al*, 2012). Therefore, based on these overlapping molecular machineries involved in generating both secretory and degradative ILVs, it is not clear at which step the MVB sorting decision is made.

However, the role of nSMase2 in generating ILVs has been exclusively described for secretory MVBs. Previous studies have shown that nSMase2 activity drives ILV biogenesis for sEV secretion by producing ceramide-induced negative membrane curvature (Trajkovic *et al*, 2008) or by generating S1P that activates its cognate MVB receptor (Kajimoto *et al*, 2013). The molecular mechanism underlying S1P receptor activation-induced ILV formation for sEV secretion remains to be elucidated. Alternatively, our study demonstrates that nSMase2 activity drives MVB trafficking for sEV secretion by counteracting V-ATPase-mediated endosomal acidification - thereby implicating both MVB lipid environment and its lumen acidification as regulatory factors determining its trafficking fate.

Similar to ceramide and sphingomyelin levels modulated by nSMase2 activity, we also show that MVB cholesterol levels also regulate sEV secretion by modulating V-ATPase-mediated endosomal acidification. Indeed, ILVs are known to harbor the highest cholesterol content in the endocytic pathway (Möbius *et al*, 2003). Moreover, the complete cryo-EM structure of the human V-ATPase complex has revealed that ordered lipid molecules including cholesterol are indeed an integral part of the V0 complex (Wang *et al*, 2020). Based on our data and these observations, we propose that cholesterol, together with ceramide generated by nSMase2 activity on the MVB membrane, drives V-ATPase subunit packaging into ILVs to attenuate its activity and thereby reduce MVB lumen acidification and promote secretory MVB trafficking.

The connection between V-ATPase mediated acidification and sEV secretion has been shown before with studies describing increased sEV secretion upon V-ATPase inhibition with bafilomycin A (Villarroya-Beltri *et al*, 2016; Edgar *et al*, 2016). Recent studies have further highlighted the role of MVB lumen acidification as a sorting signal – MVBs with less acidic lumen are sorted as secretory MVBs for sEV release. For example, ATG5 and LC3, independent of canonical macroautophagy, coordinately deacidify MVBs to promote

sEV secretion (Guo *et al*, 2017). Therefore, our findings on how changes in nSMase2-mediated endosomal acidification affect sEV secretion further substantiate these findings.

In addition to MVB lumen acidification, other molecular factors at the level of MVB cargos or their respective sorting machinery have been described to regulate MVB trafficking fates. For example, ISGylation of Tsg101, a sorting component of the ESCRT-I machinery, promotes a degradative fate for MVBs and thereby reduces sEV secretion (Villarroya-Beltri *et al*, 2016). At the cargo level, a sorting motif found in Galectin-3 was shown to be required for its efficient secretion on sEVs, albeit, in an ESCRT-dependent manner (Bänfer *et al*, 2018). Additionally, SUMOylation of hnRNPA2B1 (heterogeneous nuclear ribonucleoprotein A2/B1) controls the sorting of miRNAs into ILVs for secretion (Villarroya-Beltri *et al*, 2013) and SUMOylation of α-synuclein regulates its loading into sEV for secretion (Kunadt *et al*, 2015).

Therefore, with studies indicating regulation control at the level of cargo, cargo-sorting machinery, and mature MVBs, cells may employ a complex network of molecular regulators to determine the MVB trafficking fate depending on the cell-type and the prevailing cellular conditions.

The reported cell type-specific effects of nSMase2 inhibition on sEV secretion (Panigrahi *et al*, 2018; Gross *et al*, 2012; Matsui *et al*, 2021) may be explained by the differences in cellular endosomal acidification levels, which in turn could be affected by different cellular and physiological factors. The ESCRT components drive ILV biogenesis at the MVB (Saksena *et al*, 2007) and the knockdown of the ESCRT components HRS, STAM1, and TSG101 reduces the secretion of CD63-positive EVs (Colombo *et al*, 2013). However, the role of the ESCRT-complexes in cargo loading and ILV generation for sEV secretion is increasingly challenged by different studies. For example, a recent study has shown that knockdown of individual ESCRT subunits counterintuitively increased sEV secretion by causing lysosomal dysfunction (Matsui *et al*, 2021). These findings are also in line with studies showing that the lysosomal degradation of several endocytosed receptors requires the ESCRT machinery for proper internalization of these receptors into ILVs (Futter *et al*, 1996; Haglund *et al*, 2003; Yamashita *et al*, 2008). Therefore, based on these studies and our results, it is tempting to speculate that ESCRT complexes support ILV generation for degradative MVBs which are targeted for lysosomes. On the other

hand, ceramide generated by nSMase2 activity, in addition to aiding ILV biogenesis as previously described (Trajkovic *et al*, 2008; Kajimoto *et al*, 2013), also favors secretory MVB transport for sEV release by promoting V-ATPase invagination into ILVs. Based on our data and the above studies, it is tempting to speculate that while ESCRT machinery mainly generates degradative ILVs, ceramide exclusively drives secretory ILV biogenesis to promote sEV secretion.

In addition to its role in attenuating V-ATPase activity to promote secretory MVBs for sEV secretion, we also show that nSMase2 affects LAMP1 levels, specifically during serum starvation-induced autophagy. Therefore, how nSMase2-mediated endosomal acidification regulation affects autophagy remains an interesting question to explore. Additionally, how nSMase2-dependent MVB deacidification affects recruitment of further MVB secretory machineries, including kinesin motor proteins for its anterograde transport, Rab27a, Rab27b (Ostrowski *et al*, 2010), and SNARE proteins such as YKT6 (Gross *et al*, 2012) for plasma membrane fusion, remain interesting questions to be investigated.

3.1.2 Lipids as regulators of traffic in the endosomal system

Protein-based sorting machinery, including coat proteins and their adaptors, small GTPases, tethering factors, and fusion proteins in the regulation of endosomal trafficking is well studied at the mechanistic level (Gruenberg, 2001). However, the role of lipids in the regulation of endosomal transport is far less explored.

The vesicle compartments along the endocytic pathway are highly pleiomorphic, exhibiting tubular and vacuolar morphologies (Gruenberg, 2001). Early and recycling endosomes are characterized by extensive tubular networks, whereas late endosomes or MVBs exhibit a bulbous vacuolar morphology. Owing to their physicochemical properties, regulated lipid distribution in these compartments facilitates a geometry-based cargo-sorting mechanism. Lipids with flexible acyl chains such as glycerophospholipids are enriched in the highly dynamic and narrow tubules in which integral membrane proteins are preferentially sorted for recycling to the plasma membrane. In contrast, lipids with saturated - and therefore more rigid - acyl chain lipids such as sphingomyelin, sphingolipids, and cholesterol are enriched on the vacuolar region of the endocytic

compartments and the bulbous MVBs and thus allow the sorting of both membrane and soluble cargos into their lumen (Lippincott-Schwartz & Phair, 2010).

In addition to providing a lipid-based sorting mechanism founded in their unique lipid-lipid interaction properties, individual lipids play important role in cargo sorting and membrane transport in the endosomal pathway through their interactions with proteins (Lippincott-Schwartz & Phair, 2010). Peripheral membrane proteins often interact with membranes through diverse lipid-binding motifs and in this way lipids directly contribute to the distribution of many peripheral proteins. Many proteins involved in the regulation of endosomal transport contain a phospholipid-binding domain which allows transient interaction between them. Short-lived phosphoinositides that are rapidly turned over by kinases and phosphatases are the best-characterized lipid players during endosomal transport. For example, PI(3)P, found mostly in early endosomes, recruits different effector proteins by binding to their lipid-binding domains such as the FYVE domain and the PX (phox) domain. Effector proteins binding to the PI(3)P on the membrane facilitate further recruitment of proteins involved in early endosomal sorting and transport. For example, Rab5 effector protein EEA1 binding to PI(3)P allows the recruitment of SNARE proteins involved in membrane docking and fusion in early endosomes (Vicinanza *et al*, 2008; Di Paolo & De Camilli, 2006). Likewise, the poorly degradable lipid LBPA (lysophosphatidic acid), which exclusively resides in late endosomes, contributes to ILV generation by interacting with Alix (Matsuo *et al*, 2004; Chevallier *et al*, 2008).

Therefore, our observations on how the local lipid environment on the MVB membrane regulates its trafficking decision fit with an increasing body of work emphasizing the functions of lipids in a broader biological context. We show that at the MVB membrane, the levels of ceramide and sphingomyelin modulated by nSMase2 activity, and cholesterol regulate the MVB trafficking fate through V-ATPase. Specifically, ceramide generated by nSMase1 on the MVB drives V-ATPase subunit invagination into ILVs to attenuate its activity and thereby reduce MVB lumen acidification to promote sEV secretion.

Moreover, our observations on the regulation of V-ATPase activity by lipids are in alignment with an increasing body of work. In yeast, organelle-specific lipids modulate V-ATPase activity. The phosphatidylinositol lipid PI(3,5)P2, which is predominantly enriched

in the vacuole, directly recruits V-ATPase subunit Vph1p to the membrane and increases V-ATPase assembly and activity on the vacuolar membrane (Li *et al*, 2014; Banerjee *et al*, 2019). Likewise, PI(4)P in the Golgi membrane directly interacts with the N-terminal domain of Stv1p, a transmembrane V0A isoform, and supports the efficient localization of Golgi-V-ATPases (Banerjee & Kane, 2017). Similarly, ergosterol, the major sterol species in fungi, is required for V-ATPase-mediated vacuolar acidification in yeast (Zhang *et al*, 2010). Cryo-EM structure analysis of the yeast V0 complex suggested sterol binding sites around the C-ring, as well as specific sites for glycerophospholipids interaction with the V0 region (Vasanthakumar *et al*, 2019). The role of raft-like domains in V-ATPase activity regulation has been proposed in yeast with studies indicating sphingomyelin and possibly ceramide modulating V-ATPase function(Chen *et al*, 2004; Dawson *et al*, 2008). The first hint on the role of lipids in V-ATPase activity regulation in mammalian cells came from a study that has shown that all endosomal V-ATPase subunits are enriched in the detergent-resistance endosomal membrane fraction (Lafourcade *et al*, 2008). Moreover, a recent mass spectrometry analysis of the isolated human V0 complex has indeed shown the enrichment of different phospholipids and cholesterol in the V0 complex (Wang *et al*, 2020). Therefore, our data on the lipid-mediated V-ATPase activity regulation at the MVB - along with the aforementioned -structural and biochemical data - support an important role for lipids in V-ATPase function. Such lipids, therefore, present a possible target for modulating V-ATPase activity.

3.1.3 TNFα-nSMase2-induced sEV secretion and its implications

Sphingomyelin turnover was initially identified as an effector mechanism for the action of TNFα and gamma-interferon (Kim *et al*, 1991). Later studies identified nSMase2 as the main sphingomyelin hydrolyzing enzyme activated in response to TNFα stimulation. The resulting ceramide generated by activated nSMase1 regulates a wide array of cellular processes including inflammation (Al-Rashed *et al*, 2020; Gu *et al*, 2013), apoptosis (Kolmakova *et al*, 2004), and cell death (Luberto *et al*, 2002; Yang *et al*, 2004), cell adhesion and migration (Clarke *et al*, 2006), as well as synaptic plasticity (Wheeler *et al*, 2009).

TNFα, a pleiotropic cytokine with both homeostatic and pathogenic bioactivity, activates nSMase2 exclusively through TNF receptor 1 (TNF-R1) (Kolesnick & Krönke, 1998). Factor-associated with neutral sphingomyelinase (NSMAF) associates with TNF-R1 by binding to a domain termed neutral sphingomyelin activation domain (NSD) within TNF-R (Adam-Klages *et al*, 1996; Tcherkasowa *et al*, 2002). Through NSMAF, RACK1 also constitutively associates with TNF-R1 (Tcherkasowa *et al*, 2002). Upon TNFα binding to TNF-R1, EED, a WD-repeat protein of the Polycomb group, is translocated from the nucleus to the plasma membrane. EED then simultaneously interacts with RACK1 and nSMase2. This interaction couples EED and nSMase2 to the TFN-R1-FAN-RACK1-complex and activates nSMase2 (Philipp *et al*, 2010).

Our findings for the first time elucidate the mechanism by which TNFα-induced nSMase2 activation promotes sEV secretion: by modulating endosomal acidification. Importantly, we show that TNFα promotes sEV secretion by regulating endosomal acidification via modulating V-ATPase complex assembly. These findings establish a molecular connection between TNFα-induced nSMase2 activation and sEV secretion. In alignment with the observation that TNFα modulates endolysosomal acidification, studies have shown that TNFα stimulation compromises lysosome integrity that in turn affects the cellular degradative capacity and reduces autophagic flux (Wang *et al*, 2015; Werneburg *et al*, 2002). The exact molecular mechanism underlying defective lysosomal activity upon TNFα stimulation remains unknown. Based on our findings, it is worthwhile to investigate if this occurs via nSMase2 activation at the lysosomes that in turn affects lysosomal acidification.

TNFα is primarily released by immune cells and modulates a wide variety of cellular pathways (Holbrook *et al*, 2019). TNFα is therefore implicated in many immunology-related diseases such as rheumatoid arthritis (Farrugia & Baron, 2000), ankylosing spondylitis (Lata *et al*, 2019), and cancer (Balkwill, 2006). Tumor progression is closely associated with chronic inflammatory processes and involves dysregulated activity of various types of immune cells (Hiam-Galvez *et al*, 2021). Tumor cells release a significant amount of EVs that contribute greatly to tumor progression by modulating chronic inflammation and mediating immunosurveillance evasion (Kanada *et al*, 2016). Therefore, further study on TNFα-induced nSMase2 activation in cancer cells may shed light on the

role of TNFα and sEV in cancer progression. Moreover, the TNFα-induced-nSMase2 activation pathway may present a possible target for modulating pro-tumorigenic EV secretion in tumor cells.

EVs play a significant role not only in cancer progression but also in the pathogenesis and progression of various neurological disorders (Bellingham *et al*, 2012). For example, neuropathologic α-synuclein oligomers which cause Parkison's disease (PD) were shown to be secreted on EVs which are then taken up by surrounding cells in the brain. In this way, it is believed that EVs allow the cell-cell transmission of different neuropathogenic protein aggregates such as β-amyloid and tau in Alzheimer's disease, TAR DNA-binding protein 43 in amyotrophic lateral sclerosis, and Huntington and polyglutamine in Hungtington's disease (Candelario & Steindler, 2014). Specifically, nSMase2-induced EVs derived from the brain contribute to α-synuclein pathology in a PD mouse model (Zhu *et al*, 2021). With its predominant expression in the brain, nSMase2 is likely to play an important role in propagating these neuropathogenic protein aggregates via EVs to promote neurological diseases. Therefore, it is interesting to study if these processes also occur via the TNFα-induced-nSMase2 activation pathway in the brain.

3.2 Neutral Sphingomyelinase 1 regulates cellular fitness at the level of ER stress and cell cycle

We found that nSMase1 (encoded by *SMPD2*) plays an important role in maintaining cellular homeostasis. NSMase1 is required for activating an efficient unfolded protein response (UPR) upon ER stress induced by tunicamycin and thapsigargin. These inhibitors cause ER stress through distinct mechanisms: Tunicamycin blocks N-linked glycosylation and thereby induces ER stress and activates UPR (Heifetz *et al*, 1979; Hetz *et al*, 2020). Whereas, thapsigargin inhibits Sarco/endoplasmic reticulum Ca^{2+} ATPase (SERCA) that results in ER calcium store depletion and thereby induces ER stress and activates the UPR (Peterková *et al*, 2020). *SMPD2* KD cells failed to upregulate multiple genes involved in the UPR to resolve ER stress to the same levels as their control counterparts. Furthermore, we show that nSMase1 is necessary for proper cell cycle progression, as *SMPD2* KD led to significant G1 arrest. Moreover, the global protein

translation and Wnt-signaling activity was reduced by *SMPD2* KD. These data, for the first time, establish an important biological role for nSMase1.

3.2.1 NSMase1: Putative sphingomyelinase searching for its biological substrate

The dynamic regulation of lipids, their controlled hydrolysis by specific enzymes, or their regulated lateral or transbilayer movement in the bilayer, influences a wide range of cellular processes. Lipids not only provide structural support but also regulate transmembrane receptor activity that transduces extracellular signals into cells. By activating specific biological pathways, these extracellular signals are then translated into appropriate cellular responses. Furthermore, regulated lipid hydrolysis at specific membrane compartments generates signaling active lipids that directly participate in different cellular pathways (Holthuis & Levine, 2005; Holthuis & Menon, 2014). As described for many lipids, sphingomyelin provides both structural support and second messenger signaling lipids when metabolized (Airola & Hannun, 2013). Sphingomyelin is the most abundant lipid in the exoplasmic leaflet of the plasma membrane (Lorent *et al*, 2020) and its metabolism yields several signaling potent lipids including ceramide and sphingosine-1-phosphate (Airola & Hannun, 2013).

SMPD2 or nSMase1 was identified and cloned based on the sequence similarity to Mg^{2+}-dependent bacterial neutral sphingomyelinase, which hydrolyzes sphingomyelin into ceramide and phosphorylcholine (Tomiuk *et al*, 1998a). NSMase1 belongs to a large family of Mg2+-dependent phosphodiesterases with neutral pH optimum. The secondary structure prediction reveals two putative transmembrane domains at the C-terminus and a catalytic domain that adopts a DNase-1 like structure. Furthermore, site-directed mutagenesis experiments have shown that nSMase1 contains conserved catalytic histidine residues like the bacterial counterpart. Although we observed reduced ceramide staining upon *SMPD2* KD, studies have shown unaltered sphingomyelin and ceramide metabolism upon nSMase1 overexpression in mammalian cells (Hofmann *et al*, 2000; Sawai *et al*, 1999).

Instead, nSMase1 shows strong phospholipase C activity towards both lysoplatelet-activating factor (lyso-PAF) and lyso-phosphatidylcholine (lyso-PC) *in vitro* (Fig. 4). Based

on the higher levels of 1-alkyl-glycerol rather than 1-acyl-glycerol observed upon nSMase1 overexpression, lyso-PAF was established as its more likely biological substrate (Sawai *et al*, 1999). Of note, lyso-PC cannot be entirely ruled out as its substrate, as 1-acyl-glycerol may be rapidly degraded by lipases whereas 1-alkyl-glycerol may accumulate due to its slower metabolism (Sawai *et al*, 1999). Based on these studies, it is highly probable that nSMase1 plays a crucial role in PAF metabolism. PAF is a biologically potent molecule that mediates platelet aggregation, inflammation and granule secretion (Travers *et al*, 2021). Additionally, PAF induces cell cycle arrest and impairs the DNA damage response pathway in mast cells (Puebla-Osorio *et al*, 2015). This is in alignment with our observation that *SMPD2* KD arrests cells in the G1 phase by upregulating the two G1 cell cycle arrest markers P21 and P27. These two proteins are under the regulatory control of P53, which is activated upon cellular DNA damage (Matthews *et al*, 2022; Chen, 2016). Therefore, it is conceivable that the altered PAF metabolism upon *SMPD2* KD could accumulate PAF in cells which subsequently upregulate P21 and P27 to mediate G1 cell cycle arrest. Its ER-localization, where sphingomyelin concentration is kept very low (Holthuis & Menon, 2014), further supports the idea that lyso-PAF is its biological substrate. The observed reduced ceramide staining upon *SMPD2* KD in our study could be due to a secondary effect caused by reduced global protein translation and cell cycle arrest upon *SMPD2* KD. Therefore, it is impossible to conclusively establish sphingomyelin as the substrate for nSMase1 based on the reduced ceramide staining from our study.

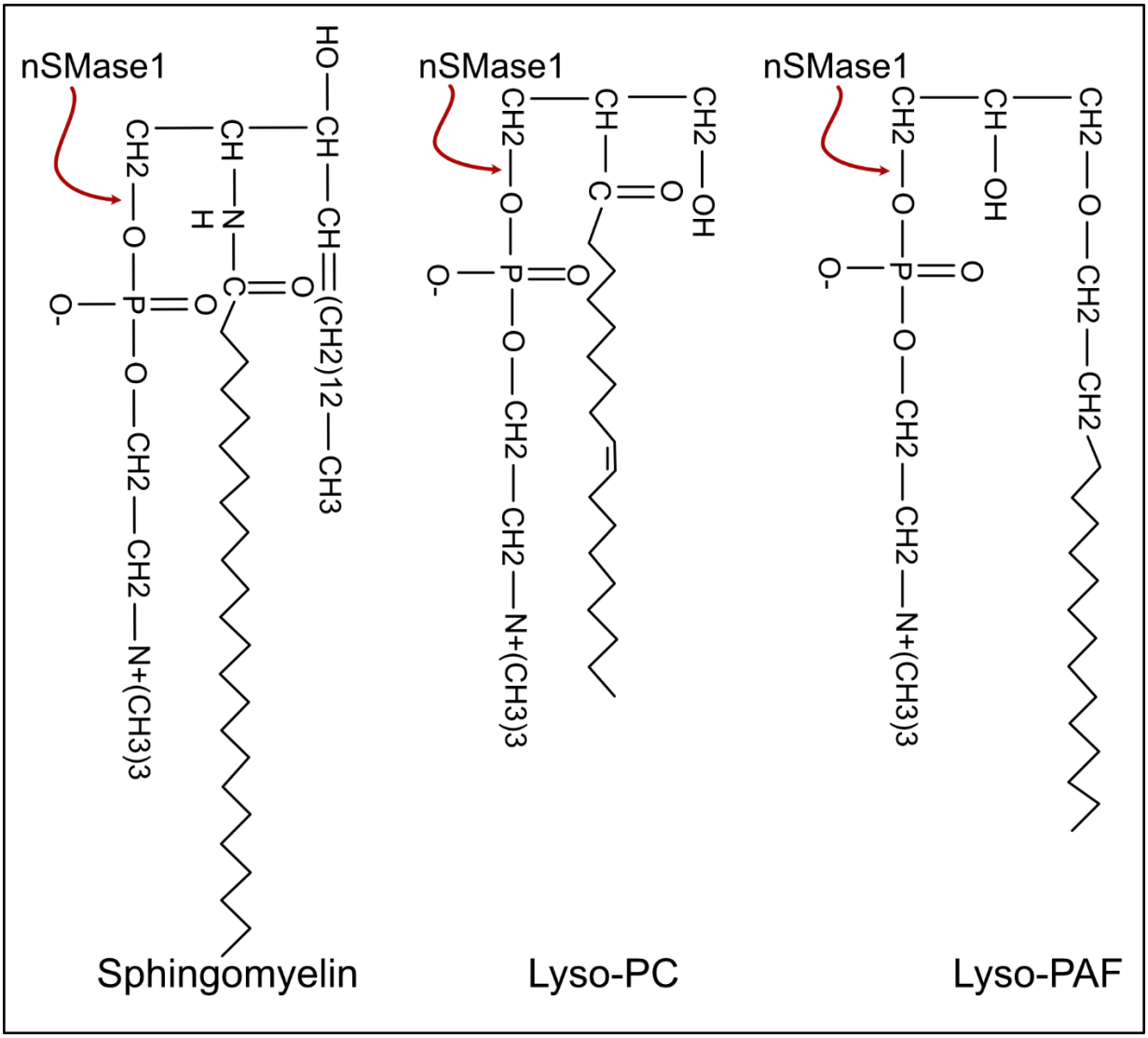

Figure 4: Potential biological substrates of nSMase1: nSMase1 shows *in vitro* phosphodiesterase activity to hydrolyze the indicated bond above to release the phosphocholine head group from sphingomyelin, lysophosphatidylcholine (lyso-PC), or lyso-platelet-activating factor. Therefore, nSMase1 is also described as a phospholipase C. Lyso-PAF was shown to be its most likely biological substrate

However, sphingomyelin as its biological substrate was not unequivocally dismissed by all studies on nSMase1. Some studies demonstrated that nSMase1 generates ceramide to mediate different cellular processes including T-cell receptor-mediated apoptosis and mitogen-activated protein kinase-mediated signal transduction (Tonnetti *et al*, 1999a; Yabu *et al*, 2015). In addition to its role as a potent signaling lipid, ceramide generated by sphingomyelinase can also be immediately metabolized into sphingosine-1-phosphate which then activates its receptor to induce a wide array of cellular responses, including

cell proliferation, angiogenesis, migration, and cytoskeleton remodeling (Ogretmen & Hannun, 2004; Pyne & Pyne, 2020). Indeed, nSMase1 was shown to interact with sphingosine-1-phosphate receptor 2 (S1PR2) (Huttlin *et al*, 2021). Furthermore, similar to our observed localization of endogenous nSMase1, S1PR2 also localizes to nuclear speckles according to the human protein atlas. Sphingomyelin has long been known to be a component of the nuclear matrix (Irvine, 2003). The presence of active sphingomyelinases and ceramidases in the nucleus indicates that these sphingolipids are actively metabolized in the nucleus as well (Martelli *et al*, 2004). Most importantly, nuclear sphingosine-1-phosphate associates with histone deacetylase 1 and 2 (HDAC1 and HDAC2) to inhibit their enzymatic activity, thereby regulating gene expression (Hait, 2009). Our study demonstrates that *SMPD2* KD not only downregulated LAMP1 and WNT3A at the mRNA level but also resulted in inefficient upregulation of genes controlled by the UPR pathways during ER stress conditions. Based on these observations, it is tempting to speculate that nSMase1 activity in the nucleus generates signal potent lipids like S1P that can directly regulate gene expression.

3.2.2 NSMase1 plays important role in maintaining ER homeostasis

Several studies have shown that overexpressed nSMase1 localizes to the ER (Fensome *et al*, 2000; Rodrigues-Lima *et al*, 2000; Tomiuk *et al*, 2000), even though nSMase1 lacks conventional ER retention sequences such as KDEL or di-lysine/di-arginine motifs found in some ER proteins (Teasdale & Jackson, 1996). A further site-directed mutagenesis study however showed that one of the two predicted transmembrane domains is required for its efficient ER localization (Rodrigues-Lima *et al*, 2000). Even though these data were challenged by another study showing that endogenous nSMase1 localizes exclusively to the nuclear matrix, there is ample evidence to support its ER localization.

The ER is a large, dynamic structure that serves multiple functions including calcium storage, protein synthesis, and lipid metabolism (Schwarz & Blower, 2016). It is responsible for the synthesis of one-third of all eukaryotic cell proteins, their post-translational modifications and assembly into complexes, and their targeted transport (Hetz *et al*, 2020). Therefore, the maintenance of a healthy proteome in the cell relies on

a functional ER to promote efficient protein folding and trafficking. Any physiological demands, such as increased protein secretion, or pathological insults like disrupted Ca^{2+} concentration level in the ER, leads to inefficient protein folding. Such unfolded or misfolded proteins accumulate in the ER lumen – a condition referred to as 'ER stress'. ER stress in eukaryotic cells activates the unfolded protein response (UPR) – a network of signal transduction pathways to reprogram gene transcription, mRNA translation, and protein modifications to restore protein folding fidelity and to maintain ER functions (Hetz *et al*, 2020).

In this study, although nSMase1 expression was upregulated upon ER stress induction, *SMPD2* depletion alone did not not induce ER stress, and therefore, UPR activation was not observed. However, *SMPD2* KD cells failed to activate a full adaptive UPR, when cells were challenged with two known ER stressors - tunicamycin and thapsigargin. In mammals, the UPR is divided into three pathways initiated by three distinct ER transmembrane protein sensors – the so-called three master regulators IRE1α, PERK, and ATF6α. These signal-transducing proteins sense ER stress through their luminal domains and further activate specific downstream effectors through three distinct pathways. Upon ER stress induction, *SMPD2* KD cells failed to upregulate multiple genes controlled by all three master regulators, which indicates that *SMPD2* KD affects all three UPR signaling pathways. The UPR signaling activation persists until an adaptive response to the ER stress is achieved. In the case of an unresolvable stress, the UPR turns pro-apoptotic to induce cell death (Hetz *et al*, 2020). Indeed, due to their inability to mount a full-potential UPR upon ER stress, *SMPD2* KD cells were also less viable. Of note, *SMPD2* KD, in contrast to inhibitors with fast mode action, might elicit a time-dependent and dose-dependent ER stress to which cells might respond differently. Since genetic knockdown is a continual process, it is hard to obtain an optimal time-point to analyze its immediate biological effect. Indeed, studies have shown that sustained ER stress attenuates the conventional adaptive and pro-survival UPR signaling and rather promotes a pro-apoptotic UPR signaling that mediates cell death (Hetz *et al*, 2020; Szegezdi *et al*, 2006). Therefore, the UPR activation measured after 4h of ER stress induction might be different from the sustained UPR activation for example induced by

gene KD. Nevertheless, the effects of *SMPD2* KD on the UPR activation after ER stress induction indicate that nSMase1 plays an important role in maintaining ER homeostasis.

In addition to an inefficient UPR activation upon ER stress, *SMPD2* KD alone significantly downregulates LAMP1 and WNT3A at both protein and mRNA levels. LAMP1 and WNT3A are integral membrane and secretory proteins respectively (Cook et al, 2004; Mikels & Nusse, 2006), that are initially translated in the cytosol. Then, a signal sequence within the nascent polypeptide chain is recognized by a signal recognition particle (SRP). and the whole mRNA:ribosome:polypeptide:SRP complex is docked to the ER, a process facilitated by SRP binding to its receptor (SRPR) on the ER membrane. Translation continues on the ER and the emerging polypeptide co-translationally enters the ER lumen through the translocon, a channel comprising several sec proteins that spans the lipid bilayer (Akopian et al, 2013; Barlowe & Miller, 2013). NSMase1 activity at the ER may regulate translation or post-translational modification of these proteins by either generating structural lipids or signaling lipids. Indeed, nSMase1 interacts with both signal recognition particle receptor B (SRPRB) and the translocon-associated signal sequence receptor 2 (SSR2) (Huttlin *et al*, 2021, 2015). Therefore, nSMase1 activity may regulate the SRP-dependent co-translational targeting of proteins such as LAMP1 and WNT3A to the ER membrane. For instance, nSMase1 activity could generate specific lipids to establish nanodomains to support efficient mRNA:ribosome:polypeptide:SRP complex docking to the ER membrane. In addition to ER membrane protein reticulon 3 and reticulon 4, nSMase1 also interacts with ER proteins such as glycosylphosphatidylinositol anchor attachment 1 (GPAA1) and phosphatidylinositol glycan anchor biosynthesis, class S (PIG-S) (Huttlin *et al*, 2021). Both of these proteins are involved in post-translational modifications by attaching glycosylphosphatidylinositol (GPI) anchors to proteins in the ER (Vainauskas & Menon, 2005).

Additionally, nSMase1 also interacts with SCAP (SREBP cleavage-activating protein) (Huttlin *et al*, 2021), a protein that functionally and physically associates with SREBP (sterol regulatory element-binding protein) (Rawson, 2003). Under homeostatic sterol levels, SCAP-SREBP resides in the ER membrane through retention factors such as INSIG-1 (Yang *et al*, 2002). Upon sterol depletion, the protein complex is transported to the Golgi where SREBP is sequentially cleaved to release its N-terminal soluble part

which translocates to the nucleus to upregulate genes involved in sterol and lipid biosynthesis (Rawson, 2003). Just as described for INSIG1, the interaction between SCAP and nSMase1 might reflect a functional connection: nSMase1 may contribute to the ER retention of the SREBP:SCAP complex. In this way, *SMPD2* KD might disrupt overall cellular sterol and lipid homeostasis which could have multiple downstream effects including G1 cell cycle arrest as we observed (Lee *et al*, 2020). Therefore, data from our study as well as other studies indicate that nSMase1 not only localizes at the ER but might play an important role in this compartment by contributing to overall ER homeostasis and function and thereby regulates overall cellular fitness.

3.2.3 A possible role of nSMase1 in the nucleus

In agreement with a previous study (Mizutani *et al*, 2001), we observed that endogenous nSMase1 localizes to the nucleus in distinct speckles. Although a conventional nuclear localization signal (NLS) is missing, nSMase1 contains a sequence at the amino acid position between 120-130 (LLVLHLSGLVL), which is homologous to the nuclear export signal (NES)(Mizutani *et al*, 2001). Specifically, nSMase1 localizes to the nuclear matrix (Mizutani *et al*, 2001). The eukaryotic nucleus contains a significant amount of phospholipids including sphingomyelin – distributed among chromatin, nuclear envelope, and in the nuclear matrix (Irvine, 2003; Martelli *et al*, 2004). The presence of active sphingomyelinases and ceramidases in the nucleus indicates that these sphingolipids are actively metabolized in the nucleus as well (Martelli *et al*, 2004; R-ledeen & G.Wu, 2009). For example, a study has shown that radiation activates nuclear neutral sphingomyelinase to generate ceramide for apoptosis (JAFFRÉZOU *et al*, 2001). Therefore, by generating signaling potent lipids such as ceramide, nuclear nSMase1 may be activated in response to different environmental stressors.

Since *SMPD2* KD cells are arrested in the G1 phase, with both P21 and P27 upregulated, nSMase1 activity might drive the remodeling of the nuclear envelope, chromatin, and nuclear matrix during cell-cycle progression by generating required structural lipids (Mizutani *et al*, 2001). Alternatively, since nSMase1 belongs to the superfamily of endo/exonucleases that cleave the phosphodiester bond between the successive

nucleotides (Bill X.Wu, Christopher J.Clarke, 2010), therefore, nSMase1, with its biological substrate still unclear, could possibly hydrolyze the phosphodiesterase bond of the DNA. As described for many endo/exonucleases (Nishino & Morikawa, 2002), nSMase1 could be involved in DNA repair and therefore in the cell cycle. In this way, inefficient DNA repair upon *SMPD2* KD might induce a DNA-damage-like response that upregulates P21 and P27 to induce G1 cell cycle arrest. Therefore, it would certainly be of interest to further investigate the activation of tumor suppressor gene P53 upon *SMPD2* KD. P53 senses DNA damage and mediates cell cycle arrest by upregulating P21 and P27 (Chen, 2016).

In summary, *SMPD2* KD cells are characterized by G1 cell cycle arrest, inefficient UPR activation upon ER stress induction, reduced global protein translation, and downregulated Wnt-signaling activity. Since *SMPD2* KD affected a wide range of cellular processes, it is possible that nSMase1, via generating signaling or structural lipid, regulates inducible gene expression in the nucleus that could have broad biological implications.

3.2.4 NSMase1: A mediator of cellular stress responses with a cell cycle connection?

So far, the best-characterized function of ceramide as a second messenger is its role in apoptosis induction upon different cellular stresses (Arana *et al*, 2010). Ceramide, generated either by *de novo* synthesis or by sphingomyelinase activity, mediates apoptosis in response to different cellular stress conditions including heat shock, chemotherapeutic agents, and β-amyloid peptides (Chang *et al*, 1995; Jaffrézou *et al*, 1996; Jana & Pahan, 2004). Some studies indicated that nSMase1 is the main sphingomyelinase activated in response to stress (Jana & Pahan, 2004; Lee *et al*, 2004; Tonnetti *et al*, 1999b; Yabu *et al*, 2008). Specifically, a study has shown that nSMase1 is activated via phosphorylation by JNK in response to different stressors including heat shock, UV exposure and hydrogen peroxide. Activated nSMase1 generates ceramide to induce apoptosis under these stress conditions in zebrafish embryonic and human Jurkat T cells (Yabu *et al*, 2015).

In contrast to *SMPD3* KD, which slightly increased cellular viability presumably due to decreased ceramide generation, *SMPD2* KD significantly reduced cell viability without inducing apoptosis. Moreover, under ER stress conditions, *SMPD2* KD reduced cell viability. These observations are in sharp contrast to the above studies that showed the role of nSMase1 in generating ceramide for apoptosis in response to cellular stress conditions. Therefore, our data rule out a role for nSMase1 in promoting cell death under both normal and ER stress conditions. Additionally, autophagy, a major cellular stress response to serum starvation, remained unaffected by *SMPD2* KD. Reduced cell viability and G1 cell cycle arrest upon *SMPD2* KD however indicate a vital role for nSMase1 in cell survival and proliferation.

Duplication of not only cellular DNA content but also of membranes and organelles is a prerequisite for cellular growth and division. Lipids play an important role in cell cycle regulation (Storck *et al*, 2018). For example, the two triacylglycerol lipases Tgl3 and Tgl4 are required for efficient cell cycle progression during the G1/S transition in yeast cells (Chauhan *et al*, 2015). Specifically, lipolysis-derived sphingolipids activate PP2A, a major cell cycle regulating protein phosphatase (Wlodarchak & Xing, 2016), to dephosphorylate SWE1 (orthologue to human WEE1) for efficient cell cycle progression (Chauhan *et al*, 2015). Therefore, it is conceivable that ceramide generated by *SMPD2* acts as a second messenger targeting proteins such as PP2A, which are involved in cell-cycle regulation. Indeed, several studies proposed PP1 and PP2A as the potential intracellular protein target of ceramides. PP2A dephosphorylates over 300 substrates involved in the cell cycle, thereby regulating almost all major pathways including the Wnt pathway and cell cycle checkpoints (Wlodarchak & Xing, 2016). Therefore, reduced Wnt-signaling could be also due to deregulated PP2A activity upon *SMPD2* KD.

With our study showing *SMPD2* KD cells arrested at the G1 phase with reduced global protein translation, inefficient UPR activation, downregulated Wnt-signaling activity, and an altered PI3K/Akt pathway, it is clear that nSMase1 plays a vital role in maintaining cellular homeostasis.

3.3 Summary and outlook

Evidence collected over the recent years has established sEV secretion as a strong driver of intercellular communication under both physiological and pathological conditions. In particular, sEVs play major roles in tumor progression and neurological disorders by propagating tumor- or disease-associated components between cells (Budnik *et al*, 2016; Shurtleff *et al*, 2018). Signaling potent intact sEVs can be readily extracted from all major bodily fluids (Bellingham *et al*, 2012). Thus, sEVs harbor great potential for both therapeutic and clinical applications. To explore the full potential of sEV secretion as a possible therapeutic target for example during tumorigenesis or for the use of these small vesicles as a vector for targeted drug delivery, it is of utmost importance to first understand the regulatory pathways involved in their biogenesis and secretion.

Current EV research disproportionately focuses on their functional aspects more than on their biogenesis mechanisms and secretion regulations. Therefore, we aimed to dissect the molecular mechanisms that underlie ILV generation for sEV secretion with a focus on nSMase2. Our data elucidates that nSMase2 regulates sEV secretion by counteracting V-ATPase activity on endosomal membranes. We delineate a so far unknown mechanism by which nSMase2 regulates sEV secretion and provide evidence that the local lipid environment at MVBs and specifically the levels of ceramide, sphingomyelin, and cholesterol regulate sEV secretion by modulating endosomal acidification. Importantly, we show that TNFα, a prominent pro-inflammatory cytokine and a known nSMase2 agonist, promotes sEV secretion by modulating endosomal acidification via modulating V-ATPase complex assembly. These findings for the first time establish a molecular link between TNFα-induced nSMase2 activation and sEV secretion.

In addition to its role in attenuating V-ATPase activity to promote secretory MVB generation/trafficking for sEV secretion, we also show that nSMase2 affects LAMP1 levels, specifically during serum starvation-induced autophagy. Therefore, how nSMase2-mediated endosomal acidification regulation affects autophagy remains an interesting question to explore. Furthermore, how nSMase2-dependent MVB deacidification affects the recruitment of further MVB secretory machineries, including kinesin motor proteins for its anterograde transport, Rab27a, Rab27b (Ostrowski *et al*,

2010) and SNARE proteins such as YKT6 (Gross *et al*, 2012) for plasma membrane fusion, remain interesting questions to be studied.

Like nSMase2, also nSMase1 belongs to the group of neutral sphingomyelinases, which hydrolyze sphingomyelin (Tomiuk *et al*, 1998b). Interestingly, however, both proteins show distinct cellular localizations and tissue expression patterns. NSMase2 is predominantly expressed in the brain (Stoffel *et al*, 2005), while nSMase1 is ubiquitously expressed (Zumbansen & Stoffel, 2002). Although nSMase2 is both functionally and structurally well-characterized, nSMase1 is far less explored and studied. Therefore, the second part of the thesis focused on investigating the biological role of nSMase1.

We found that nSMase1 is required for activating an efficient unfolded protein response upon ER stress induction by tunicamycin and thapsigargin. *SMPD2* KD cells failed to upregulate multiple genes involved in all the three UPR pathways to resolve ER stress to the same levels as their control counterparts. Furthermore, we show that nSMase1 is necessary for proper cell cycle progression, as *SMPD2* KD resulted in significant G1 arrest. Moreover, the global protein translation and Wnt-signaling activity was reduced by *SMPD2* KD. These data, for the first time, establish an important biological role for nSMase1. In summary, these findings serve as a strong basis to further dissect the role of nSMase1 in specific pathways and to ultimately find its biological substrate.

4 References

Abbas YM, Wu D, Bueler SA, Robinson C V. & Rubinstein JL (2020) Structure of V-ATPase from the mammalian brain. *Science (80-)* 367: 1240–1246

Adam-Klages S, Adam D, Wiegmann K, Struve S, Kolanus W, Schneider-Mergener J & Krönke M (1996) FAN, a novel WD-repeat protein, couples the p55 TNF-receptor to neutral sphingomyelinase. *Cell* 86: 937–947

Admyre C, Bohle B, Johansson SM, Focke-Tejkl M, Valenta R, Scheynius A & Gabrielsson S (2007) B cell-derived exosomes can present allergen peptides and activate allergen-specific T cells to proliferate and produce TH2-like cytokines. *J Allergy Clin Immunol* 120: 1418–1424

Airola M V & Hannun YA (2013) Sphingolipid metabolism and neutral sphingomyelinases. *Handb Exp Pharmacol* (215): 57–

Airola M V, Shanbhogue P, Shamseddine AA, Guja KE, Senkal CE, Maini R, Bartke N, Wu BX, Obeid LM, Garcia-Diaz M, *et al* (2017) Structure of human nSMase2 reveals an interdomain allosteric activation mechanism for ceramide generation. *Proc Natl Acad Sci* 114: E5549–E5558

Al-Nedawi K, Meehan B & Rak J (2009) Microvesicles: Messengers and mediators of tumor progression. *Cell Cycle* 8: 2014–2018

Al-Rashed F, Ahmad Z, Thomas R, Melhem M, Snider AJ, Obeid LM, Al-Mulla F, Hannun YA & Ahmad R (2020) Neutral sphingomyelinase 2 regulates inflammatory responses in monocytes/macrophages induced by TNF-α. *Sci Rep* 10: 1–12

Ananbeh H, Vodicka P & Kupcova Skalnikova H (2021) Emerging roles of exosomes in Huntington's disease. *Int J Mol Sci* 22

Aqrawi LA, Galtung HK, Vestad B, Øvstebø R, Thiede B, Rusthen S, Young A, Guerreiro EM, Utheim TP, Chen X, *et al* (2017) Identification of potential saliva and tear biomarkers in primary Sjögren's syndrome, utilising the extraction of extracellular vesicles and proteomics analysis. *Arthritis Res Ther* 19: 1–15

Arana L, Gangoiti P, Ouro A, Trueba M & Gómez-Muñoz A (2010) Ceramide and ceramide 1-phosphate in health and disease. *Lipids Health Dis* 9: 1–12

Arias-Moreno X, Velazquez-Campoy A, Rodríguez JC, Pocoví M & Sancho J (2008) Mechanism of low density lipoprotein (LDL) release in the endosome: Implications of the stability and Ca2+ affinity of the fifth binding module of the LDL receptor. *J Biol Chem* 283: 22670–22679

Babst M (2011) MVB Vesicle Formation: ESCRT-Dependent, ESCRT-Independent and Everything in Between. *Curr Opin Cell Biol* 23: 452–457

Back MJ, Ha HC, Fu Z, Choi JM, Piao Y, Won JH & Jang JM (2018) Activation of neutral sphingomyelinase 2 by starvation induces cell-protective autophagy via an increase in Golgi- localized ceramide. *Cell Death Dis*

Baietti MF, Zhang Z, Mortier E, Melchior A, Degeest G, Geeraerts A, Ivarsson Y, Depoortere F, Coomans C, Vermeiren E, *et al* (2012) Syndecan-syntenin-ALIX regulates the biogenesis of exosomes. *Nat Cell Biol* 14: 677–685

Balkwill F (2006) TNF-α in promotion and progression of cancer. *Cancer Metastasis Rev* 25: 409–416

Banerjee S, Clapp K, Tarsio M & Kane PM (2019) Interaction of the late endo-lysosomal lipid PI(3,5)P2 with the Vph1 isoform of yeast V-ATPase increases its activity and cellular stress tolerance. *J Biol Chem* 294: 9161–9171

Banerjee S & Kane PM (2017) Direct interaction of the Golgi V-ATPase a-subunit isoform with PI(4)P drives localization of Golgi V-ATPases in yeast. *Mol Biol Cell* 28: 2518–2530

Banerjee S & Kane PM (2020) Regulation of V-ATPase Activity and Organelle pH by Phosphatidylinositol Phosphate Lipids. *Front Cell Dev Biol* 8

Bänfer S, Schneider D, Dewes J, Strauss MT, Freibert SA, Heimerl T, Maier UG, Elsässer HP, Jungmann R & Jacob R (2018) Molecular mechanism to recruit galectin-3 into multivesicular bodies for polarized exosomal secretion. *Proc Natl Acad Sci U S A* 115: E4396–E4405

Barlowe CK & Miller EA (2013) Secretory protein biogenesis and traffic in the early secretory pathway. *Genetics* 193: 383–410

Bayer N, Schober D, Prchla E, Murphy RF, Blaas D & Fuchs R (1998) Effect of Bafilomycin A1 and Nocodazole on Endocytic Transport in HeLa Cells: Implications

for Viral Uncoating and Infection. *J Virol* 72: 9645–9655

Becker A, Thakur BK, Weiss JM, Kim HS, Peinado H & Lyden D (2016) Extracellular Vesicles in Cancer: Cell-to-Cell Mediators of Metastasis. *Cancer Cell* 30: 836–848

Bellingham SA, Guo BB, Coleman BM & Hill AF (2012) Exosomes: Vehicles for the transfer of toxic proteins associated with neurodegenerative diseases? *Front Physiol* 3 MAY: 1–12

Bill X.Wu, Christopher J.Clarke and YAH (2010) Mammalian Neutralsphingomyelinases: Regulation and Roles in Cell Signaling Responses. *Neuromolecular Med* 12: 320–330

Bodzęta A, Kahms M & Klingauf J (2017) The Presynaptic v-ATPase Reversibly Disassembles and Thereby Modulates Exocytosis but Is Not Part of the Fusion Machinery. *Cell Rep* 20: 1348–1359

Böttcher RT, Stremmel C, Meves A, Meyer H, Widmaier M, Tseng HY & Fässler R (2012) Sorting nexin 17 prevents lysosomal degradation of β1 integrins by binding to the β 1-integrin tail. *Nat Cell Biol* 14: 584–592

Bourne HR, Sanders DA & McCormick F (1991) The GTPase superfamily: conserved structure and molecular mechanism. *Nature* 349: 117–127

Bowman EJ & Bowman BJ (2005) V-ATPases as drug targets. *J Bioenerg Biomembr* 37: 431–435

Breton S & Brown D (2013) Regulation of luminal acidification by the V-ATPase. *Physiology* 28: 318–329

Budnik V, Ruiz-Cañada C & Wendler F (2016) Extracellular vesicles round off communication in the nervous system. *Nat Rev Neurosci* 17: 160–172

Buschow SI, Nolte-'t Hoen ENM, van Niel G, Pols MS, ten Broeke T, Lauwen M, Ossendorp F, Melief CJM, Raposo G, Wubbolts R, *et al* (2009) MHC II In dendritic cells is targeted to lysosomes or t cell-induced exosomes via distinct multivesicular body pathways. *Traffic* 10: 1528–1542

Candelario KM & Steindler DA (2014) The role of extracellular vesicles in the progression of neurodegenerative disease and cancer. *Trends Mol Med* 20: 368–374

Chairoungdua A, Smith DL, Pochard P, Hull M & Caplan MJ (2010) Exosome release of

β-catenin: A novel mechanism that antagonizes Wnt signaling. *J Cell Biol* 190: 1079–1091

Chang Y, Abe A & Shayman JA (1995) Ceramide formation during heat shock: A potential mediator of αB-crystallin transcription. *Proc Natl Acad Sci U S A* 92: 12275–12279

Chauhan N, Visram M, Cristobal-Sarramian A, Sarkleti F & Kohlwein SD (2015) Morphogenesis checkpoint kinase Swe1 is the executor of lipolysis-dependent cell-cycle progression. *Proc Natl Acad Sci U S A* 112: E1077–E1085

Chen C, Garcia-Santos D, Ishikawa Y, Seguin A, Li L, Fegan KH, Hildick-Smith GJ, Shah DI, Cooney JD, Chen W, *et al* (2013) Snx3 regulates recycling of the transferrin receptor and iron assimilation. *Cell Metab* 17: 343–352

Chen J (2016) The cell-cycle arrest and apoptotic and progression. *Cold Spring Harb Perspect Biol*: 1–16

Chen SH, Bubb MR, Yarmola EG, Zuo J, Jiang J, Lee BS, Lu M, Gluck SL, Hurst IR & Holliday LS (2004) Vacuolar H+-ATPase binding to microfilaments: Regulation in response to phosphatidylinositol 3-kinase activity and detailed characterization of the actin-binding site in subunit B. *J Biol Chem* 279: 7988–7998

Chevallier J, Chamoun Z, Jiang G, Prestwich G, Sakai N, Matile S, Parton RG & Gruenberg J (2008) Lysobisphosphatidic acid controls endosomal cholesterol levels. *J Biol Chem* 283: 27871–27880

Clancy JW, Sedgwick A, Rosse C, Muralidharan-Chari V, Raposo G, Method M, Chavrier P & D'Souza-Schorey C (2015) Regulated delivery of molecular cargo to invasive tumour-derived microvesicles. *Nat Commun* 6: 1–11

Clarke CJ, Truong T & Hannun YA (2006) Role for Neutral Sphingomyelinase-2 in Tumor Necrosis Factor ␣ -Stimulated Expression of Vascular Cell Adhesion Molecule-1 (VCAM) and Intercellular Adhesion Molecule-1 (ICAM) in Lung Epithelial Cells. *J Biol Chem* 282: 1384–1396

Clarke CJ, Truong TG & Hannun YA (2007) Role for neutral sphingomyelinase-2 in tumor necrosis factor α-stimulated expression of vascular cell adhesion molecule-1 (VCAM) and intercellular adhesion molecule-1 (ICAM) in lung epithelial cells: p38 MAPK is an upstream regulator of nSMase2. *J Biol Chem* 282: 1384–1396

Cogolludo A, Moreno L, Frazziano G, Moral-Sanz J, Menendez C, Castañeda J, González C, Villamor E & Perez-Vizcaino F (2009) Activation of neutral sphingomyelinase is involved in acute hypoxic pulmonary vasoconstriction. *Cardiovasc Res* 82: 296–302

Colacurcio DJ & Nixon RA (2016) Disorders of lysosomal acidification - the emerging role of vATPase in aging and neurodegenerative disease. *Physiol Behav* 32: 75–88

Colombo M, Moita C, Van Niel G, Kowal J, Vigneron J, Benaroch P, Manel N, Moita LF, Théry C & Raposo G (2013) Analysis of ESCRT functions in exosome biogenesis, composition and secretion highlights the heterogeneity of extracellular vesicles. *J Cell Sci* 126: 5553–5565

Del Conde I, Shrimpton CN, Thiagarajan P & López JA (2005) Tissue-factor-bearing microvesicles arise from lipid rafts and fuse with activated platelets to initiate coagulation. *Blood* 106: 1604–1611

Costa-Silva B, Aiello NM, Ocean AJ, Singh S, Zhang H, Thakur BK, Becker A, Hoshino A, Mark MT, Molina H, *et al* (2015) Pancreatic cancer exosomes initiate pre-metastatic niche formation in the liver. *Nat Cell Biol* 17: 816–826

Cotter K, Capecci J, Sennoune S, Huss M, Maier M, Martinez-Zaguilan R & Forgac M (2015) Activity of Plasma Membrane V-ATPases Is Critical for the Invasion of MDA-MB231 Breast Cancer Cells. *J Biol Chem* 290: 3680–3692

Cullen PJ & Steinberg F (2018) To degrade or not to degrade: mechanisms and significance of endocytic recycling. *Nat Rev Mol Cell Biol* 19: 679–696

Dai J, Li J, Bos E, Porcionatto M, Premont RT, Bourgoin S, Peters PJ & Hsu VW (2004) ACAP1 promotes endocytic recycling by recognizing recycling sorting signals. *Dev Cell* 7: 771–776

Dawson K, Toone WM, Jones N & Wilkinson CRM (2008) Loss of regulators of vacuolar ATPase function and ceramide synthesis results in multidrug sensitivity in Schizosaccharomyces pombe. *Eukaryot Cell* 7: 926–937

Donaldson JG & Jackson CL (2011) ARF family G proteins and their regulators: Roles in membrane transport, development and disease. *Nat Rev Mol Cell Biol* 12: 362–375

Dong L, Zieren RC, Horie K, Kim CJ, Mallick E, Jing Y, Feng M, Kuczler MD, Green J,

Amend SR, *et al* (2020) Comprehensive evaluation of methods for small extracellular vesicles separation from human plasma, urine and cell culture medium. *J Extracell Vesicles* 10

Dores MR, Chen B, Lin H, Soh UJK, Paing MM, Montagne WA, Meerloo T & Trejo JA (2012) ALIX binds a YPX 3L motif of the GPCR PAR1 and mediates ubiquitin-independent ESCRT-III/MVB sorting. *J Cell Biol* 197: 407–419

Dores MR, Grimsey NJ, Mendez F & Trejo JA (2016) ALIX regulates the ubiquitin-independent lysosomal sorting of the P2Y1 purinergic receptor via a YPX3 L motif. *PLoS One* 11: 1–20

Duan RD, Cheng Y, Hansen G, Hertervig E, Liu JJ, Syk I, Sjöström H & Nilsson Å (2003) Purification, localization, and expression of human intestinal alkaline sphingomyelinase. *J Lipid Res* 44: 1241–1250

Edgar JR, Eden ER & Futter CE (2014) Hrs- and CD63-Dependent Competing Mechanisms Make Different Sized Endosomal Intraluminal Vesicles. *Traffic* 15: 197–211

Edgar JR, Manna PT, Nishimura S, Banting G & Robinson MS (2016) Tetherin is an exosomal tether. *Elife* 5: 1–19

Erez Eitan, Suire C, Zhang S & Mattson MP (2016) Impact of Lysosome Status on Extracellular Vesicle Content and Release. *ageing Res Rev* 32: 65–74

Esmail S, Kartner N, Yao Y, Kim JW, Reithmeier RAF & Manolson MF (2018) Molecular mechanisms of cutis laxa- and distal renal tubular acidosis-causing mutations in V-ATPase a subunits, ATP6V0A2 and ATP6V0A4. *J Biol Chem* 293: 2787–2800

Farrugia M & Baron B (2000) The role of TNF-α cells in rheumatoid arthritis. *Arch Immunol Ther Exp (Warsz)* 48: 429–435

Fensome AC, Rodrigues-Lima F, Josephs M, Paterson HF & Katan M (2000) A neutral magnesium-dependent sphingomyelinase isoform associated with intracellular membranes and reversibly inhibited by reactive oxygen species. *J Biol Chem* 275: 1128–1136

Fjorback AW, Seaman M, Gustafsen C, Mehmedbasic A, Gokool S, Wu C, Militz D, Schmidt V, Madsen P, Nyengaard JR, *et al* (2012) Retromer binds the FANSHY

sorting motif in sorLA to regulate amyloid precursor protein sorting and processing. *J Neurosci* 32: 1467–1480

Forgac M (2007) Vacuolar ATPases: Rotary proton pumps in physiology and pathophysiology. *Nat Rev Mol Cell Biol* 8: 917–929

Fornoni A, Sageshima J, Wei C, Merscher-Gomez S, Aguillon-Prada R, Jauregui AN, Li J, Mattiazzi A, Ciancio G, Chen L, *et al* (2011) Rituximab targets podocytes in recurrent focal segmental glomerulosclerosis. *Sci Transl Med* 3

Frattini A, Orchard PJ, Sobacchi C, Giliani S, Abinun M, Mattsson JP, Keeling DJ, Andersson AK, Wallbrandt P, Zecca L, *et al* (2000) Defects in TCIRG1 subunit of the vacuolar proton pump are responsible for a subset of human autosomal recessive osteopetrosis. *Nat Genet* 25: 343–346

Fujii T, Sakata A, Nishimura S, Eto K & Nagata S (2015) TMEM16F is required for phosphatidylserine exposure and microparticle release in activated mouse platelets. *Proc Natl Acad Sci U S A* 112: 12800–12805

Futter CE, Pearse A, Hewlett LJ & Hopkins CR (1996) Multivesicular endosomes containing internalized EGF-EGF receptor complexes mature and then fuse directly with lysosomes. *J Cell Biol* 132: 1011–1023

Garoby-Salom S, Rouahi M, Mucher E, Auge N, Salvayre R & Negre-Salvayre A (2015) Hyaluronan synthase-2 upregulation protects *SMPD3*-deficient fibroblasts against cell death induced by nutrient deprivation, but not against apoptosis evoked by oxidized LDL. *Redox Biol* 4: 118–126

Ghoroghi S, Mary B, Asokan N, Goetz JG & Hyenne V (2021) Tumor extracellular vesicles drive metastasis (it's a long way from home). *FASEB BioAdvances* 3: 930–943

Gross JC, Chaudhary V, Bartscherer K & Boutros M (2012) Active Wnt proteins are secreted on exosomes. *Nat Cell Biol* 14: 1036–1045

Gruenberg J (2001) The Endocytic Pathway: A MOSAIC OF DOMAINS. *Nat Rev Mol Cell Biol* 2: 721–730

Gu F & Gruenberg J (2000) ARF1 regulates pH-dependent COP functions in the early endocytic pathway. *J Biol Chem* 275: 8154–8160

Gu LZ, Huang BS, Shen W, Gao L, Ding ZZ, Wu HW & Guo J (2013) Early activation of

nSMase2/ceramide pathway in astrocytes is involved in ischemia-associated neuronal damage via inflammation in rat hippocampi. *J Neuroinflammation* 10: 1–16

Guo BB, Bellingham SA & Hill AF (2015) The neutral sphingomyelinase pathway regulates packaging of the prion protein into exosomes. *J Biol Chem* 290: 3455–3467

Guo H, Chitiprolu M, Roncevic L, Javalet C, Hemming FJ, Trung MT, Meng L, Latreille E, Tanese de Souza C, McCulloch D, *et al* (2017) Atg5 Disassociates the V1V0-ATPase to Promote Exosome Production and Tumor Metastasis Independent of Canonical Macroautophagy. *Dev Cell* 43: 716-730.e7

Guo M, Wang J, Zhao Y, Feng Y, Han S, Dong Q, Cui M & Tieu K (2020) Microglial exosomes facilitate a-synuclein transmission in Parkinson's disease. *Brain* 143: 1476–1497

Gutiérrez-Vázquez C, Villarroya-Beltri C, Mittelbrunn M & Sánchez-Madrid F (2013) Transfer of extracellular vesicles during immune cell-cell interactions. *Immunol Rev* 251: 125–142

Haglund K, Sigismund S, Polo S, Szymkiewicz I, Di Fiore PP & Dikic I (2003) Multiple monoubiquitination of RTKs is sufficient for their endocytosis and degradation. *Nat Cell Biol* 5: 461–466

Hait NC (2009) Erratum: Regulation of histone acetylation in the nucleus by sphingosine-1-phosphate (Science (1254)). *Science (80-)* 326: 366

Heifetz A, Keenan RW & Elbein AD (1979) Mechanism of Action of Tunicamycin on the UDP-GlcNAc:Dolichyl-Phosphate GlcNAc-1 -Phosphate Transferase. *Biochemistry* 18: 2186–2192

Heijnen HFG, Schiel AE, Fijnheer R, Geuze HJ & Sixma JJ (1999) Activated platelets release two types of membrane vesicles: Microvesicles by surface shedding and exosomes derived from exocytosis of multivesicular bodies and α-granules. *Blood* 94: 3791–3799

Hetz C, Zhang K & Kaufman RJ (2020) Mechanisms, regulation and functions of the unfolded protein response. *Nat Rev Mol Cell Biol* 21: 421–438

Hiam-Galvez KJ, Allen BM & Spitzer MH (2021) Systemic immunity in cancer. *Nat Rev*

Cancer 21: 345–359

Hnasko TS & Edwards RH (2012) Neurotransmitter corelease: Mechanism and physiological role. *Annu Rev Physiol* 74: 225–243

Hofmann K, Tomiuk S, Wolff G & Stoffel W (2000) Cloning and characterization of the mammalian brain-specific, Mg2+-dependent neutral sphingomyelinase. *Proc Natl Acad Sci U S A* 97: 5895–900

Holbrook J, Lara-Reyna S, Jarosz-Griffiths H & McDermott M (2019) Tumour necrosis factor signalling in health and disease [version 1; referees: 2 approved]. *F1000Research* 8: 1–12

Holthuis JCM & Levine TP (2005) Lipid traffic: Floppy drives and a superhighway. *Nat Rev Mol Cell Biol* 6: 209–220

Holthuis JCM & Menon AK (2014) Lipid landscapes and pipelines in membrane homeostasis. *Nature* 510: 48–57

Hood JL, San Roman S & Wickline SA (2011) Exosomes released by melanoma cells prepare sentinel lymph nodes for tumor metastasis. *Cancer Res* 71: 3792–3801

Hsu VW, Bai M & Li J (2012) Getting active: Protein sorting in endocytic recycling. *Nat Rev Mol Cell Biol* 13: 323–328

Hu W, Song X, Yu H, Sun J & Zhao Y (2020) Released Exosomes Contribute to the Immune Modulation of Cord Blood-Derived Stem Cells. *Front Immunol* 11: 1–13

Huotari J & Helenius A (2011) Endosome maturation. *EMBO J* 30: 3481–3500

Hurley JH (2008) ESCRT complexes and the biogenesis of multivesicular bodies. *Curr Opin Cell Biol* 20: 4–11

Hurtado-Lorenzo A, Skinner M, El Annan J, Futai M, Sun-Wada GH, Bourgoin S, Casanova J, Wildeman A, Bechoua S, Ausiello DA, *et al* (2006) V-ATPase interacts with ARNO and Arf6 in early endosomes and regulates the protein degradative pathway. *Nat Cell Biol* 8: 124–136

Huttlin EL, Bruckner RJ, Navarrete-Perea J, Cannon JR, Baltier K, Gebreab F, Gygi MP, Thornock A, Zarraga G, Tam S, *et al* (2021) Dual proteome-scale networks reveal cell-specific remodeling of the human interactome. *Cell* 184: 3022-3040.e28

Huttlin EL, Ting L, Bruckner RJ, Gebreab F, Gygi MP, Szpyt J, Tam S, Zarraga G, Colby

G, Baltier K, *et al* (2015) The BioPlex Network: A Systematic Exploration of the Human Interactome. *Cell* 162: 425–440

Irvine RF (2003) Nuclear lipid signalling. *Nat Rev Mol Cell Biol* 4: 349–360

Ito H, Murakami M, Furuhata A, Gao S, Yoshida K, Sobue S, Hagiwara K, Takagi A, Kojima T, Suzuki M, *et al* (2009) Transcriptional regulation of neutral sphingomyelinase 2 gene expression of a human breast cancer cell line, MCF-7, induced by the anti-cancer drug, daunorubicin. *Biochim Biophys Acta - Gene Regul Mech* 1789: 681–690

Jabbari N, Akbariazar E, Feqhhi M, Rahbarghazi R & Rezaie J (2020) Breast cancer-derived exosomes: Tumor progression and therapeutic agents. *J Cell Physiol* 235: 6345–6356

JAFFRÉZOU J-P, BRUNO AP, MOISAND A, LEVADE T & LAURENT G (2001) Activation of a nuclear sphingomyelinase in radiation induced apoptosis. *FASEB J* 15: 123–133

Jaffrézou JP, Levade T, Bettaïeb A, Andrieu N, Bezombes C, Maestre N, Vermeersch S, Rousse A & Laurent G (1996) Daunorubicin-induced apoptosis: Triggering of ceramide generation through sphingomyelin hydrolysis. *EMBO J* 15: 2417–2424

Jana A & Pahan K (2004) Fibrillar amyloid-β peptides kill human primary neurons via NADPH oxidase-mediated activation of neutral sphingomyelinase: Implications for Alzheimer's disease. *J Biol Chem* 279: 51451–51459

Jing S, Spencer T, Miller K, Hopkins C & Trowbridge IS (1990) Role of the Human Transferrin Receptor Cytoplasmic Domain in Endocytosis: Localization Of a Specific Signal Sequence for Internalization. *J Cell Biol* 110: 283–294

Johannes M. Herrmann and Anne Spang (2015) Intracellular Parcel Service: Current Issues in Intracellular Membrane Traffi cking. *Membr Traffick Second Ed* 1270: 1–451

Kajimoto T, Okada T, Miya S, Zhang L & Nakamura SI (2013) Ongoing activation of sphingosine 1-phosphate receptors mediates maturation of exosomal multivesicular endosomes. *Nat Commun* 4

Kakarla R, Hur J, Kim YJ, Kim J & Chwae YJ (2020) Apoptotic cell-derived exosomes: messages from dying cells. *Exp Mol Med* 52: 1–6

Kalluri R & LeBleu VS (2020) The biology, function, and biomedical applications of exosomes. *Science (80-)* 367

Kanada M, Bachmann MH & Contag CH (2016) Signaling by Extracellular Vesicles Advances Cancer Hallmarks. *Trends in Cancer* 2: 84–94

Karakashian AA, Giltiay N V., Smith GM & Nikolova-Karakashian MN (2004) Expression of neutral sphingomyelinase-2 (NSMase-2) in primary rat hepatocytes modulates IL-β-induced JNK activation. *FASEB J* 18: 968–970

Karet FE, Finberg KE, Nelson RD, Nayir A, Mocan H, Sanjad SA, Rodriguez-Soriano J, Santos F, Cremers CWRJ, Di Pietro A, *et al* (1999) Mutations in the gene encoding B1 subunit of H+-ATPase cause renal tubular acidosis with sensorineural deafness. *Nat Genet* 21: 84–90

Katzmann DJ, Babst M & Emr SD (2001) Ubiquitin-dependent sorting into the multivesicular body pathway requires the function of a conserved endosomal protein sorting complex, ESCRT-I. *Cell* 106: 145–155

Kawasaki-Nishi S, Nishi T & Forgac M (2001) Yeast V-ATPase Complexes Containing Different Isoforms of the 100-kDa a-subunit Differ in Coupling Efficiency and in Vivo Dissociation. *J Biol Chem* 276: 17941–17948

Kellokumpu S (2019) Golgi pH, ion and redox homeostasis: How much do they really matter? *Front Cell Dev Biol* 7: 1–15

Van Kerkhof P, Lee J, McCormick L, Tetrault E, Lu W, Schoenfish M, Oorschot V, Strous GJ, Klumperman J & Bu G (2005) Sorting nexin 17 facilitates LRP recycling in the early endosome. *EMBO J* 24: 2851–2861

Kim MY, Linardic C, Obeid L & Hannun Y (1991) Identification of sphingomyelin turnover as an effector mechanism for the action of tumor necrosis factor α and γ-interferon. Specific role in cell differentiation. *J Biol Chem* 266: 484–489

Kim WJ, Okimoto RA, Purton LE, Goodwin M, Haserlat SM, Dayyani F, Sweetser DA, Mcclatchey AI, Bernard OA, Look AT, *et al* (2009) Mutations in the neutral sphingomyelinase gene *SMPD3* implicate the ceramide pathway in human leukemias. *Bone* 111: 4716–4723

Klausner RD & Donaldson JG (1994) ARF: a key regulatory switch in membrane traffic

and organelle structure. *Curr Opin Cell Biol* 6: 527–532

Kolesnick RN & Krönke M (1998) Regulation of ceramide production and apoptosis. *Annu Rev Physiol* 60: 643–645

Kolmakova A, Kwiterovich P, Virgil D, Alaupovic P, Knight-Gibson C, Martin SF & Chatterjee S (2004) Apolipoprotein C-I Induces Apoptosis in Human Aortic Smooth Muscle Cells via Recruiting Neutral Sphingomyelinase. *Arterioscler Thromb Vasc Biol* 24: 264–269

Kornak U, Reynders E, Dimopoulou A, Van Reeuwijk J, Fischer B, Rajab A, Budde B, Nürnberg P, Foulquier F, Dobyns WB, *et al* (2008) Impaired glycosylation and cutis laxa caused by mutations in the vesicular H+-ATPase subunit ATP6V0A2. *Nat Genet* 40: 32–34

Krämer-Albers EM, Bretz N, Tenzer S, Winterstein C, Möbius W, Berger H, Nave KA, Schild H & Trotter J (2007) Oligodendrocytes secrete exosomes containing major myelin and stress-protective proteins: Trophic support for axons? *Proteomics - Clin Appl* 1: 1446–1461

Krut O, Wiegmann K, Kashkar H, Yazdanpanah B & Krönke M (2006) Novel tumor necrosis factor-responsive mammalian neutral sphingomyelinase-3 is a C-tail-anchored protein. *J Biol Chem* 281: 13784–13793

Kunadt M, Eckermann K, Stuendl A, Gong J, Russo B, Strauss K, Rai S, Kügler S, Falomir Lockhart L, Schwalbe M, *et al* (2015) Extracellular vesicle sorting of α-Synuclein is regulated by sumoylation. *Acta Neuropathol* 129: 695–713

Lafourcade C, Sobo K, Kieffer-Jaquinod S, Garin J & van der Goot FG (2008) Regulation of the V-ATPase along the endocytic pathway occurs through reversible subunit association and membrane localization. *PLoS One* 3

Lata M, Hettinghouse AS & Liu C ju (2019) Targeting tumor necrosis factor receptors in ankylosing spondylitis. *Ann N Y Acad Sci* 1442: 5–16

Latifkar A, Ling L, Hingorani A, Johansen E, Clement A, Zhang X, Hartman J, Fischbach C, Lin H, Cerione RA, *et al* (2019) Loss of Sirtuin 1 Alters the Secretome of Breast Cancer Cells by Impairing Lysosomal Integrity. *Dev Cell* 49: 393-408.e7

Lee JT, Xu J, Lee JM, Ku G, Han X, Yang DI, Chen S & Hsu CY (2004) Amyloid-β peptide

induces oligodendrocyte death by activating the neutral sphingomyelinase-ceramide pathway. *J Cell Biol* 164: 123–131

Lee SH, Lee JH & Im SS (2020) The cellular function of SCAP in metabolic signaling. *Exp Mol Med* 52: 724–729

Leloup N, Lössl P, Meijer DH, Brennich M, Heck AJR, Thies-Weesie DME & Janssen BJC (2017) Low pH-induced conformational change and dimerization of sortilin triggers endocytosed ligand release. *Nat Commun* 8: 1–15

Levy M, Castillo SS & Goldkorn T (2006) nSMase2 activationd and trafficking are modulated by oxidative stress to induce apoptosis. *Biochem Biophys Res Commun* 344: 900–905

Levy M, Khan E, Careaga M & Goldkorn T (2009) Neutral sphingomyelinase 2 is activated by cigarette smoke to augment ceramide-induced apoptosis in lung cell death. *Am J Physiol - Lung Cell Mol Physiol* 297: 125–133

Li B, Antonyak MA, Zhang J & Cerione RA (2012) RhoA triggers a specific signaling pathway that generates transforming microvesicles in cancer cells. *Oncogene* 31: 4740–4749

Li M, Liao L & Tian W (2020) Extracellular Vesicles Derived From Apoptotic Cells: An Essential Link Between Death and Regeneration. *Front Cell Dev Biol* 8: 1–12

Li SC, Diakov TT, Xu T, Tarsio M, Zhu W, Couoh-Cardel S, Weisman LS & Kane PM (2014) The signaling lipid PI(3,5)P2 stabilizes V1-Vo sector interactions and activates the V-ATPase. *Mol Biol Cell* 25: 1251–1262

Liang Y, Wang Y, Wang W, Zhao J, Xu M & Zheng M (2021) *SMPD3*-ALK: A novel ALK fusion gene in lung adenocarcinoma. *Clin Genet* 99: 488–489

Lima LG, Chammas R, Monteiro RQ, Moreira MEC & Barcinski MA (2009) Tumor-derived microvesicles modulate the establishment of metastatic melanoma in a phosphatidylserine-dependent manner. *Cancer Lett* 283: 168–175

Lippincott-Schwartz J & Phair RD (2010) Lipids and cholesterol as regulators of traffic in the endomembrane system. *Annu Rev Biophys* 39: 559–578

Liu Z & Roche PA (2015) Macropinocytosis in phagocytes: Regulation of MHC class-II-restricted antigen presentation in dendritic cells. *Front Physiol* 6: 1–6

Lorent JH, Levental KR, Ganesan L, Rivera-Longsworth G, Sezgin E, Doktorova M, Lyman E & Levental I (2020) Plasma membranes are asymmetric in lipid unsaturation, packing and protein shape. *Nat Chem Biol* 16: 644–652

Luberto C, Hassler DF, Signorelli P, Okamoto Y, Sawai H, Boros E, Hazen-Martin DJ, Obeid LM, Hannun YA & Smith GK (2002) Inhibition of tumor necrosis factor-induced cell death in MCF7 by a novel inhibitor of neutral sphingomyelinase. *J Biol Chem* 277: 41128–41139

Maranda B, Brown D, Bourgoin S, Casanova JE, Vinay P, Ausiello DA & Marshansky V (2001) Intra-endosomal pH-sensitive Recruitment of the Arf-nucleotide Exchange Factor ARNO and Arf6 from Cytoplasm to Proximal Tubule Endosomes. *J Biol Chem* 276: 18540–18550

Marchesini N, Luberto C & Hannun YA (2003) Biochemical Properties of Mammalian Neutral Sphingomyelinase2 and Its Role in Sphingolipid Metabolism *. *J Biol Chem* 278: 13775–13783

Marchesini N, Osta W, Bielawski J, Luberto C, Obeid LM & Hannun YA (2004) Role for mammalian neutral sphingomyelinase 2 in confluence-induced growth arrest of MCF7 cells. *J Biol Chem* 279: 25101–25111

Marshansky V & Futai M (2008) The V-type H+-ATPase in vesicular trafficking: targeting, regulation and function. *Curr Opin Cell Biol* 20: 415–426

Martelli AM, Falà F, Faenza I, Billi AM, Cappellini A, Manzoli L & Cocco L (2004) Metabolism and signaling activities of nuclear lipids. *Cell Mol Life Sci* 61: 1143–1156

Matsui T, Osaki F, Hiragi S, Sakamaki Y & Fukuda M (2021) ALIX and ceramide differentially control polarized small extracellular vesicle release from epithelial cells. *EMBO Rep*: 1–11

Matsuo H, Matsuo H, Chevallier J, Mayran N, Blanc I Le, Ferguson C, Faure J, Blanc NS, Matile S, Dubochet J, *et al* (2004) Role of LBPA and Alix inMultivesicular Liposome Formationand Endosome Organization. *Science (80-)* 531: 1–4

Matthews HK, Bertoli C & de Bruin RAM (2022) Cell cycle control in cancer. *Nat Rev Mol Cell Biol* 23: 74–88

Maxfield FR & McGraw TE (2004) Endocytic recycling. *Nat Rev Mol Cell Biol* 5: 121–132

McGuire CM & Forgac M (2018) Glucose starvation increases V-ATPase assembly and activity in mammalian cells through AMP kinase and phosphatidylinositide 3-kinase/Akt signaling. *J Biol Chem* 293: 9113–9123

McMahon HT & Boucrot E (2011) Molecular mechanism and physiological functions of clathrin-mediated endocytosis. *Nat Rev Mol Cell Biol* 12: 517–533

Menck K, Sönmezer C, Worst TS, Schulz M, Dihazi GH, Streit F, Erdmann G, Kling S, Boutros M, Binder C, *et al* (2017) Neutral sphingomyelinases control extracellular vesicles budding from the plasma membrane. *J Extracell Vesicles* 6: 1378056

Mindell JA (2012) Lysosomal acidification mechanisms. *Annu Rev Physiol* 74: 69–86

Miranda KC, Bond DT, McKee M, Skog J, Punescu TG, Da Silva N, Brown D & Russo LM (2010) Nucleic acids within urinary exosomes/microvesicles are potential biomarkers for renal disease. *Kidney Int* 78: 191–199

Miura Y, Gotoh E, Nara F, Nishijima M & Hanada K (2004) Hydrolysis of sphingosylphosphocholine by neutral sphingomyelinases. *FEBS Lett* 557: 288–292

Mizutani Y, Tamiya-Koizumi K, Nakamura N, Kobayashi M, Hirabayashi Y & Yoshida S (2001) Nuclear localization of neutral sphingomyelinase 1: biochemical and immunocytochemical analyses. *J Cell Sci* 114: 3727–3736

Möbius W, van Donselaar E, Ohno-Iwashita Y, Shimada Y, Heijnen HFG, Slot JW & Geuze HJ (2003) Recycling compartments and the internal vesicles of multivesicular bodies harbor most of the cholesterol found in the endocytic pathway. *Traffic* 4: 222–231

Mueller N, Avota E, Collenburg L, Grassmé H & Schneider-Schaulies S (2014) Neutral Sphingomyelinase in Physiological and Measles Virus Induced T Cell Suppression. *PLoS Pathog* 10

Muntasell A, Berger AC & Roche PA (2007) T cell-induced secretion of MHC class II-peptide complexes on B cell exosomes. *EMBO J* 26: 4263–4272

Muralidharan-Chari V, Clancy J, Plou C, Romao M, Chavrier P, Raposo G & D'Souza-Schorey C (2009) ARF6-Regulated Shedding of Tumor Cell-Derived Plasma Membrane Microvesicles. *Curr Biol* 19: 1875–1885

van Niel G, Bergam P, Di Cicco A, Hurbain I, Lo Cicero A, Dingli F, Palmulli R, Fort C,

Potier MC, Schurgers LJ, *et al* (2015) Apolipoprotein E Regulates Amyloid Formation within Endosomes of Pigment Cells. *Cell Rep* 13: 43–51

van Niel G, Charrin S, Simoes S, Romao M, Rochin L, Saftig P, Marks MS, Rubinstein E & Raposo G (2011) The Tetraspanin CD63 Regulates ESCRT-Independent and -Dependent Endosomal Sorting during Melanogenesis. *Dev Cell* 21: 708–721

van Niel G, D'Angelo G & Raposo G (2018) Shedding light on the cell biology of extracellular vesicles. *Nat Rev Mol Cell Biol* 19: 213–228

Van Niel G, D'Angelo G & Raposo G (2018) Shedding light on the cell biology of extracellular vesicles. *Nat Rev Mol Cell Biol* 19: 213–228

Nishino T & Morikawa K (2002) Structure and function of nucleases in DNA repair: Shape, grip and blade of the DNA scissors. *Oncogene* 21: 9022–9032

Nomura S (2017) Extracellular vesicles and blood diseases. *Int J Hematol* 105: 392–405

Ochotny N, Van Vliet A, Chan N, Yao Y, Morel M, Kartner N, Von Schroeder HP, Heersche JNM & Manolson MF (2006) Effects of human a3 and a4 mutations that result in osteopetrosis and distal renal tubular acidosis on yeast V-ATPase expression and activity. *J Biol Chem* 281: 26102–26111

Ogretmen B & Hannun YA (2004) Biologically active sphingolipids in cancer pathogenesis and treatment. *Nat Rev Cancer* 4: 604–616

Oot RA, Couoh-Cardel S, Sharma S, Stam NJ & Wilkens S (2017) Breaking up and making up: The secret life of the vacuolar H+-ATPase. *Protein Sci* 26: 896–909

Ostrowski M, Carmo NB, Krumeich S, Fanget I, Raposo G, Savina A, Moita CF, Schauer K, Hume AN, Freitas RP, *et al* (2010) Rab27a and Rab27b control different steps of the exosome secretion pathway. *Nat Cell Biol* 12: 19–30

Pamarthy S, Kulshrestha A, Katara GK & Beaman KD (2018) The curious case of vacuolar ATPase: Regulation of signaling pathways. *Mol Cancer* 17: 1–9

Panigrahi GK, Praharaj PP, Peak TC, Long J, Singh R, Rhim JS, Elmageed ZYA & Deep G (2018) Hypoxia-induced exosome secretion promotes survival of African-American and Caucasian prostate cancer cells. *Sci Rep* 8: 1–13

Pant S, Hilton H & Burczynski ME (2012) The multifaceted exosome: Biogenesis, role in normal and aberrant cellular function, and frontiers for pharmacological and

biomarker opportunities. *Biochem Pharmacol* 83: 1484–1494

Di Paolo G & De Camilli P (2006) Phosphoinositides in cell regulation and membrane dynamics. *Nature* 443: 651–657

Pap E, Pállinger É, Pásztói M & Falus A (2009) Highlights of a new type of intercellular communication: Microvesicle-based information transfer. *Inflamm Res* 58: 1–8

Peterková L, Kmoníčková E, Ruml T & Rimpelová S (2020) Sarco/Endoplasmic Reticulum Calcium ATPase Inhibitors: Beyond Anticancer Perspective. *J Med Chem* 63: 1937–1963

Philipp S, Puchert M, Adam-Klages S, Tchikov V, Winoto-Morbach S, Mathieu S, Deerberg A, Kolker L, Marchesini N, Kabelitz D, *et al* (2010) The Polycomb group protein EED couples TNF receptor 1 to neutral sphingomyelinase. *Proc Natl Acad Sci U S A* 107: 1112–1117

Pietrement C, Sun-Wada GH, Da Silva N, McKee M, Marshansky V, Brown D, Futai M & Breton S (2006) Distinct expression patterns of different subunit isoforms of the V-ATPase in the rat epididymis. *Biol Reprod* 74: 185–194

Piper RC & Katzmann DJ (2010) Biogenesis and function of MVBs. *Annu Rev Cell Dev Biol* 23: 519–547

Puebla-Osorio N, Damiani E, Bover L & Ullrich SE (2015) Platelet-activating factor induces cell cycle arrest and disrupts the DNA damage response in mast cells. *Cell Death Dis* 6: 1–11

Pyne NJ & Pyne S (2020) Recent advances in the role of sphingosine 1-phosphate in cancer. *FEBS Lett* 594: 3583–3601

R-Iedeen & G.Wu (2009) Nuclear Lipids and Their Metabolic and Signaling Properties. In *Neural lipids* pp 175–191.

Rawson RB (2003) The SREBP pathway - Insights from insigs and insects. *Nat Rev Mol Cell Biol* 4: 631–640

Revill K, Wang T, Lachenmayer A, Kojima K, Harrington A, Li J, Hoshida Y, Llovet JM & Powers S (2013) Genome-wide methylation analysis and epigenetic unmasking identify tumor suppressor genes in hepatocellular carcinoma. *Gastroenterology* 145: 1–22

Rivinoja A, Hassinen A, Kokkonen N, Kauppila A & Kellokumpu S (2009) Elevated golgi pH impairs terminal N-glycosylation by inducing mislocalization of golgi glycosyltransferases. *J Cell Physiol* 220: 144–154

Rodrigues-Lima F, Fensome AC, Josephs M, Evans J, Veldman RJ & Katan M (2000) Structural requirements for catalysis and membrane targeting of mammalian enzymes with neutral sphingomyelinase and lysophospholipid phospholipase C activities: Analysis by chemical modification and site-directed mutagenesis. *J Biol Chem* 275: 28316–28325

Saksena S, Sun J, Chu T & Emr SD (2007) ESCRTing proteins in the endocytic pathway. *Trends Biochem Sci* 32: 561–573

Sanwlani R, Fonseka P, Chitti S V. & Mathivanan S (2020) Milk-derived extracellular vesicles in inter-organism, cross-species communication and drug delivery. *Proteomes* 8: 1–26

Sautin YY, Lu M, Gaugler A, Zhang L & Gluck SL (2005) Phosphatidylinositol 3-Kinase-Mediated Effects of Glucose on Vacuolar H. *Society* 25: 575–589

Sawai H, Domae N, Nagan N & Hannun YA (1999) Function of the cloned putative neutral sphingomyelinase as lyso- platelet activating factor-phospholipase C. *J Biol Chem* 274: 38131–38139

Schuchman EH, Levran O, Pereira L V. & Desnick RJ (1992) Structural organization and complete nucleotide sequence of the gene encoding human acid sphingomyelinase (SMPD1). *Genomics* 12: 197–205

Schwarz DS & Blower MD (2016) The endoplasmic reticulum: Structure, function and response to cellular signaling. *Cell Mol Life Sci* 73: 79–94

Shamseddine A, Clarke C, Carroll B, Airola M V., Mohammed S, Rella A, Obeid L & Hannun Y (2015a) P53-dependent upregulation of neutral sphingomyelinase-2: Role in doxorubicin-induced growth arrest. *Cell Death Dis* 6: e1947-10

Shamseddine AA, Airola M V. & Hannun YA (2015b) Roles and regulation of neutral sphingomyelinase-2 in cellular and pathological processes. *Adv Biol Regul* 57: 24–41

Shurtleff MJ, Temoche-diaz MM & Schekman R (2018) Extracellular Vesicles and

Cancer : Caveat Lector. 2: 395–411

Soares Martins T, Trindade D, Vaz M, Campelo I, Almeida M, Trigo G, da Cruz e Silva OAB & Henriques AG (2021) Diagnostic and therapeutic potential of exosomes in Alzheimer's disease. *J Neurochem* 156: 162–181

Stoffel W, Hammels I, Jenke B, Binczek E, Schmidt-Soltau I, Brodesser S, Schauss A, Etich J, Heilig J & Zaucke F (2016) Neutral sphingomyelinase (*SMPD3*) deficiency disrupts the Golgi secretory pathway and causes growth inhibition. *Cell Death Dis* 7: e2488

Stoffel W, Hammels I, Jenke B, Schmidt-Soltau I & Niehoff A (2019) Neutral Sphingomyelinase 2 (*SMPD3*) Deficiency in Mice Causes Chondrodysplasia with Unimpaired Skeletal Mineralization. *Am J Pathol* 189: 1831–1845

Stoffel W, Jenke B, Blöck B, Zumbansen M & Koebke J (2005) Neutral sphingomyelinase 2 (*SMPD3*) in the control of postnatal growth and development. *Proc Natl Acad Sci U S A* 102: 4554–4559

Storck EM, Özbalci C & Eggert US (2018) Lipid Cell Biology: A Focus on Lipids in Cell Division. *Annu Rev Biochem* 87: 839–869

Stransky L, Cotter K & Forgac M (2016) The function of v-atpases in cancer. *Physiol Rev* 96: 1071–1091

Stransky LA & Forgac M (2015) Amino acid availability modulates vacuolar H+-ATPase assembly. *J Biol Chem* 290: 27360–27369

Stuffers S, Sem Wegner C, Stenmark H & Brech A (2009) Multivesicular endosome biogenesis in the absence of ESCRTs. *Traffic* 10: 925–937

Sun-Wada GH, Imai-Senga Y, Yamamoto A, Murata Y, Hirata T, Wada Y & Futai M (2002) A proton pump ATPase with testis-specific E1-subunit isoform required for acrosome acidification. *J Biol Chem* 277: 18098–18105

Sun-Wada GH, Murata Y, Yamamoto A, Kanazawa H, Wada Y & Futai M (2000) Acidic endomembrane organelles are required for mouse postimplantation development. *Dev Biol* 228: 315–325

Sun-wada GH, Toyomura T, Murata Y, Yamamoto A, Futai M & Wada Y (2006) The a3 isoform of V-ATPase regulates insulin secretion from pancreatic β-cells. *J Cell Sci*

119: 4531–4540

Sun-Wada GH & Wada Y (2015) Role of vacuolar-type proton ATPase in signal transduction. *Biochim Biophys Acta - Bioenerg* 1847: 1166–1172

Szegezdi E, Logue SE, Gorman AM & Samali A (2006) Mediators of endoplasmic reticulum stress-induced apoptosis. *EMBO Rep* 7: 880–885

Tani M & Hannun YA (2007) Neutral sphingomyelinase 2 is palmitoylated on multiple cysteine residues: Role of palmitoylation in subcellular localization. *J Biol Chem* 282: 10047–10056

Taub N, Teis D, Ebner HL, Hess MW & Huber LA (2007) Late Endosomal Traffic of the Epidermal Growth Factor Receptor Ensures Spatial and Temporal Fidelity of Mitogen-activated Protein Kinase Signaling. *Mol Biol Cell* 18: 3250–3263

Tcherkasowa AE, Adam-Klages S, Kruse M-L, Wiegmann K, Mathieu S, Kolanus W, Krönke M & Adam D (2002) Interaction with Factor Associated with Neutral Sphingomyelinase Activation, a WD Motif-Containing Protein, Identifies Receptor for Activated C-Kinase 1 as a Novel Component of the Signaling Pathways of the p55 TNF Receptor. *J Immunol* 169: 5161–5170

Teasdale RD & Jackson MR (1996) Signal-mediated sorting of membrane proteins between the endoplasmic reticulum and the Golgi apparatus. *Annu Rev Cell Dev Biol* 12: 27–54

Theos AC, Truschel ST, Tenza D, Hurbain I, Harper DC, Berson JF, Thomas PC, Raposo G & Marks MS (2006) A lumenal domain-dependent pathway for sorting to intralumenal vesicles of multivesicular endosomes involved in organelle morphogenesis. *Dev Cell* 10: 343–354

Théry C, Witwer KW, Aikawa E, Alcaraz MJ, Anderson JD, Andriantsitohaina R, Antoniou A, Arab T, Archer F, Atkin-Smith GK, *et al* (2018) Minimal information for studies of extracellular vesicles 2018 (MISEV2018): a position statement of the International Society for Extracellular Vesicles and update of the MISEV2014 guidelines. *J Extracell Vesicles* 7

Toei M, Saum R & Forgac M (2010) Regulation and isoform function of the V-ATPases. *Biochemistry* 49: 4715–4723

Tomiuk S, Hofmann K, Nix M, Zumbansen M & Stoffel W (1998a) Cloned mammalian neutral sphingomyelinase: Functions in sphingolipid signaling? *Proc Natl Acad Sci* 95: 3638–3643

Tomiuk S, Hofmann K, Nix M, Zumbansen M & Stoffel W (1998b) Cloned mammalian neutral sphingomyelinase: Functions in sphingolipid signaling? *Proc Natl Acad Sci U S A* 95: 3638–3643

Tomiuk S, Zumbansen M & Stoffel W (2000) Characterization and subcellular localization of murine and human magnesium-dependent neutral sphingomyelinase. *J Biol Chem* 275: 5710–5717

Tonnetti L, Verí MC, Bonvini E & D'Adamio L (1999a) A role for neutral sphingomyelinase-mediated ceramide production in T cell receptor-induced apoptosis and mitogen-activated protein kinase-mediated signal transduction. *J Exp Med* 189: 1581–9

Tonnetti L, Verí MC, Bonvini E & D'Adamio L (1999b) A role for neutral sphingomyelinase-mediated ceramide production in T cell receptor-induced apoptosis and mitogen-activated protein kinase-mediated signal transduction. *J Exp Med* 189: 1581–1589

Traini M, Quinn CM, Sandoval C, Johansson E, Schroder K, Kockx M, Meikle PJ, Jessup W & Kritharides L (2014) Sphingomyelin phosphodiesterase acid-like 3A (SMPDL3A) is a novel nucleotide phosphodiesterase regulated by cholesterol in human macrophages. *J Biol Chem* 289: 32895–32913

Trajkovic K (2008) Ceramide triggers budding of exosome vesicles into multivesicular endosomes (Science (1244)). *Science (80-)* 320: 179

Trajkovic K, Hsu C, Chiantia S, Rajendran L, Wenzel D, Wieland F, Schwille P, Brügger B & Simons M (2008) Ceramide triggers budding of exosome vesicles into multivesicular endosomes. *Science (80-)* 319: 1244–1247

Travers JB, Rohan JG & Sahu RP (2021) New Insights Into the Pathologic Roles of the Platelet-Activating Factor System. *Front Endocrinol (Lausanne)* 12: 1–12

Tricarico C, Clancy J & D'Souza-Schorey C (2017) Biology and biogenesis of shed microvesicles. *Small GTPases* 8: 220–232

Truman LA, Ford CA, Pasikowska M, Pound JD, Wilkinson SJ, Dumitriu IE, Melville L, Melrose LA, Ogden CA, Nibbs R, *et al* (2008) CX3CL 1/fractalkine is released from

apoptotic lymphocytes to stimulate macrophage chemotaxis. *Blood* 112: 5026–5036

Vainauskas S & Menon AK (2005) Endoplasmic reticulum localization of Gaa1 and PIG-T, subunits of the glycosylphosphatidylinositol transamidase complex. *J Biol Chem* 280: 16402–16409

Vasanthakumar T, Bueler SA, Wu D, Beilsten-Edmands V, Robinson C V. & Rubinstein JL (2019) Structural comparison of the vacuolar and Golgi V-ATPases from saccharomyces cerevisiae. *Proc Natl Acad Sci U S A* 116: 7272–7277

Vasanthakumar T & Rubinstein JL (2020) Structure and Roles of V-type ATPases. *Trends Biochem Sci* 45: 295–307

Vicinanza M, D'Angelo G, Di Campli A & De Matteis MA (2008) Function and dysfunction of the PI system in membrane trafficking. *EMBO J* 27: 2457–2470

Villarroya-Beltri C, Baixauli F, Mittelbrunn M, Fernández-Delgado I, Torralba D, Moreno-Gonzalo O, Baldanta S, Enrich C, Guerra S & Sánchez-Madrid F (2016) ISGylation controls exosome secretion by promoting lysosomal degradation of MVB proteins. *Nat Commun* 7

Villarroya-Beltri C, Gutiérrez-Vázquez C, Sánchez-Cabo F, Pérez-Hernández D, Vázquez J, Martin-Cofreces N, Martinez-Herrera DJ, Pascual-Montano A, Mittelbrunn M & Sánchez-Madrid F (2013) Sumoylated hnRNPA2B1 controls the sorting of miRNAs into exosomes through binding to specific motifs. *Nat Commun* 4: 1–10

Wang L, Wu D, Robinson C V., Wu H & Fu T-M (2020) Structures of a Complete Human V-ATPase Reveal Mechanisms of Its Assembly. *Mol Cell*: 1–11

Wang MX, Cheng XY, Jin M, Cao YL, Yang YP, Wang J Da, Li Q, Wang F, Hu LF & Liu CF (2015) TNF compromises lysosome acidification and reduces α-synuclein degradation via autophagy in dopaminergic cells. *Exp Neurol* 271: 112–121

Wang R, Wang J, Hassan A, Lee CH, Xie XS & Li X (2021) Molecular basis of V-ATPase inhibition by bafilomycin A1. *Nat Commun* 12

Wang T, Gilkes DM, Takano N, Xiang L, Luo W, Bishop CJ, Chaturvedi P, Green JJ & Semenza GL (2014) Hypoxia-inducible factors and RAB22A mediate formation of microvesicles that stimulate breast cancer invasion and metastasis. *Proc Natl Acad*

Sci U S A 111

Werneburg NW, Guicciardi ME, Bronk SF & Gores GJ (2002) Tumor necrosis factor-α-associated lysosomal permeabilization is cathepsin B dependent. *Am J Physiol - Gastrointest Liver Physiol* 283: 947–956

Wheeler D, Knapp E, Bandaru VVR, Wang Y, Knorr D, Poirier C, Mattson MP, Geiger JD & Haughey NJ (2009) Tumor necrosis factor-α-induced neutral sphingomyelinase-2 modulates synaptic plasticity by controlling the membrane insertion of NMDA receptors. *J Neurochem* 109: 1237–1249

Willms E, Johansson HJ, Mäger I, Lee Y, Blomberg KEM, Sadik M, Alaarg A, Smith CIE, Lehtiö J, El Andaloussi S, *et al* (2016) Cells release subpopulations of exosomes with distinct molecular and biological properties. *Sci Rep* 6: 1–12

Wlodarchak N & Xing Y (2016) PP2A as a master regulator of the cell cycleThe Impact of Pollution on Worker Productivity. *Crit Rev Biochem Mol Biol* 51: 162–184

Wolf P (1967) The nature and significance of platelet products in human plasma. *Br J Haematol* 13: 269–288

Wu BX, Rajagopalan V, Roddy PL, Clarke CJ & Hannun YA (2010) Identification and characterization of murine mitochondria-associated neutral sphingomyelinase (MA-nSMase), the mammalian sphingomyelin phosphodiesterase 5. *J Biol Chem* 285: 17993–18002

Yabu T, Imamura S, Yamashita M & Okazaki T (2008) Identification of Mg2+-dependent neutral sphingomyelinase 1 as a mediator of heat stress-induced ceramide generation and apoptosis. *J Biol Chem* 283: 29971–29982

Yabu T, Shiba H, Shibasaki Y, Nakanishi T, Imamura S, Touhata K & Yamashita M (2015) Stress-induced ceramide generation and apoptosis via the phosphorylation and activation of nSMase1 by JNK signaling. *Cell Death Differ* 22: 258–273

Yamashita Y, Kojima K, Tsukahara T, Agawa H, Yamada K, Amano Y, Kurotori N, Tanaka N, Sugamura K & Takeshita T (2008) Ubiquitin-independent binding of Hrs mediates endosomal sorting of the interleukin-2 receptor β-chain. *J Cell Sci* 121: 1727–1738

Yang CL, Chiou SH, Tai WC, Joseph NA & Chow KC (2017) Trivalent chromium induces autophagy by activating sphingomyelin phosphodiesterase 2 and increasing cellular

ceramide levels in renal HK2 cells. *Mol Carcinog* 56: 2424–2433

Yang DI, Yeh CH, Chen S, Xu J & Hsu CY (2004) Neutral sphingomyelinase activation in endothelial and glial cell death induced by amyloid beta-peptide. *Neurobiol Dis* 17: 99–107

Yang T, Espenshade PJ, Wright ME, Yabe D, Gong Y, Aebersold R, Goldstein JL & Brown MS (2002) Crucial step in cholesterol homeostasis: Sterols promote binding of SCAP to INSIG-1, a membrane protein that facilitates retention of SREBPs in ER. *Cell* 110: 489–500

Yang Z & Klionsky DJ (2010) Eaten alive: A history of macroautophagy. *Nat Cell Biol* 12: 814–822

Zhang YQ, Gamarra S, Garcia-Effron G, Park S, Perlin DS & Rao R (2010) Requirement for ergosterol in V-ATPase function underlies antifungal activity of azole drugs. *PLoS Pathog* 6

Zhong L, Kong JN, Dinkins MB, Leanhart S, Zhu Z, Spassieva SD, Qin H, Lin HP, Elsherbini A, Wang R, *et al* (2018) Increased liver tumor formation in neutral sphingomyelinase-2-deficient mice. *J Lipid Res* 59: 795–804

Zhu C, Bilousova T, Focht S, Jun M, Elias CJ, Melnik M, Chandra S, Campagna J, Cohn W, Hatami A, *et al* (2021) Pharmacological inhibition of nSMase2 reduces brain exosome release and α-synuclein pathology in a Parkinson's disease model. *Mol Brain* 14: 1–8

Zumbansen M & Stoffel W (2002) Neutral sphingomyelinase 1 deficiency in the mouse causes no lipid storage disease. *Mol Cell Biol* 22: 3633–3638

Curriculum Vitae

Personal Data

Name: Dolma Choezom **Date of birth:** 03.09.1992 **Place of birth:** Lithang, Tibet

Email: dolma.choezom@med.uni-goettingen.de **Address**: Waldweg19A, 37073 Göttingen

EDUCATION and RESEARCH EXPERIENCE

PhD in Molecular Medicine 2018 - present

Georg-August-University Göttingen, Göttingen, Germany

PhD Thesis Title: Investigating the role of neutral sphingomyelinases in membrane vesicle trafficking

Supervisor: Prof. Dr. Julia Groß, Department of Developmental Biochemistry/ Hematology and Oncology

Master of Science in Molecular Medicine 2016 - 2018

Georg-August-University Göttingen, Göttingen, Germany

Thesis Title: The role of neutral sphingomyelinases in extracellular vesicle secretion in tumor cell lines

Supervisor: Prof. Dr. Julia Groß, Department of Developmental Biochemistry/ Hematology and Oncology

Bachelor of Science in Biochemistry and Cell Biology 2013 - 2016

Jacobs University Bremen, Bremen, Germany

Thesis Title: Gamma-toxin activity on *Dictyostelium discoideum* tRNA

Supervisor: Prof. Dr. Christian Hammann, Ribogenetics and RNA Biochemistry Laboratory

All India Senior School Certificate Examination 2010 - 2012

Tibetan Childen's Village Selakui, Dehradun, India

PUBLICATIONS:

- **Choezom** D & Gross JC (2022) Neutral Sphingomyelinase 2 controls exosomes secretion by counteracting V-ATPase-mediated endosome acidification. J Cell Sci
- **Choezom** D & Gross JC (2022) Neutral sphingomyelinase 1 regulates cellular fitness at the level of ER stress and cell cycle Dolma. bioRxiv

- Pradhipa Karuna M, Witte L, Linnemannstoens K, **Choezom** D, Danieli-Mackay A, Honemann-Capito M & Gross JC (2020) Phosphorylation of ykt6 snare domain regulates its membrane recruitment and activity. Biomolecules 10: 1–19
- He W, Yuan T, **Choezom** D, Hunkler H, Annamalai K, Lupse B & Maedler K (2018) Ageing potentiates diet-induced glucose intolerance, β-cell failure and tissue inflammation through TLR4. Sci Rep 8: 2767

SCIENTIFIC MEETINGS

• BSCDB-BESEV Joint Autumn meeting 2019: “Neutral sphingomyelinases in the interplay between autophagy and EV secretion.” Poster Presentation

• GBM/DGZ Fall Conference 2019: “Neutral sphingomyelinases in the interplay between autophagy and EV secretion.” Poster Presentation

• GSEV Autumn Meeting 2018: “Neutral sphingomyelinases in the interplay between autophagy and EV secretion.” Poster Presentation

TEACHING EXPERIENCE

Biochemistry Practical Course for Medical Students 2018-2021

Instruction and supervision of experiments (15 students per course day, 1 week per semester).

Supervision of lab rotation students 2018-2021

Planning and supervision of independent research projects for Bachelor’s and Master’s students and evaluation of written reports (One to two students for 8-10 weeks per semester).

Languages:

Tibetan: Native **English:** Full professional proficiency

Hindi: Professional working proficiency **German:** Intermediate (B1)